UNDERSTANDING BLENDED CORROSION CONTROL CHEMICALS FOR CONTROLLING LEAD RELEASE AND WATER QUALITY IN DRINKING WATER

By

Javier Augusto M. Locsin

Submitted in partial fulfilment of the requirements

for the degree of Doctor of Philosophy

at

Dalhousie University

Halifax, Nova Scotia

December 2022

Table of Contents

List of Tables

List of Figures

Abstract

This thesis provided a comprehensive review of the occurrence, measurement, and characterization of colloidal lead in drinking water. Colloids have been underestimated in conventional drinking water monitoring, where metals are defined as soluble based on their ability to pass through a 0.45 µm filter. Field studies show that colloidal lead can represent a significant proportion of total lead concentrations. This work also explored various approaches to controlling iron and lead release, and manganese sequestration using blends of orthophosphate and one of three model polyphosphates -- tripoly-, trimeta- and hexametaphosphate— , or orthophosphate and sodium silicate. Polyphosphate structure was a significant factor for determining their behavior with lead, iron, and manganese. Blends with linear polyphosphates provided greater capacity for chelating metal ions than cyclophosphates. Longer chain lengths increased lead but decreased iron release. This was attributed to the steric constraints of cyclophosphates inhibiting their interactions with metals. Unlike cyclophosphates, linear polyphosphates also appeared to remain in solution rather than adsorb to mineral surfaces, resulting in greater metals release. Sequesterants may increase manganese mobility by forming soluble metal-complexes or via their mobilization with iron colloids. Here, polyphosphates or silicate sequestered 2.3-7.4 and 3 times more manganese than orthophosphate, respectively. Orthophosphate-silicate was the most effective blend for reducing iron corrosion. Moreover, field flow fractionation (A4F) data were consistent with the mobilization of manganese via adsorption to suspended iron colloids. Small colloids present unique challenges for maintaining drinking water quality. Techniques used for sampling and colloids characterization can shape corrosion control decisions. The use of sequestrants entails considerable risk and may be counterproductive to minimizing consumer exposure to lead and manganese. The dispersive properties of sequestrants resulted in the mobilization of manganese via its attachment to iron colloids or maintain dissolved metals in solution.

List of Abbreviations Used

24HS	24 h stagnation
30MS	30 minute stagnation
BET-N2	Brunauer-Emmett-Teller analysis
CSTR	Continuous-flow stirred-tank reactor
DIC	Dissolved inorganic carbon
$Pb_{0.2\mu m}$	Dissolved lead
PO_4	Dissolved phosphate
EDS	Energy dispersive X-ray spectroscopy
ATR-FTIR	Fourier transform infrared spectroscopy in attenuated total reflectance mode
HexametaP	Hexametaphosphate
HRT	Hydraulic retention time
ICP-MS	Inductively coupled plasma mass spectrometry
IR	Infrared spectrum
$Pb_{0.45\mu m}$	Lead in the 0.45 µm filtrate
OrthoP	Orthophosphate
OrthoP-HexametaP	Orthophosphate-Hexametaphosphate
OrthoP-TrimetaP	Orthophosphate-Trimetaphosphate
OrthoP-TripolyP	Orthophosphate-Tripolyphosphate
SEM	Scanning electron microscopy
$Pb_{0.2\text{-}0.45\mu m}$	Small colloidal lead

TrimetaP	Trimetaphosphate
TrimetaP	Tripolyphosphate
XRD	X-ray powder diffraction

Acknowledgements

This thesis was completed with the help from colleagues and several organizations. First, I acknowledge the financial support provided by NSERC through the Industrial Research Chair in Water Quality and Treatment grant.

Second, I would like to thank my supervisor Dr. Graham Gagnon for the opportunity and encouragement to pursue research. I would also like to thank my supervisory committee, consisting of Dr. Margaret Walsh and Dr. Paul Bishop for providing valuable feedback throughout the process of grad school.

Third, I thank fellow students and staff who have assisted me in completing this degree. This includes undergraduate students Kelly Hines, Gillian Stanton, Ryan Swinamer, Almothanna Karfoul, Alyssa Chiasson, Jorginea Bonang, and Aaron Bleasdale-Pollowy. Fellow graduate students Lindsay Anderson, Jessica Bennett, Kyle Rauch, Kaycie Lane, and Dave Redden who provided important feedback on experiment design and manuscript drafts. I also recognize the technical and administrative support provided by post-doctoral fellows Drs. Benjamin Trueman, Evelyne Doré, Yuri Park, and Yaohuan Gao; research staff Heather Daurie and Tarra Chartland; and Halifax Water employees Dr. Wendy Krkošek and Caitlin Sampson.

Finally, I would like to thank my family for being supportive of this process. Thank you to my parents for being a continuous source of support.

1. Chapter 1 Introduction

1.1. Research Rationale

1.1.1. Lead corrosion and regulation in drinking water

Drinking water can be a significant source of lead (Pb) exposure (Triantafyllidou et al., 2007). Lead contamination may occur through contact with lead service lines (LSLs) or premises plumbing components such as lead solder and brass or bronze fixtures, fittings and joints (Elfland et al., 2010). Lead is a potent toxin. Even at low concentrations, lead exposure is associated with attention disorders (Canfield et al., 2003; Nigg et al., 2008), life-long cognitive deficits (Reuben et al., 2017), renal disfunction (Loghman-Adham, 1997), and cognitive decline (Shih et al., 2007).

Due to human health risks, lead is regulated as a contaminant. Lead sampling protocols can be used to meet various sampling objectives including confirming regulatory compliance, assessing corrosion control effectiveness, and estimating exposure. Regulatory sampling protocols vary between countries and regions. In the U.S., the Lead and Copper rule (LCR) specifies an action level of 15 µg L^{-1} measured in first-draw regulatory compliance samples collected at the point-of-use following a >6-hour stagnation (US EPA, 1991). Revisions to the LCR will require a 1st and 5th litre sample taken after a 6-hr stagnation (US EPA, 2021). Meanwhile, Health Canada recommends a maximum allowable concentration of 5 µg L^{-1} in either 30-minute stagnant or random daytime samples collected from drinking water outlets (Health Canada, 2019a). Although guided by Health Canada, Canadian provinces are responsible for the selection of sampling protocol. In Ontario (Government of Ontario, 2002) and Quebec (Government of

Quebec, 2021), 30-mininute stagnant samples taken after a 5-minute flush are used to measure lead levels. Meanwhile, Alberta (Government of Alberta, 2022) adopts a 1L random daytime sampling protocol.

Field studies show that colloidal lead exists in size fractions smaller than ≤0.45 µm and can represent a significant proportion of the total concentration (Figure 2). Metals are operationally defined as soluble or particulate based on their ability to pass through a 0.45 µm membrane filter (Baird, 2017; US EPA, 1994a, 1994b). This highlights a critical shortcoming of this operational definition: the potential to misclassify colloidal or nanoparticulate lead and other contaminants as soluble. The concern is that the remedial actions taken to reduce soluble lead concentrations (i.e., increased orthophosphate dose) may differ from those used to target colloidal lead (i.e., improved NOM removal, controlling iron oxides), and in some cases could exacerbate the problem.

With the variability in lead sources, water use patterns, and water quality, regulated sampling protocols may not accurately provide lead concentrations representative of actual consumer exposure. Moreover, a greater understanding of particle formation will ultimately inform water treatment processes and decrease exposure at the tap. As lead regulations become more stringent, it is essential that decision makers can confidently extrapolate consumer lead exposure. There is a need to better understand how each sampling protocol and colloids analysis can provide a reliable estimate of lead exposure.

1.1.1. Manganese occurrence and regulation in drinking water

Manganese (Mn) accumulation and release in drinking water degrades water quality and can pose risks to public health. In Canada, manganese concentrations in drinking water a limited to

a maximum acceptable concentration of 120 µg L^{-1} and an aesthetic objective of 20 µg L^{-1} (Health Canada, 2019b).

While discoloration of water caused by manganese can compromise public confidence, it may also be detrimental to children's health. Manganese exposure has been associated with lower cognitive development(Bouchard et al., 2018; Dion et al., 2018) and impaired fetal growth(Rahman et al., 2015). Moreover, manganese has been found to increase lead risk in distribution systems(Trueman et al., 2019a).

While a variety of studies have investigated manganese accumulation in full scale distribution systems(Cerrato et al., 2006; Gerke et al., 2016; Schock et al., 2014; Sly et al., 1990), there has been limited research at the bench scale investigating the effects of various distribution conditions on Mn accumulation in a controlled setting.

1.1.2. Controlling lead release with Polyphosphates and Orthophosphate-Polyphosphates

Several water systems add phosphate based corrosion inhibitors and sequestrants - orthophosphate, polyphosphate, and orthophosphate-polyphosphates- to their water (Hazen and Sawyer, 2019; L. S. McNeill & Edwards, 2002). While polyphosphates are effective for controlling aesthetic water quality issues (i.e. discoloration, calcium scaling), they increase lead release by inhibiting lead phosphate mineral formation (Li, Trueman, Locsin, et al., 2021a) and through complexation (T. R. Holm & Shock, 1991b; Rashchi & Finch, 2002). However, the comprehensive understanding of lead-polyphosphate interactions are confounded by two factors: First, polyphosphates encompass a broad range of compounds with varying chain lengths and structures which directly determines polyphosphate's behavior with metal ions

(Rashchi & Finch, 2000). For example, shorter chain polyphosphates are more effective at sequestering heavy metal ions, while longer chains are more effective for lighter metal ions (i.e. Ca, Mg) (Van Wazer & Callis, 1958b). Second, polyphosphates hydrolyze into smaller polyphosphates or orthophosphate (Edwards & McNeill, 2002a; McCullough et al., 1956) resulting in the simultaneous presence of different phosphate species. It is therefore difficult to attribute certain effects exclusively to orthophosphate or polyphosphate because the total effect is due to the interaction of both.

Owing to the complexities mentioned above and the proprietary nature of commercially available orthophosphate-polyphosphates, the mechanisms by which it acts to limit lead release is unclear. Specifically, the effect of orthophosphate:polyphosphate ratios and polyphosphate structural properties on lead release and mineral formation. Previous studies have suggested that the successful used of blended phosphates were dependent on having a high ratio of orthophosphates to polyphosphate (Cantor, 2017).

1.1.3. Potential impacts of sequestrant stabilized Iron (Oxyhydr)Oxides on Lead release

Corroded iron mains release iron (oxyhydr)oxide particles to distributed water that are detectable at the point-of-use (Trueman et al., 2018a). During stagnation within a lead pipe, lead adsorption to iron oxides may promote lead dissolution by suppressing the activity of the lead cation in solution. Similarly, manganese can be transported through the distribution system by iron colloids (Gora et al., 2020; Trueman, Anaviapik-Soucie, et al., 2019) When sequestrants are used, adsorption to stabilized, suspended iron particles could increase lead and manganese at the point-of-use.

1.1.4. Orthophosphate-Silicate- A possible alternative for simultaneous corrosion control and sequestration

While sodium silicate is an effective sequestrant (B. Li et al., 2019; Robinson et al., 1992), it performs poorly for lead control compared to orthophosphate or pH adjustment (Kogo et al., 2017; B. Li, Trueman, Locsin, et al., 2021a; Pinto et al., 1997). This effect is owing to the minimal direct interaction between silicate and lead (B. Li, Trueman, Locsin, et al., 2021a). However, silicates can mobilize lead via colloidal co-transport with other distribution system metals (B. Li, Trueman, Munoz, et al., 2021b).

Some drinking water utilities apply phosphate-silicate blends for corrosion control (Hazen and Sawyer, 2019) but there is a lack of understanding of orthophosphate-silicate treatment found in peer-reviewed literature. The combination of phosphates and silicates have been effective in reducing carbon steel corrosion in industrial settings (Naderi et al., 2014; Salasi et al., 2007) but there are no studies in the drinking water context.

1.2. Thesis Objectives

The goal of this thesis was to comprehensively understand and evaluate the performance of blended phosphates -Orthophosphate-Polyphosphate and Orthophosphate-Silicate- for simultaneously controlling lead release and mitigating discoloration in drinking water.

The main objectives of the work presented in this thesis document are as follows:

1. Investigate the impacts of polyphosphate structure on lead corrosion control with orthophosphate-polyphosphate blends.

2. Evaluate the performance of orthophosphate-polyphosphate and orthophosphate-silicate blends for reducing iron corrosion, and sequestering manganese.

1.3. Organization of Thesis

To achieve these objectives, the research approach was organized into six chapters.

The chapters of this thesis are arranged in the style of a series of journal papers. Each of those chapters contains an abstract, introduction, materials and methods, results and discussion. Methods that are repeated in multiple chapters are only described in their initial appearance and subsequent chapters will refer to these instances appropriately.

Chapter 2 provides a brief overview of the state of understanding of lead colloids –particles between 0.001 and 1 µm- in drinking water, including relevant published material that it pertinent to this work. This section also includes an overview of the occurrence and factors affecting colloidal lead release and mobility, and summary of colloid characterization methods as well as highlights their potential applications and benefits to drinking water utilities.

Chapter 3 presents results of a field study on the impact of the recent reduction in maximum allowable concentration (MAC) and the change in recommended sampling protocols on lead regulatory compliance by means of a multi-community monitoring program. Lead occurrence in Nova Scotia was compared against the new MAC using four regulatory sampling protocols — flushed, random daytime, 30-minute stagnation, and 6-hour stagnation — and the implications for future compliance monitoring in Canada are discussed.

Chapter 4 focuses on the effect and efficacy of orthophosphate-polyphosphate blends on dissolved and colloidal lead release. The dissolution of lead (II) carbonate was determined as a

function of polyphosphate structure (cyclophosphate vs linear chain) and chain length (short vs long), orthophosphate:polyphosphate ratio (1:1, 1:2) and hydraulic retention time using continuously stirred tank reactors (CSTR). The changes in chemical and structural properties were probed by scanning electron microscopy (SEM), X-ray diffraction (XRD) and Fourier transform infrared spectroscopy in attenuated total reflectance mode (ATR-FTIR) and used to describe the mechanistic interaction between lead and phosphates.

Chapter 5 covers the experimental study of iron and manganese sequestration and iron corrosion with blended phosphate- orthophosphate-polyphosphate and orthophosphate-silicate- treatment. Iron and manganese precipitation experiments were used to evaluate sequestering ability of blended phosphates. Corrosion cells were used to determine the impact of blended phosphates on iron corrosion and manganese deposition. Corrosion scales were developed on new iron coupons at environmentally relevant pH, dissolved inorganic carbon, and free chlorine concentrations. The release of colloidal iron and its interaction with manganese was investigated via asymmetrical flow filed flow fractionation (A4F).

Chapter 6 provides a summary and conclusion of the work included in this thesis.

2. Chapter 2 Colloidal lead in drinking water: formation, occurrence, and characterization

This chapter is reprinted with permission from the following:

Locsin, J. A., Hood, K. M., Doré, E., Trueman, B. F., & Gagnon, G. A. (2022). Colloidal lead in drinking water: Formation, occurrence, and characterization. *Critical Reviews in Environmental Science and Technology*, 1-27.

J.A.L coordinated data collection, analyzed the data, wrote the paper, and prepared the figures.

2.1. Abstract

Lead colloids—particles between 0.001 and 1 µm—present unique challenges for maintaining drinking water quality. Most of the published literature on lead in drinking water adopts a threshold for soluble lead of <0.45 µm, yet strong evidence of lead colloids occurring below this threshold has been reported across North America and Europe. This highlights the potential to misclassify colloidal lead as soluble. Remedial actions taken to reduce soluble lead concentrations can differ from those used to target colloidal lead, and in some cases may exacerbate the problem.

Concentrations of colloidal lead are difficult to measure and to predict from water quality data. Nevertheless, advances in analytical techniques have allowed for more precise identification and characterization of lead colloids and their interactions with other compounds in drinking

water. Analytical cost or expertise may be a barrier to utilizing some of these techniques. A critical analysis, weighing practicality and data quality, of the strengths and weaknesses of these methods is presented.

This review identifies and discusses four key factors that promote colloidal lead formation and mobility in drinking water: natural organic matter, adsorption of lead to colloidal iron particles, precipitation with orthophosphate, and complexation or dispersion by sequestrants. This review also summarizes previous observations of lead colloids originating from the corrosion of drinking water distribution system and premises plumbing components and evaluates the use of colloidal analysis as a diagnostic tool. Despite the challenges and need for further research, colloidal analysis is a useful tool to inform better lead mitigation strategies.

2.2. Introduction

Lead exposure *via* drinking water is a significant public health concern (Levallois et al., 2014). In drinking water, lead service lines are the dominant source of lead (Trueman et al., 2016), while brass fixtures and fittings, solders, goosenecks, and galvanized steel pipes represent other potential sources (Clark et al., 2015). Colloids—particles between 0.001 and 1 μm in diameter (Nic et al., 2019) have been an underestimated source of lead. However, there is emerging recognition of their importance. For example, Santucci & Scully (2020) highlighted persistent challenges of addressing lead in drinking water while advocating for a renewed commitment to corrosion science and engineering. The authors acknowledged the formation and mobility of colloidal lead but were unable to quantify its presence and concentration using known thermodynamic models. The occurrence of lead colloids in drinking water represents a critical

gap in our efforts to control lead at the tap.

Despite evidence of colloidal lead in drinking water contributing to regulatory exceedances (de Mora et al., 1987; Lytle, Schock, et al., 2020; Trueman et al., 2019b), sampling may fail to accurately quantify colloids. Neither regulatory sampling protocols nor common analytical methods are designed to quantify colloid-bound metals. Standard corrosion control practices—such as orthophosphate or sodium silicate addition—may also promote lead colloid formation under certain conditions (Aghasadeghi et al., 2021; B. Li, Trueman, Munoz, et al., 2021a; Zhao et al., 2018a). Moreover, recent research has demonstrated that NSF/ANSI-42/53 certified point-of-use (POU) filters may not remove lead-phosphate nanoparticles, which may expose consumers to lead (Doré et al., 2021; Lytle, Schock, et al., 2020; Pan et al., 2021). For example, a study in Newark, New Jersey, reported that water filtered through POUs had high lead concentrations (22–45 µg/L) (Lytle, Schock, et al., 2020). These levels exceeded both the United States Environmental Protection Agency (US EPA) action level (15 µg/L) and the 2015 NSF/ANSI-53 certification limits (10 µg/L)—later lowered to 5 µg/L in 2019—in three of the four homes sampled (NSF International, 2015, 2019; US EPA, 2010). The same study found lead-phosphate nanoparticles were prevalent in those samples. This work highlights that POU removal may fail, under specific water qualities, to effectively reduce total lead concentrations below certification requirements when lead colloids are present in the water. Effective mitigation of lead exposure at the tap may require a comprehensive understanding of both the prevalence and formation of colloids in drinking water systems.

Colloidal lead may occur as a result of the dispersion of lead corrosion products, partitioning of dissolved lead to other colloids (de Mora et al., 1987), or nucleation in the bulk water (Dai et al., 2018). For example, lead has been associated with both iron and natural organic matter (NOM) in tap water samples (de Mora et al., 1987). Additionally, colloidal matter rich in lead may detach from lead corrosion scale or other deposits in distribution systems (McFadden et al., 2011; L. Xie & Giammar, 2007). However, lead may not always precipitate on pipe surfaces, but rather in solution and remain in the bulk water (Dai et al., 2018), which can be cause for concern as it can be associated with elevated lead concentrations at the tap.

Complementing previous work on the importance of nanoparticulate corrosion by-products to drinking water quality (Westerhoff et al., 2018), this article focuses on the characterization, occurrence, and formation of colloids that contain lead originating from drinking water distribution systems. Specifically, this review critically evaluates (1) size separation and analytical techniques for colloid identification and size characterization; (2) the occurrence of lead colloids in drinking water distribution systems; (3) factors that promote lead colloid formation and mobility; and (4) the use of colloid analysis as a diagnostic tool to determine the causes of elevated lead concentrations in drinking water distribution systems.

2.3. Colloids characterization techniques

This section will briefly mention important characterization methods and techniques that will be referred to throughout the remainder of this article (Table 1). The most important parameters for characterizing colloids include size, shape, crystalline phase, charge, and elemental composition. Understanding the interaction between lead with organic or inorganic

constituents in water requires being able to distinguish between different mechanisms such as adsorption of soluble lead or agglomeration of lead colloids. Information on the size, shape, elemental composition, and surface charge is essential for differentiating between interaction mechanisms. For environmental samples, the limit of detection should be lower than the concentration (≤ μg L^{-1}) and cover the size range of particles in water. Since natural colloids may be present in drinking water samples, matrix sensitivity also becomes an important criterion. In addition, if the quantity and diversity of measurements needed are large, then it is important to reduce the amount of sample preparation or duration for each measurement. Therefore, the ideal analytical technique is dependent on the type of analyte, expected concentrations, sample matrix components, and the parameters to be determined. For challenging samples with complex matrixes or many analytical requirements, then a combination of complementary techniques may be used for the full characterization of colloidal suspensions.

Table 1 Comparison of analytical methods for drinking water colloid characterization.

Method	Size range (µm)	Output parameter	Advantages	Disadvantages	References
Membrane filtration	0.01 – 12 µm	• Discrete size range	• Diverse selection of filter pore sizes and membrane materials • Minimal sample preparation requirements • Ease of use	• Size selectivity not completely efficient • High variability in filtrate concentration • Size speciation and recovery may differ by membrane material	(Barkatt et al., 2009; de Mora & Harrison, 1983; Doré et al., 2021; Hulsmann, 1990)
Size-exclusion chromatography (SEC)	0.001 – 1 µm	• Continuous size distribution • Effective diameter	• High resolution over small size range • SEC columns can cover a wide variety of size ranges	• Analyte components can interact with the column material. • Trade-off between resolution and overall size separation range	(Štulík et al., 2003)
Hydrodynamic chromatography (HDC)	0.01 – 1 µm	• Continuous size distribution • Effective diameter	• low sample consumption • HDC columns can cover a wide variety of size ranges	• Low chromatographic resolution • possibility for degradation of very large and fragile macromolecules	(Brewer & Striegel, 2008, 2010; Striegel & Brewer, 2012)
Field-flow fractionation (FFF) 0.001 - 1µm (Flow-FFF) 0.03 -1 µm (Sedimentation-FFF)		• Continuous size distribution • Hydrodynamic radius	• High resolution, continuous analyte separation based on hydrodynamic radius or equivalent spherical diameter • Minimal sample perturbation • Unlike SEC, no interaction with a stationary phase	• Sample dilution, preconcentration, and on-channel concentration can lead to artifacts • Non-uniform density and shape in environmental samples may skew actual size distribution • Particle-wall or particle-membrane interaction may contribute to lower analyte recovery and artifacts	(Baalousha et al., 2011; Dubascoux et al., 2010; Geckeis et al., 2002; Jackson et al., 2005)

Method	Size range (µm)	Output parameter	Advantages	Disadvantages	References
Ultra-centrifugation (UC)	0.005 - 300µm	• Size distribution via gradient separation	• Useful for sample preparation for imaging techniques	• Current analytical UC detectors not appropriate for trace concentrations • The particle under investigation needs to sediment in a reasonable amount of time	(Balnois et al., 2007; Wohlleben, 2012)
Single particle inductively coupled plasma mass spectrometry (spICP-MS)	0.02 – 1 µm	• Particle count • Particle mass • Elemental composition	• Provides size determination and distribution, particle number concentration, and elemental composition of individual particles in a single measurement • Provides a distinction between dissolved and particulate fractions at concentrations down to parts-per-trillion levels	• Provides size estimates using assumptions about compositions, density and a spherical shape, which may not reflect some complex or non-uniform environmental samples	(Mitrano et al., 2012; Montaño et al., 2016; Pace et al., 2012)
Magnetic particle spectroscopy (MPS)		• Particle size	• Primarily useful for superparamagnetic iron oxide particles • Can be used to separate iron colloids with adsorbed metals by size.	• Limited environmental application since not all metal oxides have superparamagnetic properties. • May not be useful for detection of lead colloids	(Barkatt et al., 2009; Senftle et al., 2007; Woodward et al., 2007)

Method	Size range (µm)	Output parameter	Advantages	Disadvantages	References
Dynamic light scattering (DLS)	0.006 – 10 µm	• Bulk size distribution • Hydrodynamic diameter	• Normally used for unimodal particle distributions • Minimal sample preparation •	• Low resolution • Not well suited for low-sample concentrations or large aggregates • Cannot provide information on chemical composition • Inconsistencies in particle surface can affect diffusion and alter the apparent size • Larger particles may block smaller ones, skewing size measurements	(Boyd et al., 2011; Langevin et al., 2018; Stetefeld et al., 2016)
Multi angle light scattering (MALS)	0.001 – 10 µm	• Bulk size distribution • Hydrodynamic diameter	• When combined with separation techniques (i.e. SEC, FFF) or analytical tools (i.e. ICP-MS), MALS allows for molar mass calculation, composition, and characterization of each population in a mixed sample	• Need to assume certain parameters (i.e. refractive index, shape) to calculate size • Cannot provide information on chemical composition •	(Kammer et al., 2005; Moore & Cerasoli, 2017)
Nanotracking analysis (NTA)	0.01 – 2 µm	• Particle count • Hydrodynamic diameter	• Colloids are analyzed in solution. Prevents drying artifacts • Ability to visually size and count individual particles • Can detect individual particles and agglomerates • Provides hydrodynamic diameter	• Does not provide morphology or imaging • Need to assume particle shape	(Boyd et al., 2011; Filipe et al., 2010; Kim et al., 2019)

Method	Size range (µm)	Output parameter	Advantages	Disadvantages	References
Scanning electron microscopy (SEM)	0.01 – 1 µm	• Particle shape • Particle size	• SEM can provide morphology, size, and, if paired with Energy Dispersive X-Ray Spectroscopy (EDS), can provide elemental composition • Minimal sample preparation • Produces 3D image	• Samples need to be conductive to prevent charging. (i.e gold coating) • Sample drying can introduce artifacts • Need to measure individual particles • Analysis and sample preparation time restrict sample size	(Goldstein et al., 2017; Harmon et al., 2020)
Environmental scanning electron microscopy (ESEM)	0.01 – 1 µm	• Particle shape • Particle size	• Minimal sample preparation • wet or insulated samples can be examined • can observe dynamic physiochemical processes in real time	• Need to measure individual particles • Analysis time restricts sample size	(Hülsey et al., 2019)
Transmission electron microscopy (TEM)	0.001 – 1 µm	• Particle shape • Particle size	• No need to coat samples to be conductive • Can provide direct visual information on particle size and shape, and crystal structure and chemical composition if paired with X-ray energy dispersive spectroscopy (X-EDS) • Able to capture nanoparticle images, from which its size can be determined	• Difficult to apply TEM to quantify particles in environmental samples at low concentrations (≤ µg L^{-1}) • Sample drying can introduce artifacts • Need to measure individual particles • Analysis and sample preparation time restrict sample size	(Domingos et al., 2009; Egerton, 2011; Wilkinson et al., 1999)

Method	Size range (µm)	Output parameter	Advantages	Disadvantages	References
Liquid transmission electron microscopy (liquid TEM)	0.01 – 1 µm	• Particle shape • Particle size	• Lower vacuum pressure compared to conventional TEM • Preserved the liquid state of samples • Allows for in-situ sample observation	• Poor resolution	(Daulton et al., 2001; Peckys & de Jonge, 2011)
Atomic force microscopy (AFM)	0.001 – 1 µm	• Particle shape • Particle size • Mechanical and electrical properties	• Provides topographical, mechanical, and electrical properties • Can be operated under the ambient conditions of the sample • Can be used for both conductive and non-conductive samples • relative differences in chemistry can be determined by using chemically modified AFM tips	• Sample preparation is tedious. • Nanoparticles must be strongly adhered to a substrate. • chemical information cannot be directly obtained. • Potential sample and tip damage may skew measurements	(Baalousha & Lead, 2013; Boyd et al., 2011)
X-ray diffraction (XRD)	0.003 – 1 µm	• Crystalline phase • Particle size if crystalline phase is known	• Provides crystalline mineral phase and particle size	• Not always suitable for amorphous particles, disordered crystals, or very small colloids. • Need to assume the colloid mineral phase for particle sizing	(Mourdikoudis et al., 2018; Patterson, 1939)
X-ray absorption (XAS)	0.001 – 1 µm	• Particle composition • Particle size	• Minimal sample preparation • Structural information can be obtained from disordered crystalline samples.	• Requires synchrotron light source for dilute environmental samples	(Alp et al., 1990; Yano & Yachandra, 2009)

2.3.1. Size separation

In environmental samples, colloids are mixed with larger particles, therefore the sample may need to be size fractionated. Common fractionation methods include membrane filtration, size exclusion chromatography (SEC), hydrodynamic chromatography (HDC), field flow fractionation (FFF), and ultracentrifugation (UC). Membranes are used to physically separate particles that are passing through a medium with fixed pore size to provide discrete size fractions (de Mora & Harrison, 1983). With membrane filtration, particles can be separated *via* micro (0.05–10 µm), ultra (0.001–0.05 µm), and nano filtration (0.0005–0.001 µm) (R. Singh & Hankins, 2016). However, size separation by filtration is prone to measurement variability: filter material, imperfections in filter construction, filtration technique, degree of particle agglomeration, adsorption onto the membrane, filter clogging, and water quality can impact analyte recovery, particle size distributions, and reproducibility (de Mora & Harrison, 1983; Doré et al., 2021; Lytle, Formal, et al., 2020).

More specialized methods provide continuous size discrimination *via* the mobility of the particles when exposed to a medium (i.e., column) or external field (Figure 1). In SEC and HDC, smaller, lower molecular mass, colloids diffuse more slowly through the column (Figure 1). By contrast, larger colloids will elute from the column more quickly. The mechanism of retention of the two techniques is different, however: in SEC, retention is due to preferential sampling of the pore volume (Prazeres, 1997), while in HDC it is due to preferential sampling of the streamlines of flow (Striegel & Brewer, 2012). SEC has a limited size separation range and surface adsorption may result in unintended intermolecular interactions of analyte components with the stationary

phase (i.e. column packing material) (Štulík et al., 2003). Unlike SEC, the use of non-porous beads as the stationary phase in HDC considerably reduces interactions with particles but may be less efficient compared to other techniques (Striegel & Brewer, 2012).

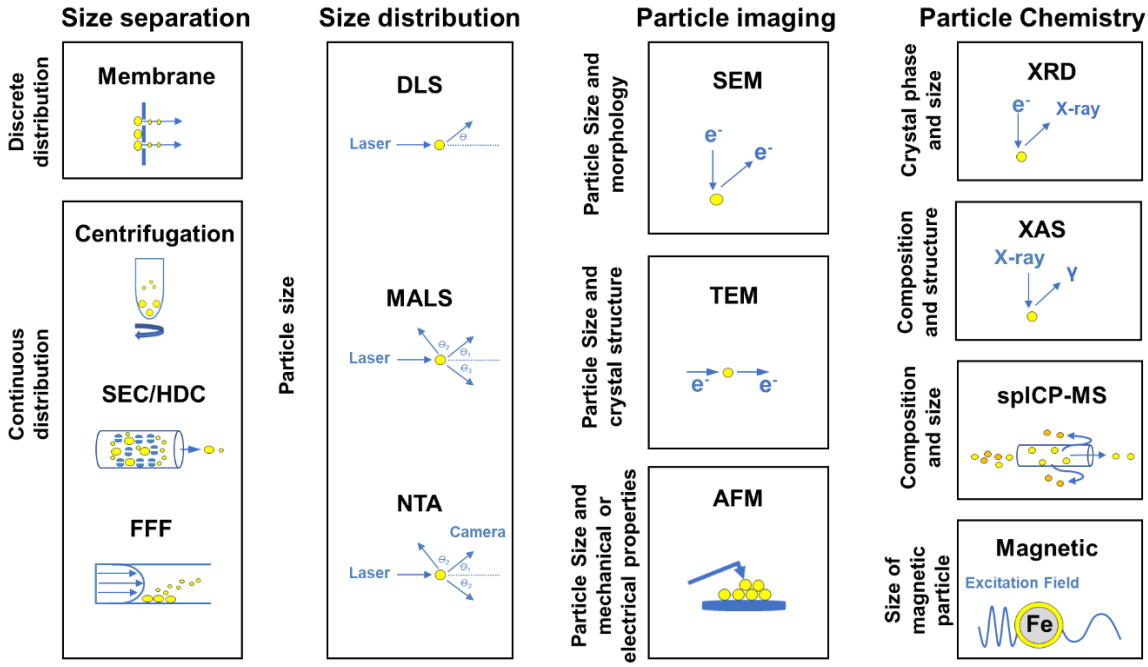

Figure 1 Analytical tools available for colloidal size characterization and their general working principle. SEC: Size exclusion chromatography, HDC: hydrodynamic chromatography, FFF: Field flow fractionation, DLS: Dynamic light scattering, MALS: Multi angle light scattering, NTA: Nanotracking analysis, SEM: Scanning electron microscopy, TEM: Transmission electron microscopy, AFM: Atomic force microscopy, XRD: X-ray diffraction, XAS: X-ray absorption spectroscopy, spICP-MS: Single particle inductively coupled plasma mass spectrometry.

An advantage of field-flow fractionation (FFF) over SEC or HDC is its ability to provide a continuous separation of analyte components over a wider dynamic range without the disadvantage of interaction with a stationary phase. FFF comprises different sub-techniques that utilize the same basic separation principle. A force field (e.g., liquid flow, centrifugal force, temperature, or electric gradients) is applied perpendicular to the main parabolic flow and

separates particles based on their mobility in the field (Giddings, 1993) (Figure 1). One of the major advantages of FFF is the ability to preconcentrate the samples, without any extra sample preparation, during the focusing step (Lyvén et al., 1997).

Ultracentrifugation (UC) is a high-speed, high-volume technique for size fractionation. Since analytical UC detectors are not selective or appropriate for detecting trace amounts of environmental colloids, therefore it is rarely used for environmental samples (Wohlleben, 2012). On the other hand, preparative UCs are useful in sample preparation for particle imaging techniques. For example, gradient separations or depositing aquatic nanoparticles on electron microscopy substrates (Balnois et al., 2007). One obvious limitation of UC is the requirement of the particle under investigation to sediment in a reasonable amount of time.

2.3.2. Size distribution and particle imaging

Size distribution can be accomplished using a variety of techniques such as light scattering, atomic force, and electron microscopy. Basic operations of light scattering methods require little operator training and measure the bulk sample size distribution *in situ*. Light scattering cannot distinguish between individual particles and agglomerates or between particles of different compositions (Langevin et al., 2018), nor provide information on chemical composition. Dynamic light scattering (DLS) obtains a hydrodynamic diameter based on the Brownian diffusion of particles. DLS suffers from low resolution and is susceptible to skewed measurements from large aggregates present in the sample (Stetefeld et al., 2016). Furthermore, measurements may be unreliable when sample concentrations are too low or particles are very small (Hassan et al., 2015). Moreover, particles may not be spherical in

environmental samples (Lytle, Schock, et al., 2020; Trueman, Anaviapik-Soucie, et al., 2019), a limitation that can be addressed by taking multiple measurements at various angles. But this is only possible when the particles are large enough (radius > 10 nm) and not too polydisperse (Langevin et al., 2018).

Static, multi-angle light scattering (MALS) addresses the single measurement angle limitations of DLS by simultaneously measuring the intensity of scattered light at different scattering angles. This technique can provide users with information on the shape and structure of particles. There are some limitations in using MALS, particularly in environmental samples where neither the analyte concentration, the molecular weight, nor the refractive index increment are known (Kammer et al., 2005).

With nanotracking analysis (NTA), a particle under Brownian motion can be measured individually and simultaneously *via* laser light scattering captured by an optical microscope (Kim et al., 2019). Analysis can be performed *in situ* and requires minimal sample preparation.

In some cases, direct visualization of colloids may also be desired, which is impossible in methods previously discussed. Electron microscopes use electrons to produce an image of an object with magnification controlled by electric fields (Figure 1). Two common electron microscopy methods are scanning electron microscopy (SEM) and transmission electron microscopy (TEM). Since conventional SEM and TEM must be operated under a high vacuum, samples are dried. Thus, sample preparation is critical: the drying process may make it difficult to distinguish between agglomeration due to drying and aggregates already present in the

sample or induce the crystallization of salts and structural alteration of colloids (Domingos et al., 2009). In contrast, environmental SEM (ESEM) and liquid TEM allows the *in-situ* observation of the sample (Daulton et al., 2001; Hülsey et al., 2019). However, they suffer from lower resolution due to electron interactions with the liquid layer (Peckys & de Jonge, 2011).

Atomic force microscopy (AFM) is a versatile tool, not only limited to topographical measurements but also able to assess mechanical and electrical material properties. AFM can be operated under the ambient conditions of the liquid sample and topographic images in the sub-nanometer size can be obtained (Baalousha & Lead, 2013). However, analytes have to be fixed on a flat surface for imaging, making sample preparation for environmental samples more tedious (Baalousha & Lead, 2013). Particle measurements via electron microscopy (i.e. TEM, SEM, and ESEM) or AFM are selective enough to avoid matrix effects and can provide particle size and distribution, albeit with some difficulty. Particles in environmental samples may be polydisperse (Lead & Wilkinson, 2007) and, owing to the single-particle measurement property of electron microscopy, characterization of these samples can be tedious. However, AFM and electron microscopy can give a clear and easily understandable picture of structure, which, in turn, can inform us about the chemical behavior of a system.

2.3.3. Particle chemistry

Once size parameters have been obtained, particle chemistry information can determine colloid reactivity or origin in the environment. X-ray diffraction can be used to identify both mineral phase and particle size however, it is not suitable for amorphous materials or very small colloids (Mourdikoudis et al., 2018). A key parameter needed for particle sizing is knowledge of the

colloid's mineral phase. This can be problematic for environmental samples in that not all colloids are crystalline nor are they uniform in size or composition.

X-ray absorption (XAS) is an excellent tool for providing the local structure of the colloid without interference from matrix effects. XAS is uniquely suited to environmental samples due to its limited sample preparation requirements, independence from crystallinity, and ability to preserve the original physical and chemical states of the sample (Yano & Yachandra, 2009). Two XAS techniques applicable for colloidal metals are X-ray absorption fine structure (EXAFS) and X-ray absorption near structure (XANES). EXFAS can identify the chemical state of a colloid even at very low concentrations (B. Singh & Grafe, 2010). Whereas, XANES probes the electron density of states to provide oxidation states and coordination environment (B. Singh & Grafe, 2010). Furthermore, XAS is element-specific and since it's not limited by the state of the sample, can be done on solid or aqueous samples. One major limitation of XAS is that dilute environmental samples are measured in fluorescence mode and require a synchrotron light source (Alp et al., 1990). Due to the limited number of institutions with synchrotron light sources, instrument accessibility becomes challenging.

Single particle inductively coupled plasma mass spectrometry (spICP-MS) simultaneously provides the determinations of size, size distribution, particle number concentration, and elemental composition of colloids in suspension (Montaño et al., 2016). While particle size can be calculated from its mass, these calculations require assumptions about particle density and geometry; particles are generally assumed to be spherical (Pace et al., 2012). Accordingly, spICP-MS can detect lead containing particles but may not distinguish between different particle

compositions (i.e., PbO_2, $PbCO_3$, etc.). In these cases, assumptions about particle geometry or density influences the ability to determine particle size with spICP-MS. Generally, these assumptions are not ideally suited for complex environmental nanoparticle compositions and morphologies and may result in biased particle sizing (Montaño et al., 2016). Nonetheless, there are several advantages of spICP-MS, including its high sensitivity and ability to detect colloids in environmental samples (Mitrano et al., 2012; Pace et al., 2012). Additionally, this method can distinguish between particles of interest from other particles of the same size *via* their elemental composition.

Magnetic particle measurement methods have been used to characterize superparamagnetic nanoparticles; particles having no permanent magnetic dipole (Senftle et al., 2007; Woodward et al., 2007). The moment for each particle fluctuates between different directions at a rate given by the temperature and the applied magnetic field. For superparamagnetic particles, there is no magnetization or agglomeration in the absence of an applied magnetic field (Senftle et al., 2007; Woodward et al., 2007). This method is a good bulk sampling technique that works better with narrow particle size distributions. However, it is limited by the need to assume a particle shape and size distribution range, as well as can be subject to experimental artifacts (e.g. ferromagnetic hysteresis) when attempting to determine quantitative results (Woodward et al., 2007). Its application to environmental samples is limited as the particles need to be superparamagnetic, which is problematic for Pb since they exhibit diamagnetic behavior (Das & Misra, 1972). This method may only be useful for the detection of adsorbed species on magnetic particles like iron oxides.

2.4. Integrating analytical approaches to colloid characterization

Changes in speciation or losses of trace metals during storage present challenges in the study of environmental colloids since environmental samples are not usually analyzed immediately after sampling. Long term storage can produce significant alterations in the chemical composition (Quevauviller & Donard, 1991) or size distribution (Tso et al., 2010) of colloids due to chemical reactions between species, microbial activity, pH, light action, and adsorption to the container (Daye et al., 2019; Tso et al., 2010). There are very few reports on the impacts of sample storage conditions and time on drinking water colloids. Therefore, it is important to consider the influence of these factors with respect to sample storage to get a representative analytical assessment of the sample.

Most often, the characterization of multiple parameters is required to determine the presence, effects, and origins of colloids in drinking water. The combination of membrane filtration with element detection, electron microscopy, and mineral phase identification (i.e. X-ray diffraction) allows for comprehensive identification of important size fractions in drinking water samples and overcomes the inherent limitations of each technique. For example, TEM-XRD can identify colloidal mineral species present, while the total elemental concentrations (i.e. dissolved, colloidal, and particulate) species in each size fraction can be accounted for via ICP-MS. While the drying process in conventional electron microscopy results in artifacts, *in situ* electron microscopy techniques, like liquid TEM or ESEM, allow for the characterization of the sample in its native environment. They can provide unique insights into the fundamental mechanisms,

such as the relationship between surface energy and morphology of a nanoparticle (Chen et al., 2015).

One advantage light scattering techniques have over electron microscopy is that they can be coupled with continuous size distribution separation techniques (i.e. SEC, HDC, and FFF) to provide a quantitative assessment of the particle size directly in the solution phase. Further colloidal characterization can be accomplished by coupling size separation, light scattering, and element detection. For instance, a study on colloidal organic matter from a wastewater treatment plant (WWTP) observed that WWTP effluent organic matter is a primary contributor to total organic matter in urban water systems and that it has similar reactivity and metal complexing abilities as natural organic matter (Worms et al., 2010). To circumvent the non-selective limitation of light scattering, metal binding was measured via FFF-MALS-UV-ICP-MS and further characterization with fluorescence and total organic carbon detectors showed that the effluent was mainly a low aromatic, humic-like fraction.

In cases where sample preparation should be minimal, and where colloids, natural or inorganic, are within the same size range as the target analyte (i.e. Pb), then spICP-MS may be the most suitable. Additionally, this method can distinguish between particles of interest from other particles of the same size *via* their elemental composition and can measure trace concentrations. There is also a clear advantage of spICP-MS over FFF in simultaneously quantifying dissolved from nanoparticulate components, as any dissolved components move through the FFF membrane and cannot be directly quantified (Mitrano et al., 2012). In spICP-MS, dissolved metals contribute to the background and can be quantified by subtracting the

baseline measurement (Mitrano et al., 2012) but matrix effects (ex. high concentrations of organics or dissolved solids) may reduce the instrument sensitivity. Alternatively, size separation coupled with spICP-MS can help overcome the limitations of spICP-MS, specifically the need for assumptions on particle density. Size separation can provide size distribution, mass, and number of particles to complement the particle number concentration and elemental composition provided by spICP-MS. Another key advantage of spICP-MS is its ability to nearly simultaneously capture multiple isotopes (Montaño et al., 2014).

2.5. Occurrence of colloidal lead in drinking water

Over the last three decades, evidence of colloidal lead occurring in drinking water distribution systems has been reported throughout the United States, Canada, and the United Kingdom. This article's review of lead occurrences was limited to field studies to assess the prevalence of colloids and factors associated with their presence in drinking water. One observation was persistent and clear: colloidal lead in the distribution system is prone to be included within the operational definition of soluble lead (<0.45 μm) (Figure 2). Both total lead concentrations (expressed here as mass concentration) and colloidal size distributions (proportional) differed across studies, and this variation may be explained by differences in water quality, sampling method, and type of site sampled (Details provided in Table S1, Supplementary Information).

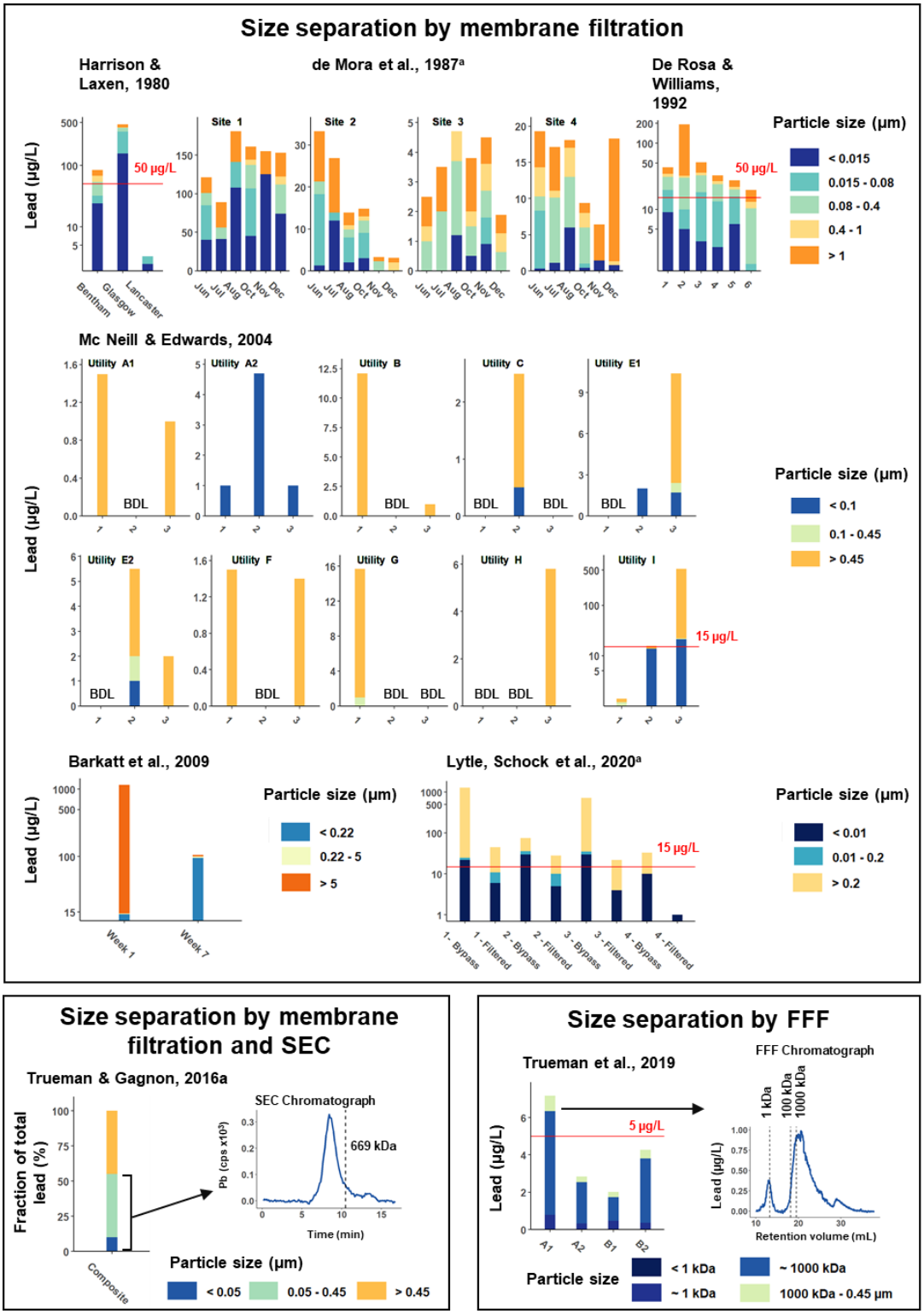

Figure 2 Size fractions of drinking water lead. Horizontal red lines represent the regulatory or recommended maximum lead concentrations depending on the location of the study. Notes: (a) Values estimated from graphs; (b) BDL: Below detection limits.

Early work using various filter pore sizes found evidence of small lead colloids that would have otherwise been classified as soluble. In first draw samples from homes in Bentham and Glasgow (United Kingdom), 37% and 69% of total lead, were between 0.08–0.4 µm, while 29% and 15% were ≤0.015 µm, respectively (Harrison & Laxen, 1980). Similarly, De Rosa and Williams (1992) observed that significant proportions of lead occurred between 0.08–0.4 µm (10–45%) and 0.015–0.08 µm (2–32%), with lead ≤0.015 µm accounting for between 0–21% across all homes sampled after 6-hour stagnation.

Continuous size separation techniques provided better distinction between small colloids and soluble lead species. In random daytime samples from a Northern Canadian community, FFF chromatograms indicated that 8–23 % of total lead was present in the 1 kDa size fraction, which was clearly resolved from dissolved species. An estimated 63–80% total lead was present in the 1000 kDa size fraction (Trueman et al., 2019b). Although lead concentrations were not reported in an SEC analysis of samples from the same community, data presented similar colloidal lead distributions as the FFF samples (Trueman et al., 2019a).

Using a combination of membrane filtration, SEM, TEM, and XRD, Lytle and colleagues (2020) measured particulate lead in homes with elevated lead concentrations passing through POU filters in Newark, NJ, a system with orthophosphate treatment. The findings indicated that the majority of lead was particulate (58–98%), and mostly colloidal in the 0.01–0.2 µm size range (Lytle, Schock, et al., 2020). Moreover, solids analyses revealed most of the colloidal lead was composed of lead (II)-orthophosphate.

When examining drinking water samples from a building with copper piping and lead solder via XRD, Barkatt et al., (2009) observed a significant amount of iron particles—namely magnetite and lepidocrocite, and iron oxides, which effectively adsorbed dissolved lead.

Despite the differences in methods, colloidal size fractions, and proportions of total lead, there are common themes across these studies, highlighting the impacts of iron, NOM, and corrosion control treatment on the occurrence and size distribution of colloidal lead. Further, very few studies determined the chemical species of lead, limiting the ability to identify its source or appropriate treatment. More extensive analysis, other than simple size separation, should be considered to better identify the conditions that promote lead colloid formation and mobility.

2.6. Factors that influence colloidal lead formation and mobility in drinking water distribution systems

The release of colloidal lead is determined by the physical and chemical interactions of lead corrosion by-products with organic and inorganic species in the distribution system. Lead corrosion by-products differ between distribution systems and water qualities. For example, lead service line scale from 22 Midwestern utilities in the US included a variety of minerals. Most had a mixture of amorphous layers rich in iron, manganese, calcium, or phosphorous and lead carbonates or phosphates, while only two featured lead (IV) oxides (Tully et al., 2019a). Figure 3 summarizes factors affecting lead colloid formation and mobility in drinking water distribution systems; a discussion of each factor is provided below.

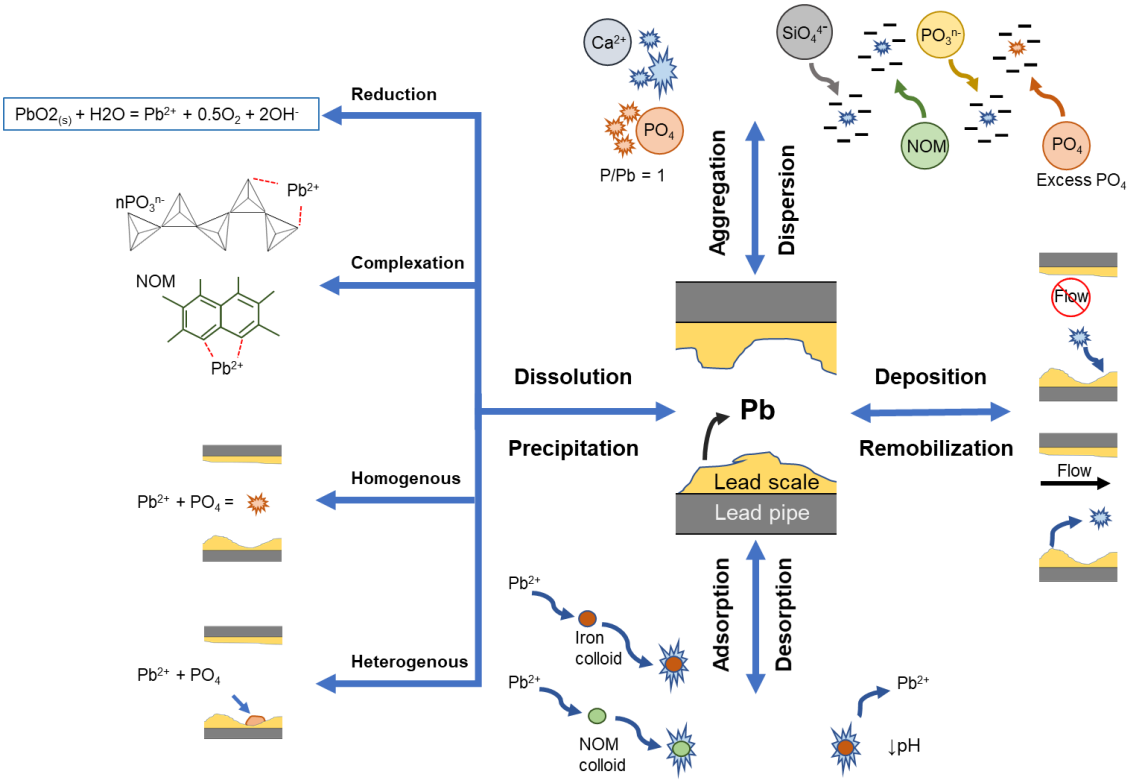

Figure 3 Graphical representation of possible reactions of colloidal lead in drinking water distribution systems.

2.6.1. Natural organic matter increases lead release

Some drinking water utilities rely on source waters where NOM is increasing over time (Anderson et al., 2017). Several surface waters in North America and Europe are experiencing brownification—a change in source-water color, due to climate change, changes in land use, or declining atmospheric acid deposition—which is characteristically accompanied by increased NOM concentrations (Anderson et al., 2021). Changes in source water have implications for treatment and drinking water quality, given the link between NOM in surface waters and lead colloids (≤0.45 µm) (Trueman et al., 2019b). de Mora et al. (1987) noted that total and colloidal lead concentrations decrease with NOM removal (i.e. via coagulation). The same study observed that this effect was particularly pronounced for colloids <0.08 µm in waters with

coagulation (Sites 3 and 4) compared to the water with no NOM removal (Site 1) (Figure 2).

NOM is rich in functional groups that, (1) promote reductive dissolution of lead minerals (Z. Shi & Stone, 2009), (2) complex dissolved lead ions (Christl et al., 2001), (3) retard lead precipitation (Lang & Kaupenjohann, 2003), and (4) stabilize lead bearing colloids (Korshin & Liu, 2019) (Figure 3). NOM is a key driver for the reduction of lead (IV) oxides. This was demonstrated by Dryer and Korshin (2007) and Lin and Valentine (2008), who noted that the amount of lead from dissolving lead (IV) increased with NOM concentrations. Additionally, Lin and Valentine (2008) provided direct evidence of the reductive dissolution of lead by NOM by specifically measuring lead (II) ions released during the reaction via anodic stripping voltammetry. Shi and Stone (2009) explained their results via two distinct NOM fractions: a reductant fraction, responsible for reductive lead (IV) dissolution, and an inhibitory fraction, which prevents reductive lead dissolution. Reductant capacity was hypothesized to be tied to less reactive, nonaromatic NOM moieties, while the inhibitory fraction may adsorb onto active sites, preventing reductant access (Z. Shi & Stone, 2009).

Dissolved lead may bind to NOM colloids, an effect that is positively associated with pH (Christl et al., 2001). As pH increases, NOM is more negatively charged and may readily accumulate lead ions (Christl et al., 2001). While conventional water treatment (i.e., coagulation, settling, etc.) removes the strongest complexing fractions of NOM, metal-binding NOM may remain in treated water (Z. Shi & Stone, 2009). The binding of lead ions to NOM is mainly due to the presence of acidic (e.g., carboxylic and phenolic) functional groups (Christl et al., 2001). Lead ions preferentially interact with phenolic rather than carboxylic groups (Lishtvan et al., 2005).

However, when lead has exhausted all phenolic binding sites, excess lead ions may bind with carboxylic groups as well (Lishtvan et al., 2005).

NOM adsorption may also retard lead precipitation by blocking active crystal sites, inhibiting nucleation, and resulting in smaller particles (Lang & Kaupenjohann, 2003; Zhao et al., 2018a). For instance, inhibited chloropyromorphite precipitation and smaller particle sizes due to NOM blocking active surface sites have been observed, thus preventing crystal growth at pH 5–7 (Lang & Kaupenjohann, 2003). Greater negative surface charge accumulation (Korshin et al., 2005) or steric interference (Mosley et al., 2003) in the presence of NOM may also result in increased metal colloid stability. For instance, colloidal dispersion of Pb oxides by NOM has been observed in laboratory experiments (Korshin & Liu, 2019).

2.6.2. Iron particles transport Lead

Iron particles represent important transport vectors for lead (Deshommes et al., 2010; Q. Shi et al., 2020; Trueman & Gagnon, 2016b). Given the diversity in water qualities (e.g. acidity, redox conditions, temperature, presence of inorganic/organic ligands), the structure and chemistry of iron oxi(hydroxi)des is very rich and a mixture of iron oxide phases at different size fractions can be found (Demangeat et al., 2018). Considerable proportions of total lead (16–93% between 0.015–1 µm) and iron (12–82% between 0.015–1 µm) concentrations have been observed in the same colloidal size range (de Mora et al., 1987; Hulsmann, 1990) in drinking water samples. More recently, Trueman and Gagnon (2016b) observed considerable fractions of lead (45 ± 10%) and iron (40 ± 6%) in drinking water samples in the 0.05–0.45 µm size range, with the universal coelution of lead and iron in SEC chromatograms. Another study (Barkatt et al., 2009) with

different premises plumbing—a 90-year old building with copper piping, supplied by a cast iron main—reported that tap water had a significant concentration of iron particles associated with lead and copper.

It has been proposed that dissolved lead adsorbs onto suspended iron from upstream iron corrosion and may deposit onto pipe scale or be transported through to the tap (Deshommes et al., 2010; Trueman & Gagnon, 2016b). Moreover, particles rich in both iron and lead can detach from lead service line scale (Masters & Edwards, 2015; McFadden et al., 2011) (Figure 3). Lead ions can bind directly to the surface (inner sphere) or within a hydration shell (outer sphere) of iron oxides (Bargar et al., 1997; Glover et al., 2002). Inner sphere complexes are generally stronger and less reversible than adsorption via ion exchange (outer sphere). The adsorption of lead ions onto iron oxide surfaces is strongly dependent on pH (Q. Shi et al., 2020; Trivedi et al., 2003; L. Xie & Giammar, 2007) and can be explained as surface complex formations with deprotonated [-OH] groups (Leung & Criscenti, 2017).

At pH >8, more iron functional groups are deprotonated, and lead binding at deprotonated sites is more energetically favorable and provides stronger electrostatic interactions (Leung & Criscenti, 2017). However, the precipitation of non-adsorbing lead species may decrease this effect (Ostergren et al., 2000). Although lead generally hydrolyzes above pH 7, its high electronegativity allows for the formation of covalent bonds with oxygen atoms on iron oxide surfaces even at low pH (Glover et al., 2002). At pH >7, dissolved lead carbonate complexes may inhibit lead ion adsorption onto iron oxides (Ostergren et al., 2000). Moreover, the aggregation of iron oxides at higher pH may result in fewer available adsorption sites (Trivedi et al., 2003).

Lead sorption to iron oxides may be further enhanced when ligands such as chloride, sulfate, and phosphate are present (Elzinga et al., 2001; Q. Shi et al., 2020; Trivedi et al., 2003; Weesner & Bleam, 1998). For instance, phosphate used in corrosion control may increase lead adsorption through two mechanisms: Lead may form ternary complexes with phosphate on iron oxides (Q. Shi et al., 2020), and phosphate adsorption onto iron oxides may reduce their surface charge and increase their affinity for positively charged lead ions (L. Xie & Giammar, 2007). Lead-phosphate phases may also form if lead binds directly to isolated phosphate present on iron oxides (Weesner & Bleam, 1998). Alternatively, negatively charged lead phosphate particles may adsorb onto positively charged iron oxides (Q. Shi et al., 2020). Adsorbed lead phosphate particles may slowly dissolve, with free lead ions being re-adsorbed through the formation of surface ternary complexes (Q. Shi et al., 2020). Similar interactions between lead, iron oxides, and sulfate have been reported (Elzinga et al., 2001). Conditions that favor increased adsorption of lead to suspended colloidal iron may result in increased lead concentrations at the tap.

2.6.3. Nuances of orthophosphate corrosion control

Orthophosphate is widely considered the most effective corrosion control treatment for reducing lead corrosion (Dodrill & Edwards, 1995). Its addition is intended to form a layer of insoluble lead-phosphate mineral on the pipe (Schock, 1989). However, lead phosphates may, instead, precipitate in solution (homogeneous nucleation) and be transported with flow (Dai et al., 2018) (Figure 3), increasing colloidal lead mobility (Y. Xie & Giammar, 2011). Zhao et al (2018) argued that elevated total lead concentrations observed post phosphate addition can be attributed to the formation and stability of colloidal lead phosphates in solution. Although the slow formation of lead phosphate minerals on the pipe surface occurs, the total lead

concentration may be dominated by colloids.

Orthophosphate can stabilize lead phosphate colloids by imparting a negative surface charge (Figure 3), keeping them suspended (B. Li, Trueman, Locsin, et al., 2021a; Zhao et al., 2018a). Waters with low hardness (<50 mg $CaCO_3$/L) may have optimal conditions for the formation of stable colloidal lead phosphate (Pan et al., 2021). However, high ionic strength, calcium (Ca), and magnesium have been observed to counteract the dispersion effect (Dai et al., 2018; Pan et al., 2021; Zhao et al., 2018a), promoting aggregation and possibly reducing colloidal lead mobility through deposition.

While traveling through the distribution system, concentrations of phosphate in the bulk water may decrease due to the formation of phosphate containing solids (Bae et al., 2020). Other metal ions (e.g. Ca) may compete with lead for phosphate (Bae et al., 2020). If initial phosphate concentrations are too low or are depleted below a critical level, other lead minerals, potentially those with higher solubility, like lead carbonates, may dominate lead release (Y. Xie & Giammar, 2011).

2.6.4. Complexation and dispersion by sequestrants

Polyphosphates and blended phosphates (a combination of ortho- and polyphosphates) are generally used to sequester iron and manganese by binding the metals, preventing precipitation, or by aiding in dispersion. However, polyphosphate may significantly increase lead release by forming soluble lead complexes (T. R. Holm & Shock, 1991a; Trueman et al., 2018a) or stabilizing lead particles by imparting negative surface charge over a wide pH range (7–9) (B.

Li, Trueman, Locsin, et al., 2021a). Polyphosphate has been shown to influence the size distributions of colloidal metals: iron and lead were observed at different sizes in two distribution systems, one with high and another with negligible residual polyphosphate, respectively (Trueman et al., 2018a). With the high polyphosphate residual, lead and phosphorous were strongly associated at a low apparent molecular weight (<1.5 kDa) which was attributed to the complexation of lead by polyphosphate (Trueman et al., 2018a). In contrast, lead, iron, and trace phosphorous in the low polyphosphate residual system were strongly associated at a higher apparent molecular weight (>669 kDa), indicative of lead adsorbing onto iron colloids, perhaps stabilized by phosphate (Trueman et al., 2018a). Polyphosphates chelating ability is strongly dependent on its structural properties. In regards to complexation, linear are more effective compared to cyclic polyphosphates (Miyahima et al., 1981; Van Wazer & Callis, 1958a). The difference in lead complexation behavior can be attributed to two mechanisms: First, linear polyphosphates can sterically conform around lead ions or colloids, the structure of cyclic polyphosphates inhibits this deformation (Lambert & Watters, 1957). Secondly, linear polyphosphates can form partial covalent bonds with lead whereas cyclic polyphosphates can form weaker electrostatic bonds (Van Wazer & Callis, 1958a).

Silicates are not effective compared with orthophosphate for lead corrosion control (Aghasadeghi et al., 2021; B. Li, Trueman, Locsin, et al., 2021a), but silicate treatment has been linked with lower lead release relative to polyphosphate treatment (Schock et al., 2005). In pilot studies, a substantial concentration of colloids (~ 1000 kDa, 0.008 μm) has been observed in the presence of silicate, with a negligible amount present with orthophosphate (Aghasadeghi et al.,

2021; B. Li, Trueman, Munoz, et al., 2021a). For silicate concentrations found in drinking water conditions, rapid and complete depolymerization occurs resulting in the dominance of monomeric species ($Si(OH)_4$ and $HSiO_3^-$) (Iler, 1979) that imparts a significant negative surface charge on lead particles (B. Li, Trueman, Locsin, et al., 2021a). The depolymerization and its dispersion effect is expected to be greater as pH increases (Iler, 1979).

The sequestering capacity of polyphosphates and silicates can also impact iron related colloidal lead mobility. Information on how phosphates and silicates can stabilize iron oxides in the colloidal size range can be found elsewhere (B. Li et al., 2019; Lytle & Snoeyink, 2002a). Notably, phosphates and silicates reduce the size of iron colloids and inhibit their crystallization (B. Li et al., 2019). Increased adsorptive capacity and surface charge density of smaller colloids or amorphous iron have been reported in other studies (Furusawa et al., 1992; Xu et al., 2006; H. Zhang et al., 1999). For instance, partitioning of lead ions to silicate-stabilized colloidal iron or the dispersion of lead directly from corrosion scale may increase lead release (B. Li, Trueman, Munoz, et al., 2021a).

2.6.5. Effects of flow rate and ionic strength

Once suspended, the settling behavior of lead particles or lead containing colloids are partly dependent on solution ionic strength (Napper, 1970) and hydraulic considerations (i.e., flow rates, stagnation) (Abokifa & Biswas, 2017; Clark et al., 2015; Doré et al., 2019).

The impact of ionic strength can be described by DVLO theory. The thickness of the diffuse double layer of a colloid determines its dispersivity. The effective thickness of the double layer is

directly proportional to the dielectric constant of the solution and zetapotential of the colloid but is inversely proportional to the surface charge density. Consequently, the double layer is thicker when solutions are dilute, resulting in higher colloidal dispersion. Since the dielectric constant is inversely proportional to the electrolyte concentration, the double layer thickness decreases with increasing ionic strength (Napper, 1970). Since most of the studies in the preceding section were carried out in soft waters, the colloidal concentrations can be partly explained by their dispersion due to low ionic strength. In water with higher ionic strength, groundwater for instance, colloidal dispersion would be expected to be lower, allowing more colloids to settle out.

While the release of particulate (≥ 0.45 µm) compared to dissolved lead can depend on consumer water use patterns, the effect of flow on colloidal Pb is unknown. However, a comparison between particulate and dissolved lead release may provide some idea of colloidal lead mobility. If lead release is controlled by dissolution, lead concentrations should decrease as flow through the service line increases due to lower contact time (P. Cardew, 2009). But particulate lead tends to increase with higher flow rates. Particulate release from flow conditions can be attributed to shear stress, which is strongly dependent on the velocity and acceleration of flow (Zidouh, 2009). Varying water demands in homes can create regular shear stress events in lead service lines which would mobilize lead (Cartier et al., 2012; Clark et al., 2015; Deshommes et al., 2010).

2.6.6. Variability from sampling methods

Other factors that influence colloidal lead measurements at the tap include temporal variability

and hydraulic factors (i.e. stagnation time, flow rates). Regarding the former, variations in both colloidal lead size distributions and total lead concentrations from the same sites varied temporally in studies reviewed (Figure 2). For instance, in Scotland, 30-minute stagnation samples taken from Site 1, supplied with untreated water (pH = 7.4 ± 0.2), in June (121 μg/L) were dominated by lead ≤0.4 μm (83%) (de Mora et al., 1987). By contrast, samples taken in November had higher total lead concentrations (155 μg/L), a majority of which were ≤0.015 μm (81%). Additionally, random daytime samples taken from the same sites on different days exhibited day-to-day variations (Trueman, Anaviapik-Soucie, et al., 2019). Further evidence of temporal variation has been found in other work (Barkatt et al., 2009), but in that study, the effects are more difficult to extract from those of varied stagnation time. Barkatt and colleagues (2009) found first draw samples taken after months-long stagnation presented extreme lead concentrations that were predominantly (98.8%) in the large particulate fraction (>5 μm), whereas samples taken in the same building after a shorter, week-long stagnation were mostly present in the ≤0.22 μm size fraction (90.1%). The variability of lead concentrations and size distribution between studies and within sites may also be a result of the sampling method used.

Long stagnation sampling (i.e. 6-hour stagnant) has been used to approximate maximum lead exposure by allowing more time for dissolving lead to reach soluble equilibrium concentrations with stagnant bulk water (Lytle et al., 2021; Riblet et al., 2019). However, stagnant bulk water may facilitate the settling of larger inorganic colloids (Abokifa & Biswas, 2017). Random daytime and 30-minute stagnation sampling have been used to approximate average consumer exposure to lead. However, the lack of fixed stagnation time inherent in random daytime sampling may

produce higher variability in total lead concentrations (Cartier et al., 2011). Currently, there is no clear understanding of the effect of sampling protocol on colloidal lead measurements making meaningful comparisons between studies complicated.

2.7. Colloid characterization provides practical guidance for drinking water providers

When lead concentrations exceed maximum acceptable concentrations or action levels, researchers and utilities often seek to determine the cause. Scale analysis—examination of the corrosion by-products on a harvested pipe—has been used to identify how corrosion control treatment (Wasserstrom et al., 2017a) and other water quality parameters (Tully et al., 2019a) interact with existing scale. Colloidal analysis could be used analogously, or complementarily, to identify factors associated with elevated lead concentrations at the tap.

Colloidal analysis may require determination of both size distribution and elemental composition, but it can provide practical guidance to better target appropriate mitigation measures. For example, colloidal analysis can reveal whether lead is associated with NOM or iron particles, or how the existing corrosion control strategy is functioning. The diagnostic capability of colloidal analysis can reduce the need for time-intensive, complicated, and expensive experimental tests, such as pipe loop studies. This type of analysis can aid in determining the cause and prevalence of the colloidal fraction, and ultimately minimize consumers' exposure to lead. Some examples of researchers using different characterization techniques to study colloids in drinking water samples are reviewed in more detail below. To date, these studies (de Mora et al., 1987; Gora et al., 2020; Lytle, Schock, et al., 2020; Trueman,

Anaviapik-Soucie, et al., 2019; Trueman et al., 2017; Trueman & Gagnon, 2016b) have been conducted by academics or researchers to inform utilities or small systems, rather than directly conducted by utilities themselves.

2.7.1. Membrane filtration identifies key water quality characteristics: NOM and pH

Although simple, membrane filtration can be a potent tool in identifying the impact of water quality characteristics on colloidal lead release. Using membrane filtration, de Mora and colleagues (1987) reported that lead colloid occurrence was markedly different between five single family homes, supplied by the same source water but serviced by different water treatments: NOM removal *via* slow sand filtration or coagulation, or corrosion control *via* pH adjustment. Generally, treatment improved both total and colloidal lead concentrations, but the effect was particularly pronounced for waters with both NOM removal and pH adjustment (pH ~ 9) (Sites 3 and 4).

2.7.2. SEC-ICP-MS/UV identifies lead mobility due to colloidal iron

Size separation via SEC or FFF paired with element detection (e.g. ICP-MS) and UV spectroscopy are effective methods for examining colloid-lead interactions. SEC paired with UV detection (254 nm) along with ICP-MS was used to identify lead and iron in a common size fraction in >6-hour stagnant samples collected at houses in Halifax, Nova Scotia (Trueman & Gagnon, 2016a). A total of 23 sites were sampled and analyzed with SEC-ICP-MS, with 8 of these sites also being analyzed with SEC-UV. Trueman and Gagnon (2016) found a sizable fraction of iron and lead eluted with NOM in a single colloidal fraction. This study provided evidence that lead mobility was due to adsorption to mobile iron colloids. In a subsequent study further examining the role

of iron corrosion on lead release, Trueman et al. (2017) observed increased lead release associated with greater iron corrosion from unlined cast iron compared to cement-lined iron mains. The implication of these findings highlighted the importance of minimizing iron corrosion as a mitigation strategy for lead release.

2.7.3. FFF analysis reveals elevated lead linked to corrosive source water

Determining factors affecting lead release may be crucial in formulating a mitigation strategy, particularly for small or remote communities with limited resources. For instance, FFF coupled with ICP-MS and UV detection was used in a remote Arctic community to demonstrate the link between high organic carbon, iron, and manganese concentrations in source water and high lead and copper concentrations in tap water (Gora et al., 2020; Trueman, Anaviapik-Soucie, et al., 2019). Drinking water for the Hamlet of Pond Inlet (Nunavut, Canada) is drawn from a surface water reservoir, dosed with sodium hypochlorite, and transported directly to consumers via water trucks. No additional water treatment is provided, and distributed water is stored in indoor cisterns until it is used. Sequential sampling in the community identified that lead occurrence is localized and building specific. TEM micrographs determined that colloidal matter was in the 0.05–0.2 µm size range. FFF-ICP-MS-UV analysis on random daytime samples from three buildings discovered that supplied water in Pond Inlet is conducive to the corrosion of premise plumbing components and metals transport to the tap. Drinking water in Pond Inlet is abundant in NOM, iron, and manganese, and colloidal fractions of these analytes were associated with the occurrence of colloidal lead (Gora et al., 2020; Trueman, Anaviapik-Soucie, et al., 2019).

2.7.4. Membrane filtration, SEM, TEM, and XRD find lead-phosphate nanoparticles

Colloidal analysis can evaluate and diagnose problems with a corrosion control program, such as was the case with Newark, NJ. After switching to orthophosphate treatment, high lead concentrations were found in tap water filtered through NSF/ANSI-42/53 certified POU filters (Lytle, Schock, et al., 2020) Membrane filtration, SEM, TEM, and XRD were used to attribute the source of elevated lead concentrations in filtered water to lead-phosphate nanoparticles. Two membrane sizes were used to further separate filtered water into small colloidal matter (≤0.2 µm) and soluble lead (≤30 kDa, ~ 0.001 µm). Membrane filtered samples paired with ICP-MS provided both colloid concentrations and size distributions. SEM and TEM, coupled with EDS, were used to both confirm size measurements as well as provide other physical characteristics (e.g. shape and crystal structure). In certain cases, colloids were too small to identify their crystalline structure using SEM or TEM. To overcome this, XRD was used to identify lead-phosphate particles retained on 0.2 µm membranes. In combination, membrane filtration, SEM, TEM, and XRD determined the prevalence, size, and structure of colloidal lead passing through the POU device.

2.8. The case for colloidal analysis as a diagnostic tool

The use of colloid characterization was useful, in these cases, for three reasons: First, the identification of sources and causes of colloidal lead using routine water sampling procedures can help large, small, and remote utilities better target their corrosion control strategies without the need for costly experimental set-ups. Secondly, evidence of lead adsorbing onto

iron colloids can direct utilities to reducing iron corrosion by-product release as a strategy to minimize lead at the tap; likewise, evidence of lead binding to NOM might highlight treatment process improvements to minimize lead release. Finally, when lead mitigation strategies are failing, colloid characterization can be used to identify unintended consequences of corrosion control treatment, such as the formation of lead-phosphate nano-particles (Lytle, Schock, et al., 2020) or the complexation of lead by polyphosphate (Trueman et al., 2018a).

2.9. Conclusion

The evidence of lead colloids in tap water dates back to the work of Hulsmann and colleagues (1980), and despite relatively little research attention for decades, the landscape is changing. Newark, NJ represents a prominent case study on the role of lead nanoparticles in lead exceedances at the tap (Lytle, Schock, et al., 2020), but a growing body of work highlights the importance of these small colloids from source to tap. Colloidal lead and other metals have been measured in tap waters (Gora et al., 2020; Lytle, Schock, et al., 2020; Trueman, Anaviapik-Soucie, et al., 2019; Trueman, Gregory, et al., 2019). Given their link with elevated total lead concentrations, and the challenges of controlling their formation and mobility, the presence of lead colloids poses potentially significant public health concerns. Lead colloids can occur in different size ranges and concentrations and even differ between sampling events from the same sites. Moreover, under specific water qualities, colloids have been shown to pass POU filters, such as NSF/ANSI-42/53 certified POU filters (Lytle, Schock, et al., 2020), which are typically viewed as an effective mitigation strategy when elevated lead concentrations are present at the tap.

Despite the growing interest, colloids have been underestimated in conventional drinking water monitoring, where metals are operationally defined as soluble or particulate based on their ability to pass through a 0.45 µm membrane filter (Baird, 2017; US EPA, 1994a, 1994b). However, field studies show that colloidal lead exists in size fractions smaller than ≤0.45 µm and can represent a significant proportion of the total concentration (Figure 2). This highlights a critical shortcoming of this operational definition: the potential to misclassify colloidal or nanoparticulate lead and other contaminants as soluble. Here, the issue is not the lack of distinction during routine monitoring, rather it is the potential to misdiagnose, and thus, mistreat the source of the exceedance. The concern is that the remedial actions taken to reduce soluble lead concentrations (i.e. increased orthophosphate dose) may differ from those used to target colloidal lead (i.e. improved NOM removal, controlling iron oxides), and in some cases could exacerbate the problem.

When lead concentrations exceed regulatory levels, size separation can determine if the increased lead concentrations are caused by soluble, colloidal, or particulate (>0.45 µm) fractions. There are a range of methods available to characterize colloids in drinking water samples. Each of these tools presents its own strengths and limitations—some methods are more accessible and require less specialized training (e.g., filtration) compared to others (i.e. spICP-MS, TEM/SEM, SEC, FFF). These distinctions are important: while more sophisticated analytical techniques present some obvious advantages in research spheres, they may require more capital and operational costs, and may not be suitable or necessary for frequent analysis. Utilities may also be ill-equipped to characterize colloids in their distribution systems under

routine monitoring, but colloidal analysis may be beneficial in some circumstances. A few, well targeted samples paired with colloidal analysis can provide a great deal of information. Nevertheless, advancements in particle detection and characterization will be critical in future research beyond trace metals analysis, including emergent topics such as micro/nano-plastics in source waters and distribution systems.

Finally, a greater understanding of particle formation will ultimately inform water treatment processes and decrease exposure at the tap. To minimize colloidal lead transport and formation in distribution systems, a utility can potentially modify the following water quality parameters/treatments of drinking water: (1) reducing natural organic matter (NOM), (2) controlling iron corrosion, (3) optimizing orthophosphate corrosion control and (4) optimizing the use of sequestrants.

Based on the review presented, there are important gaps in the literature required to advance our understanding, which can broadly be categorized into questions related to formation and water quality, and exposure prevention and monitoring. The former include: (1) determining what water quality conditions are favorable to colloidal lead formation, and (2) understanding the role of NOM in lead release. Whereas the latter involves, (3) how colloidal lead in drinking water can be controlled if existing POUs fail, (4) determining what are the appropriate sampling methods and types of samples needed to identify colloids. Finally, another important research area will be improving predictive capabilities for lead colloid formation.

3. Chapter 3 Potential regulatory implications of Health Canada's new lead guideline

This chapter is reprinted with permission from the following:

Locsin, J. A., Trueman, B. F., Serracin-Pitti, D., Stanton, G. M., & Gagnon, G. A. (2020). Potential regulatory implications of Health Canada's new lead guideline. *AWWA Water Science*, 2(4), e1182.

J.A.L coordinated data collection, analyzed the data, wrote the paper, and prepared the figures.

3.1. Abstract

Health Canada's guideline for lead in drinking water was updated in March 2019. Two new sampling protocols were introduced — random daytime and 30-minute stagnation sampling — and the maximum acceptable concentration (MAC) of lead in drinking water was decreased from 10 to 5 μg/L. This study examined the possible impacts that changes in guideline might have on water utilities in Canada. A lead monitoring survey of seven drinking water distribution systems was conducted using the random daytime and 30-minute stagnation protocols. Random daytime sampling captured an estimated 45% more lead than 30-minute stagnation sampling. However, both protocols yielded samples above the new MAC: 7.5% and 5.4% of random daytime and 30-minute stagnation samples exceeded it. These data indicate that some

drinking water providers — especially those supplying systems with legacy lead plumbing — may have difficulty achieving 100% compliance with the new guideline.

3.2. Introduction

Drinking water can be a significant source of lead exposure (Triantafyllidou & Edwards, 2012). It is usually lead-free upon leaving the water treatment plant, but lead contamination may occur through contact with lead service lines (LSLs) or premises plumbing components such as lead solder and brass or bronze fixtures, fittings and joints (Elfland et al., 2010). While many water utilities use corrosion inhibitors to control lead in drinking water, lead release can still be a problem in homes with lead plumbing components (Cardew, 2003; Hayes et al., 2008) Water characteristics (e.g. pH, dissolved inorganic carbon (Schock, 1989), temperature (Masters, Welter, et al., 2016), orthophosphate concentration (Noel et al., 2014), the age of materials (Schock & Lemieux, 2010), the duration of stagnation (Cartier et al., 2012) , and consumer behavior (Del Toral et al., 2013) affect lead leaching into drinking water.

In light of the health risks linked to lead exposure, Health Canada has updated its guidance on lead in drinking water (Health Canada, 2019a). The new guidelines reduce the maximum acceptable concentration (MAC) of lead from 10 to 5 μg/L and introduce two new sampling protocols to better estimate lead exposure: random daytime and 30-minute stagnation. The former specifies sample collection during the day without a fixed stagnation time or prior flushing, while the latter specifies that sample collection be preceded by a 5-minute flush of a drinking water outlet and thirty minutes without water use prior to sample collection. This

represents a significant change; Nova Scotia, where this study was conducted, currently regulates based on a 5-minute fully flushed sample and a 10 μg/L MAC (Nova Scotia Environment, 2010). While flushed samples have been previously recommended for compliance monitoring (Health Canada, 1992; Nova Scotia Environment, 2010), they tend to grossly underestimate lead exposure (Baron, 2001; Deshommes et al., 2013; Riblet et al., 2019; van den Hoven, et al., 1999). By contrast, the new sampling methods require a stagnation period, albeit one of unspecified duration in the case of random daytime sampling.

The European commission (European Commission, 2018) has also recommended random daytime or 30-minute stagnation sampling for compliance monitoring, and both protocols provide reasonable estimates of lead exposure(Cardew, 2003; Hayes & Croft, 2012; van den Hoven, et al., 1999). Thirty-minute stagnation sampling may, however, underestimate lead exposure in homes with lead service lines (Riblet et al., 2019). Nevertheless, the 30-minute stagnation period is approximately representative of consumer inter-use stagnation time (Riblet et al., 2019; van den Hoven, et al., 1999). van den Hoven *et al.* (1999) noted that mean inter-use stagnation time is 30 minutes. This was derived from a statistical analysis of water use patterns in the United Kingdom. Riblet *et al.* (2019) found that 68 % of inter-use stagnation times at the kitchen tap were less than 45 minutes and just 15% of those events were less than 15 minutes. For optimizing corrosion control, first draw, 6-hour stagnant sampling is recommended by regulators (Health Canada, 2009; Nova Scotia Environment, 2010), but this method is likely to overestimate lead exposure (Riblet et al., 2019).

This study attempted to predict the impact of the recent reduction in MAC and the change in recommended sampling protocols on regulatory compliance by means of a multi-community monitoring program. Lead occurrence in Nova Scotia was compared against the new MAC using four regulatory sampling protocols — flushed, random daytime, 30-minute stagnation, and 6-hour stagnation — and the implications for future compliance monitoring in Canada are discussed.

3.3. Methods

3.3.1. Lead sampling at the tap

Drinking water samples were collected from 147 homes in seven communities across Nova Scotia. Sample sites were selected by the participating water utilities with emphasis on single family homes with suspected or known lead plumbing. Lead service line locations were confirmed in communities A and B using utility records, but service line or premises plumbing materials data were limited for communities C - G. In order to capture the seasonal maximum lead exposure, samples were collected in the warmer months between May and October of 2018. Six of the seven communities added a phosphate-based inhibitor for corrosion control and free chlorine for disinfection. Community C did not use a phosphate-based inhibitor and used chloramine for disinfection (Table 2). Distributed water pH for all communities fell between 7 and 7.8.

Table 2 Summary of water quality conditions.

Community	Homes Sampled (#)	pH	Corrosion Inhibitor	Disinfectant
A	30	7.3	Orthophosphate (1mg PO_4/L)	Chlorine Gas (1 mg/L)
B	17	7.5	Orthophosphate (1mg PO_4/L)	Chlorine Gas (1 mg/L)
C	10	7.8	None	Chloramine (unknown)
D	31	7.5	Blended phosphate (3mg/L as product)	Chlorine Gas (1.5 mg/L)
E	13	7.6	Blended phosphate (0.4 mg/L as Product)	Chlorine Gas (2.7 mg/L)
F	6	7.5	Blended phosphate (0.6 mg/L as Product)	Chlorine Gas (2.5 mg/L)
G	40	7.2	Blended phosphate (1.75 mg/L as Product)	Chlorine Gas (1.8 mg/L)

Three 1L samples were collected at each site at the maximum achievable flow rate; flushing was also performed at maximum flow. First, a 1L random daytime sample from a kitchen cold water tap was collected during work hours (Mon - Fri, 8 am - 5 pm) and without prior flushing. Afterward, the tap was flushed for 5 minutes and then left undisturbed for 30 minutes; during this time no water use was permitted in any part of the home. After the stagnation period, two sequential 1L samples were collected representing the first 2L drawn from the tap. Taps were

checked for point-of-use filters, and if a filter was present, an alternate tap (e.g. bathroom sink) was selected for sampling. If present, aerators were not removed.

Additional paired 6-hour stagnant and flushed samples were collected in communities A and B from the same drinking water tap within the same week. The presence of LSLs at these sites was confirmed by visual inspection and water utility records. At each site, a 1L sample volume was collected after a minimum 6 hour stagnation period without pre-flushing. The tap was then flushed for 5 minutes and a second 1L, representing the flushed sample, was collected.

Lead samples were sent to an accredited laboratory for analysis. All samples were acidified with concentrated nitric acid (Fischer Chemical, Trace metal grade) (20 mL per litre) in their original containers and held for a minimum of 16 hours at room temperature before metals analysis via inductively coupled plasma mass spectrometry (Perkin Elmer – Nexion 300X) per standard method 3125B(American Public Health Association, American Water Works Association, Water Environment Federation, 2012). The reported detection limit (RDL) for lead was 0.5 μg/L. For data quality assurance, blanks and spiked solutions of known concentrations were measured every 10 samples. In 40 randomly selected homes, aliquots from each of the three acidified sample litres was measured to ensure pH was below 2 prior to storage.

All 1L wide mouth high density polyethylene sample bottles used in this study were first soaked for 24 hours in 2M nitric acid (Fischer Chemical, Certified ACS Plus). Bottles were then rinsed three times with deionized water and once with ultrapure water (18 MΩ-cm, TOC <2 µg/L), and left to dry completely.

3.3.2. Statistical analysis methods

As described in the Health Canada guideline, the two 30-minute stagnation samples were averaged to yield a representative value for comparison with the MAC(Health Canada, 2019a). When one of the two samples were below RDL, the average was calculated by substituting the RDL (0.5 μg/L).

Since a substantial fraction of the data were left-censored (i.e., below the RDL of 0.5 μg/L), sample protocols were compared using the paired-Prentice Wilcoxon test, a non-parametric procedure for comparing matched pairs with censoring, using the R software and contributed package "smwrQW" (De Cicco, 2017; Team, 2013). A Wilcoxon signed rank test was used to compute a difference estimate between the lead concentrations yielded by each sampling protocol.

In communities A and B, lead levels via four sampling protocols were compared using a three-way ANOVA on ranks, with protocol and the presence of LSLs as independent variables and site as a blocking factor (Brownie & Boos, 1994). To account for censored observations, a rank transformation was applied by assigning left-censored values the minimum rank prior to conducting ANOVA (Conover & Iman, 1981). For multiple comparisons of sampling protocols paired by site, adjustments to the p-values that control the family wise error rate (FWER) (S. Holm, 1979) and false discovery rate (FDR) (Hochberg, 1988) were applied.

3.4. Results and Discussion

3.4.1. Lead occurrence across seven communities

To examine lead occurrence and estimate future compliance using the revised Health Canada guideline, statistical estimates and exceedance rates were calculated by protocol (random daytime and 30-minute stagnation sampling) using the full data set (N = 147). Although a large number of homes were sampled, knowledge on lead plumbing was limited: just 16 homes (Community A = 13, Community B = 3) were known to have LSLs, 27 were known not to have LSLs (Community A = 13, Community B = 14), and the remaining 104 had unknown plumbing configurations. Across the full data set, 74 homes yielded lead concentrations below the RDL in all three sample litres. Lead levels for each community can be found in Table 3.

Over the full data set, random daytime (median = 1.85 μg/L, 10^{th} - 90^{th} percentile = <0.5 - 12.1 μg/L) yielded a greater exceedance rate than the 30-minute stagnation protocol (median = 1.05 μg/L, 10^{th} - 90^{th} percentile = <0.5 - 6.35 μg/L): 7.5% and 4.8% of random daytime samples exceeded 5 and 10 µg/L, respectively, compared with 5.4% and 1.4% of 30-minute stagnation samples (Figure 4).

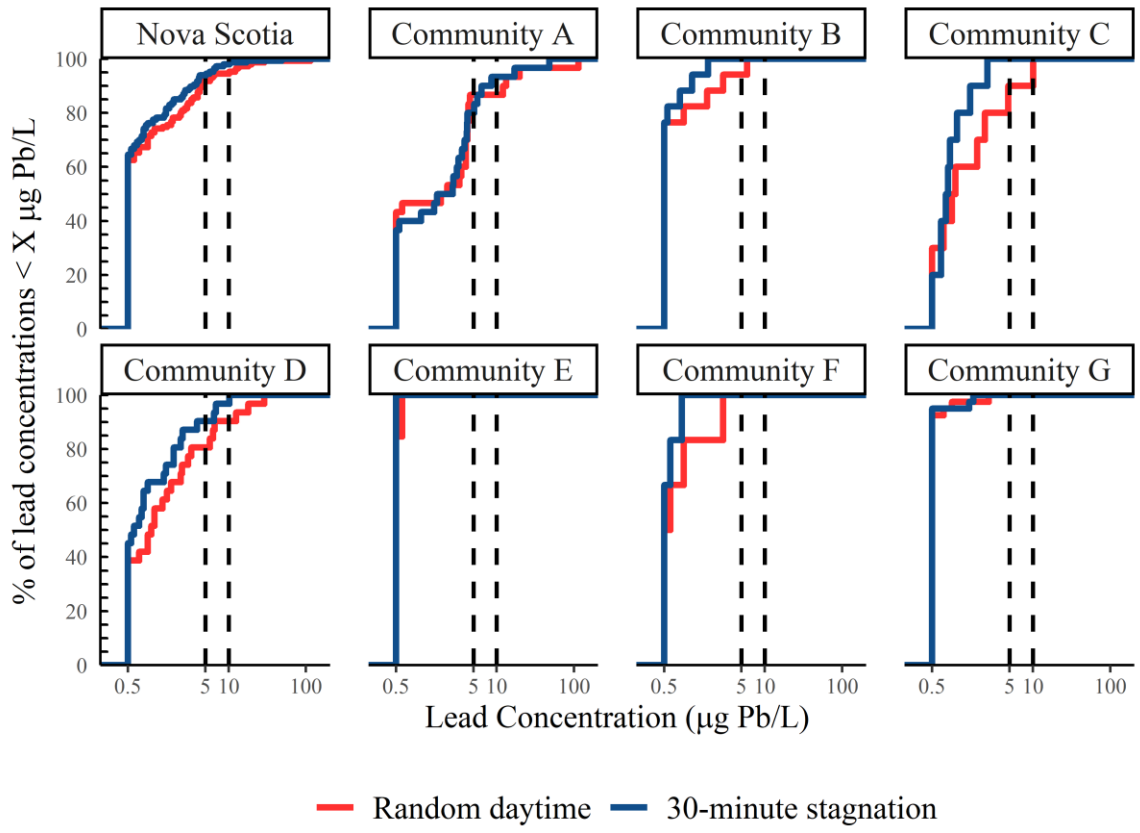

Figure 4 Cumulative distribution of lead concentrations by sampling protocol and community (N = 147). The dotted lines represent the 5 and 10 µg/L guideline MACs.

These rates varied substantially by location: in communities A - D, 0 - 10% of random daytime samples exceeded 10 μg/L and 6 - 17% exceeded 5 μg/L (Table 3). In the same communities, 0 - 3% of 30-minute stagnation samples exceeded 10 μg/L and 0 - 16.7%, exceeded 5 μg/L. No samples collected in communities E - G exceeded 5 μg/L. Moreover, a large proportion of sites in these communities yielded sample sets with lead concentrations below the RDL in all three sample litres, and there was no confirmation of leaded plumbing at any of these sites.

Table 3 Summary of lead sampling results from seven communities in Nova Scotia.

Community	Number of homes	Number of homes with no lead[a]	Random Daytime							30-minute Stagnation						
			Lead concentration (μg/L)					% samples > MAC[b]		Lead concentration (μg/L)					% samples > MAC[b]	
			10th	Median	Mean	90th	Max	5 μg/L	10 μg/L	10th	Median	Mean	90th	Max	5 μg/L	10 μg/L
A	30	4	<0.5	2.1	7.03	12.7	114	10%	10%	<0.5	2.2	4.42	7.45	48.15	16.7%	6.7%
B	17	12	<0.5	<0.5	1.06	2.9	5.9	6%	0%	<0.5	<0.5	0.64	1.15	1.85	0%	0%
C	10	2	<0.5	0.95	2.33	7.45	10.1	20%	10%	<0.5	0.78	0.99	2.08	2.6	0%	0%
D	31	8	<0.5	1	3.41	6.6	28.9	17%	7%	<0.5	0.6	1.66	3.9	10.2	7%	3%
E	13	11	<0.5	<0.5	0.52	0.6	0.6	0%	0%	<0.5	<0.5	0.5	0.5	0.5	0%	0%
F	6	2	<0.5	0.55	0.98	2.9	2.9	0%	0%	<0.5	<0.5	0.58	0.85	0.85	0%	0%
G	40	35	<0.5	<0.5	0.57	0.5	2.7	0%	0%	<0.5	<0.5	0.56	0.5	1.7	0%	0%
Nova Scotia	147	74	<0.5	1.85	5.2	12.1	114	7.5%	4.8%	<0.5	1.05	2.9	6.35	48.15	5.4%	1.4%

[a] Lead concentrations in all sample litres were below reported detection limit (<0.5 μg/L).

[b] Maximum acceptable concentration.

Communities A and B have similar water quality and corrosion control. Higher lead levels in random daytime and 30-minute stagnation samples from community A may be, in part, due to a significant proportion of homes with LSLs (43.3%). In contrast, lower lead levels in community B were likely due to a lower proportion of homes with LSLs (17.6%), with many homes (70.6%) having all samples below RDL (Table 3).

Community C experienced the highest rate of non-compliance across all the communities and sample protocols (Figure 1). This may be due to the lack of corrosion inhibitors used in this system. Lead levels in systems with corrosion control are expected to be much lower than systems without(Cartier et al., 2013). Phosphate addition has been shown to decrease average lead levels by up to 86% (28 to 8.4 μg/L) (Sandvig et al., 2009) and reduce rates of non-compliance by up to 50.3% (City of Toronto, 2018).

Plumbing information on community D was limited. However, three homes with a galvanized steel service line on the private side of the property experienced lead levels above 5 μg/L (random daytime = 17.9, 12.5, 6.3 μg/L, 30-minute = 6.5, 10.2, 6.9 μg/L). The utility could not confirm the material of the service line on the public side. Galvanized steel may serve as a significant source of lead with concentrations reaching 67 μg/L in 6-hour stagnation profile samples (Clark et al., 2015; McFadden et al., 2011; Schock & Oliphant, 1996; Triantafyllidou & Edwards, 2012).

Since lead plumbing information was limited in communities E - G, samples were taken from homes at higher risk of having an LSL (built before 1960 and with no records of LSL replacements). A significant number of homes in communities E (11 of 13) and G (35 of 40) had lead levels below the RDL in all sample volumes. Over both sampling protocols, the majority of samples taken from community F (5 of 6) had lead levels below or close to the RDL, with only one sample exceeding 1 μg/L (via random daytime sampling). This may suggest a low probability of having LSLs at those homes. This along with the use of corrosion control may partly explain the low lead levels from these communities (Table 3).

3.4.2. Comparison of four sampling protocols

The greater propensity for random daytime sampling to yield elevated lead in this study was confirmed by a direct pairwise comparison of the method with 30-minute stagnation sampling. Over the full data set, sites yielding samples (N = 68) with lead above the RDL in at least one litre were used to compare the two protocols.

Random daytime samples captured an estimated 45% more lead than 30-minute stagnation (Paired-Prentice Wilcoxon, N = 68, Z = 0.399, p-value <0.05) (Figure 5). Of the 68 sites,

47 (69.2%) and 13 (19.1%) yielded the highest lead levels via random daytime sampling and the 30-minute stagnation average, respectively, while 8 (11.8%) yielded equivalent levels via the two methods. Higher lead concentrations in random daytime samples may be due to collection, on average, after greater than 30 minutes of stagnation. Differences in stagnation time can cause significant variability in lead levels (e.g. 10-30% difference between 30 minutes and 60

minutes) (Schock, 1989). Stagnation times (no distinction between LSLs and tap) may vary between single occupant (47 minutes) to multi-occupant (18 minutes) homes (Bailey et al., 1986). In Montreal, median stagnation time at the kitchen tap (18 minutes, 90th percentile = 394 minutes) was longer than in the service line (11 minutes, 90th percentile = 72 minutes) with 33% of stagnation events lasting more than 45 minutes (Riblet et al., 2019). Inter-use stagnation time was not measured in this study but is expected to vary in a similar fashion.

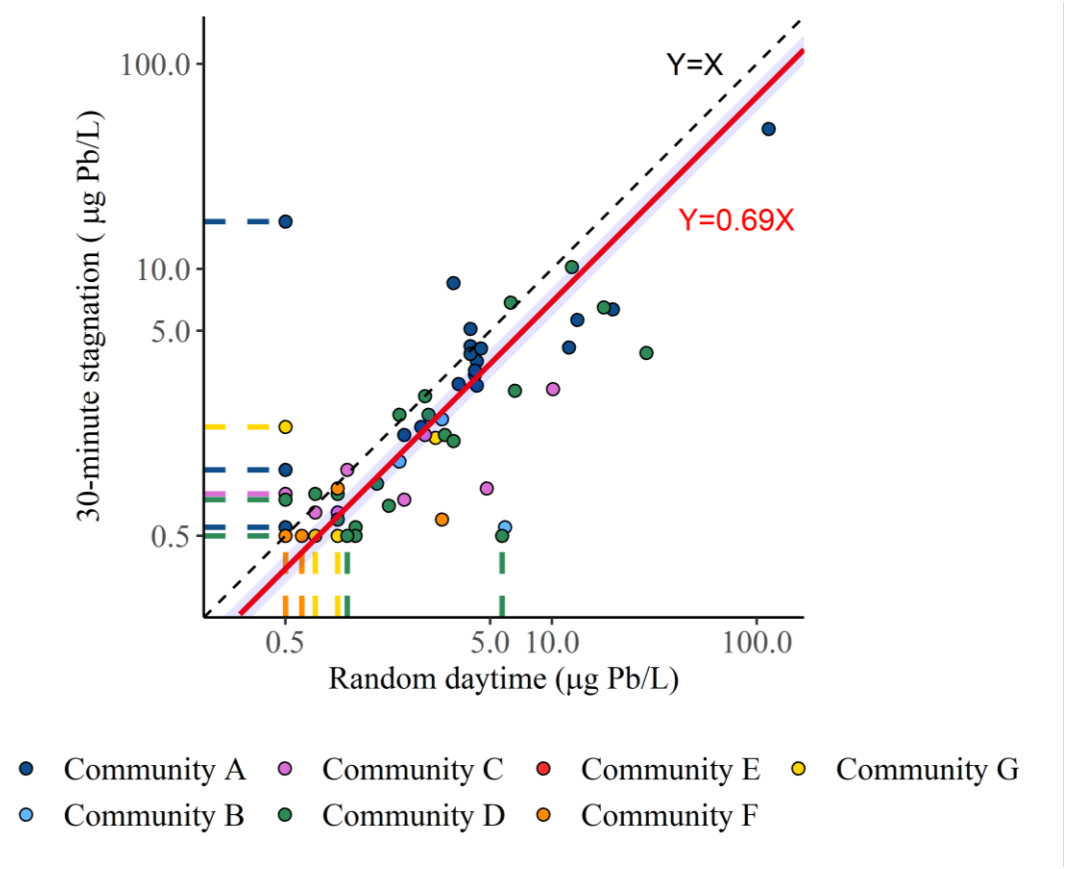

Figure 5 Lead concentrations from random daytime vs the averaged 30-minute stagnation samples separated by community (N = 68 homes). The shaded band represents the 95% confidence interval (0.58 - 0.81) around the difference estimate. Lead concentrations below reporting limit are represented by colored dashed lines.

The tendency of random daytime to yield greater lead levels compared to 30-minute stagnation is consistent with previous studies (Baron, 2001; Hayes et al., 2016; Riblet et al., 2019; van den

Hoven, et al., 1999). Several studies have estimated true exposure by composite proportional sampling, wherein a portion of each volume of water drawn for dietetic consumption is retained for analysis; this protocol captures all the factors influencing average lead intake through drinking water (Riblet et al., 2019; van den Hoven, et al., 1999). Sampling protocols were evaluated against true exposure and yielded similar results. Random daytime was similar (random daytime = composite = 10 μg/L) (Riblet et al., 2019) or overestimated true exposure by up to 27% (slope = 1.27, R^2 = 0.61) (van den Hoven, et al., 1999). In contrast to both the European study (van den Hoven, et al., 1999) and this work, sampling in the Montreal study (Riblet et al., 2019) was carried out by participating homeowners, thus eliminating the issues with possible exaggerated inter-use stagnation times due to sampling during working hours. Conversely, 30-minute stagnation sampling underestimated true lead exposure by 20% (slope = 0.8, R^2 = 0.58) (van den Hoven, et al., 1999) to 25% (mean = 7.9 - 8.8 μg/L) (Riblet et al., 2019).

Random daytime has been found to exceed 10 μg/L more frequently than 30-minute stagnation(Baron, 2001; Hayes et al., 2016). Using random daytime and a modified 30-minute stagnation protocol (4 x 1L average), Hayes *et al.* (2016) found that 15.3% and 13.9% of random daytime and 30-minute stagnation samples exceeded 10 μg/L, respectively. Due to its larger overall volume drawn, the modified 30-minute stagnation profile would be expected to result in much higher lead levels in homes with LSLs compared to the 30-minute stagnation

(2 x 1L average) protocol used in this study. The contribution of LSLs may be seen after the 1st litre resulting in higher lead levels in succeeding litres (Deshommes et al., 2016; Lytle et al., 2019).

To evaluate lead capture via new versus previously-recommended sampling protocols, additional 6-hour stagnation and flushed samples (N = 40, 32.5% LSL) were collected in communities A and B and compared with their paired 30-minute stagnation (2x 1L average) and random daytime samples. Sampling protocol (ANOVA, N = 40, F= 4.704, p-value < 0.05) was a significant predictor of lead concentration. The p-values for multiple comparison tests can be found in Table 4; Lead concentrations were significantly lower in flushed (median = <0.5 μg/L, 10^{th} - 90^{th} percentile = <0.5 - 3.3 μg/L) compared with 6-hour samples (median = 1.05 μg/L, 10^{th} - 90^{th} percentile = <0.5 - 7.6 μg/L) (Paired-Prentice Wilcoxon, N=40, p-value < 0.05) but were similar in flushed compared with random daytime (median = 0.55 μg/L, 10^{th} - 90^{th} percentile = <0.5 - 10.6 μg/L, Paired-Prentice Wilcoxon, N = 40, p-value >0.05) and 30-minute samples (median = 0.55 μg/L, 10^{th} - 90^{th} percentile = <0.5 - 5.37 μg/L, Paired-Prentice Wilcoxon, N = 40, p-value >0.05). In this subset of data, the lead concentrations in 6-hour, 30-minute, and random daytime samples were not significantly different (Paired-Prentice Wilcoxon, N = 40, p-values > 0.05).

Table 4 Comparison of sampling protocols using Paired-Prentice Wilcoxon tests with multiple comparison corrections controlling the family wise error and false discovery rates separately.

Protocol A	**Protocol B**	**p-value$_{FWER}$[a]**	**p-value$_{FDR}$[b]**
30-min	Random daytime	0.423	0.241
Random daytime	Flushed	0.187	0.097
Random daytime	6-hour	0.423	0.241
30-min	Flushed	0.216	0.108
30-min	6-hour	0.193	0.097
Flushed	6-hour	<0.001	<0.001

[a] Family wise error rate
[b] False discovery rate

Six-hour stagnation sampling is used for compliance monitoring in the USA (US EPA, 2010). In both Canada and the USA, it is also used to assess the effectiveness of corrosion control treatment (Health Canada, 2009, p. 200; US EPA, 2010). However, it was not intended to provide estimates of consumer exposure, overestimating true exposure (composite = 10 μg/L) by up to 29% (6-hour = 14 μg/L) (Riblet et al., 2019). Long stagnation times (e.g. > 6 hours) substantially increase particulate (Cartier et al., 2013) and total (Lytle & Schock, 2000) lead release. Lead levels in a 1.6 (5/8) - 1.9 (3/4) cm (inch) diameter lead pipe are estimated to be between 80 - 100% of equilibrium concentrations after a 6-hour stagnation (Kuch & Wagner, 1983). Here, the median lead level via 6-hour stagnation was low; however, some homes encountered up to 150 μg/L. High lead levels have been reported in Brandon, MB (median = 21 μg/L, 90th percentile = 44 μg/L, max = 110 μg/L) (L. Winning, 2015), Winnipeg, MB (median = 7.3 μg/L, 90th percentile = 23 μg/L, max = 35 μg/L) (L. Winning, 2015), and Flint, MI (after orthophosphate addition, median < 1 μg/L, 90th percentile = 9 μg/L, max = 221.1 μg/L) (Pieper et al., 2018).

Lead levels were the lowest in flushed samples with 57.5% of them being below the RDL. All but one (7.6 μg/L) of the samples had lead levels below 5 μg/L. Estimates of lead levels via flushed sampling range from 47% (mean = 5.5 μg/L) (Riblet et al., 2019) to 57% (slope = 0.57, R^2 = 0.29) (van den Hoven, et al., 1999) of true exposure. Flushed samples may also fail to identify at risk homes(Riblet et al., 2019; van den Hoven, et al., 1999). Homes in communities A and B had lead levels above 5 μg/L in random daytime (N = 6, 5.9 - 114 μg/L) and 30-minute stagnation (N = 5, 5.1 - 48.2 μg/L) when paired flushed samples were below 5 μg/L (<0.5 - 4.9 μg/L).

3.4.3. Lead release may be sporadic and unpredictable

Similar to findings by Cartier *et. al.* (2011), the difference between random daytime and 30-minute was not as impactful as the difference in household plumbing. This was confirmed by a one-way ANOVA on ranks with site as the independent variable, wherein the variation among sites was significantly greater than the variation between sampling protocols (p-value < 0.001, N = 68).

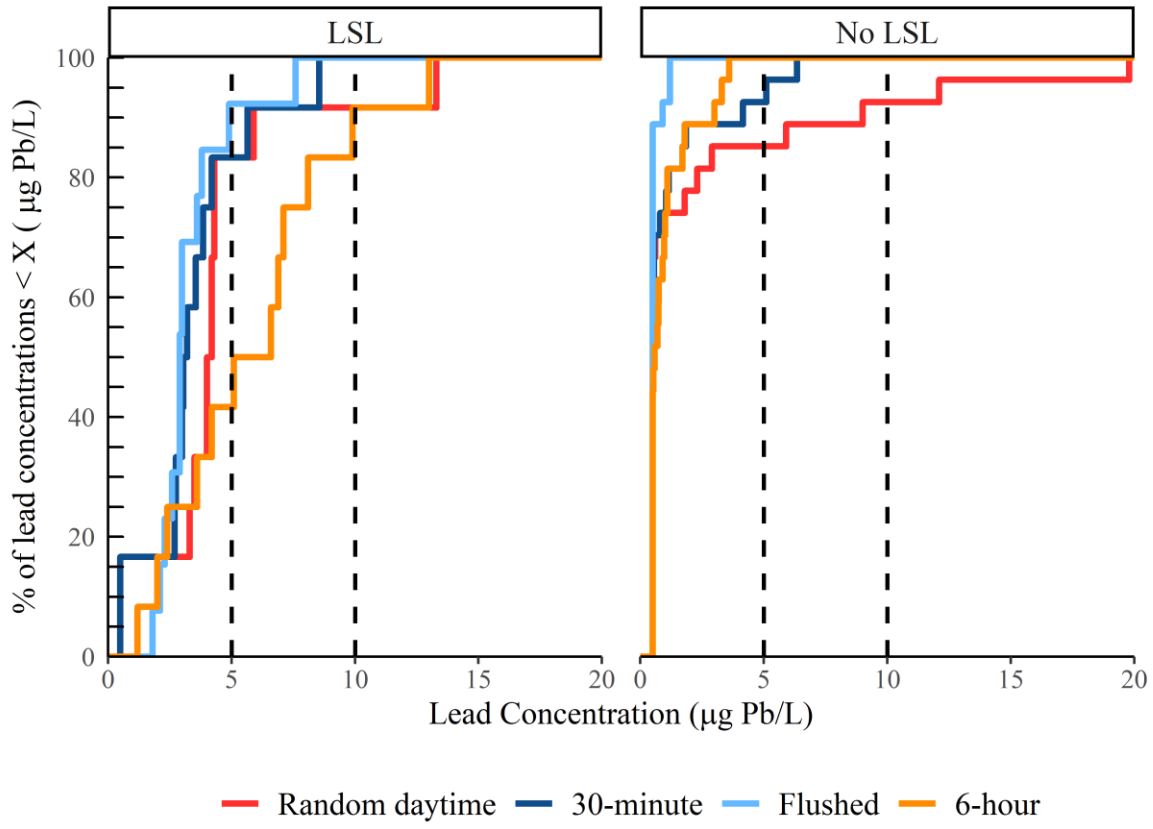

Figure 6 Cumulative distribution of lead concentrations for homes with (N = 13) and without LSLs as a function of sampling protocols for community A & B. The dotted lines represent the 5 and 10 µg/L guideline MACs.

The presence of LSLs (ANOVA, N = 40, F = 209.8, p-value < 0.05) was a significant predictor of lead release. Across all the sampling protocols, lead levels in homes with LSLs were an estimated 5.8 times greater (Wilcoxon, N = 40, 95% CI = 5.4 - 6.6) than homes without LSLs (Figure 6). Even with the use of phosphate corrosion control, median lead levels from 6-hour stagnation samples in homes with LSLs (6.6 μg/L) were 11 times that of homes without LSLs (0.6 μg/L). This trend carried through the other sampling protocols as well. Median lead levels in homes with LSLs (13 homes) were the highest in 6-hour stagnant (6.6 μg/L), followed by

random daytime (4.2 μg/L), 30-minute stagnant (3.2 μg/L) and flushed samples (2.9 μg/L) (Table 5). Lead concentrations exceeding 5 μg/L occurred in 2, 3, 3, and 8 homes via flushed, 30-minute, random daytime and 6-hour sampling, respectively. Additionally, for the small sample of homes with LSLs (N = 13), median lead levels via random daytime (Wilcoxon,

p-value = 0.2809) and 30-minute stagnation (Wilcoxon, p-value = 0.1239) were similar to 6-hour stagnation samples. Other studies have found that these methods can be used to assess corrosion control (Cardew, 2000, 2003; Hayes et al., 2016; Hayes & Croft, 2012; Riblet et al., 2019). Cardew (2003) cautioned that the sampling size requirement to determine representativeness is unique to each distribution system and water quality conditions, requiring a good understanding of lead variability in the area. It has been suggested that at least 8 (up to 100) random daytime samples analyzed annually over several years are required to represent a distribution system (Cardew, 2003; Hayes & Croft, 2012).Lead service lines provide a consistently high source of lead (Cartier et al., 2011; Schock & Oliphant, 1996; Y. Xie & Giammar, 2011) and can contribute up to 75% of the total lead at the tap (Sandvig et al., 2009). Lead corrosion by-products from an LSL may be incorporated into corrosion scale on premises plumbing (Sandvig et al., 2009). In homes where an LSL was completely removed, lead levels after 6 months decreased significantly (by 40%) in 6-hour stagnation samples (Trueman et al., 2016).

Table 5 Summary of lead sampling results from homes with lead service lines (N = 13).

	Lead Service Line							
	Lead concentrations (μg/L)					% samples > guideline value		
Protocol	Median	Mean	10th	90th	Max	5 μg/L	10 μg/L	15 μg/L
Flushed	2.9	3.4	2.1	4.9	7.6	6.8%	0.0%	0.0%
30-minute stagnation	3.2	6.9	<0.5	8.6	48.2	15.4%	7.7%	0.0%
Random daytime	4.2	12.8	<0.5	13.3	114	23.1%	7.7%	7.7%
6-hour stagnation	6.6	16.9	2	13	150	53.8%	15.4%	7.7%

Median lead levels in homes without LSLs (N = 27) were the highest in 6-hour stagnant (0.6 μg/L), with flushed, random daytime and 30-minute stagnation having lead levels below RDL (Table 6). None of the 6-hour or flushed samples collected exceeded 5 μg/L, but two 30-minute stagnation and four random daytime samples did. Notably, two homes without LSLs had lead concentrations of <0.5 μg/L, 5.3-5.4 μg/L, 12.1-19.8 μg/L, and <0.5-1.1 μg/L via flushed, 30-minute, random daytime, and 6-hour stagnant sampling, respectively.

Table 6 Summary of lead sampling results from homes without lead service lines (N = 27).

	No Lead Service Line							
	Lead concentrations (μg/L)					% samples > guideline value		
Protocol	Median	Mean	10th	90th	Max	5 μg/L	10 μg/L	15 μg/L
Flushed	<0.5	<0.5	<0.5	0.9	1.2	0.0%	0.0%	0.0%
30-minute stagnation	<0.5	1.2	<0.5	4.2	6.4	3.7%	0.0%	0.0%
Random daytime	<0.5	2.3	<0.5	9	19.8	11.1%	3.7%	3.7%
6-hour stagnation	0.6	1	<0.5	3	3.6	0.0%	0.0%	0.0%

Surprisingly, lead levels in random daytime and 30-minute stagnation samples from these two homes exceeded the paired 6-hour stagnation samples, median lead concentrations in homes with LSLs, and the recommended 5 μg/L MAC (Figure 6). Higher lead levels would be expected

in 6-hour stagnation compared to either random daytime or 30-minute stagnation (Riblet et al., 2019). However, lead release is not only dependent on stagnation time. The variability in premises plumbing materials and construction can result in unpredictable spikes of lead due to the semi-random release of particulate (Masters, Parks, et al., 2016; Sandvig et al., 2009). Compared to paired 6-hour stagnation, higher lead concentrations in some random daytime and 30-minute stagnation samples may indicate a sporadic but significant contribution of particulate lead from the premises plumbing; brass fixtures or faucets and lead-tin solder are possible sources in this case (Deshommes et al., 2010; Elfland et al., 2010; Sundberg et al., 2003; Y. Zhang & Edwards, 2011) (Figure 6). Distinguishing between lead levels due to characteristics of the home (e.g. consistent particulate lead levels from premises plumbing) or sporadic release of lead particles was not possible as each home was only sampled once using the four protocols.

3.4.4. Lead service lines increase rates of non-compliance

Homes with LSLs would see increased exceedance of the MAC (Figure 6). To highlight the effect of the guideline change on non-compliance, sampling protocols were compared against their respective guideline values. Non-compliance is defined in this study as having a value above the guideline value: flushed > 10 µg/L (Health Canada, 1992), random daytime and 30-minute stagnation > 5 µg/L (Health Canada, 2019a), and 6-hour stagnation > 15 µg/L (Health Canada, 2009). Flushed samples did not exceed 10 µg/L in either type of home. Comparing homes without and with LSLs, exceedance of 5 µg/L increased from 3.7% to 15.4% and 11.1% to 23.1% via 30-minute stagnation and random daytime, respectively. Similarly, exceedance of 15 µg/L in 6-hour stagnation samples increased from 0% (no LSL) to 7.7% (LSL).

Substantial rates of exceedance have been reported in other studies using the same protocols. Using a Monte Carlo simulation for a system with low plumbosolvency, Hayes (2009) reported that 30-minute stagnation and random daytime samples exceeded the 10 μg/L were 0%, and between 0.41 - 3.47%, respectively. Rates of non-compliance increased with an increasing proportion of homes with LSLs (10 - 90%) and plumbosolvency. In three communities across North America, Deshommes *et al.* (2018) reported that the exceedance of 10 μg/L via flushed sampling was greater in homes with LSLs (0 - 82%, depending on community) than those without LSLs (0%). Random daytime samples in Montreal exceeded 5 μg/L 82% and 32% of the time in homes with and without LSLs, respectively (Riblet et al., 2019). In two Manitoba distribution systems, 75% and 0% of homes with (Brandon) and without (Steinbach) LSLs exceeded 15 μg/L, respectively (L. Winning, 2015).

3.5. Implications for water utilities

3.5.1. Increased non-compliance and corrective action

The reduction in MAC from 10 to 5 μg/L, paired with the change in sampling protocol, may increase rates of non-compliance. None of the flushed samples collected from communities A and B (N = 40 homes) exceeded 10 μg/L but 2 samples exceeded 5 μg/L. Conversely, random daytime (10% > 10 μg/L, 17.5% > 5 μg/L) and 30-minute stagnation (2.5% > 10 μg/L, 12.5% > 5 μg/L) sampling exceeded these thresholds at much higher rates. Other studies show consistent results: data from Montreal show that the reduction in MAC and change in sampling protocol from flushed to 30-minute stagnation would be expected to increase the exceedance rate by up to 76% and 7% for homes with and without LSLs, respectively (Riblet et al., 2019). The

exceedance rates were even higher when the same comparison was made with random daytime and flushed sampling: rates increased by 82% and 32% for homes with and without LSLs, respectively (Riblet et al., 2019). Similarly, a comparison between random daytime and flushed sampling data from Winnipeg showed a 20.5% increase in non-compliance (City of Winnipeg, 2019). Additionally, systems without corrosion control or homes with LSLs experienced higher instances of non-compliance.

Unlike the Lead and Copper rule, which assesses compliance against a 90th percentile lead level, Health Canada measures against the MAC on a per site basis. This means that each home with lead levels above the MAC will require corrective action. Increased rates of non-compliance may pose new challenges and add significant cost to utilities. Repeated sampling using the same or a more appropriate sampling protocol (e.g. 6-hour stagnation profiles) may be needed to help determine the sources of lead in a home. However, additional sampling would, again, require homeowner participation. Premises plumbing (e.g. brass fittings, lead solder) may also be a significant source of lead in drinking water, contributing up to 55% of total lead measured at the tap by some estimates (Kimbrough, 2001; Korshin et al., 2000; Sandvig et al., 2009; Y. Zhang & Edwards, 2011). Lead contamination is not restricted to older properties. Lead levels above 100 μg/L have been observed in newer construction (Elfland et al., 2010). If lead plumbing is present in a home, utilities may recommend replacing leaded plumbing components. If a large proportion of homes have lead levels exceeding 5 μg/L, additional systemwide corrosion control measures (e.g. phosphate addition, pH adjustment) or water treatment processes may need to be optimized or applied. Phosphate used for corrosion

control can effectively limit lead release by adsorbing to lead scale or forming low solubility lead phosphates (Edwards & McNeill, 2002b; Noel et al., 2014). Natural organic matter (Korshin et al., 2000; Lin & Valentine, 2008), iron (Masters & Edwards, 2015; Schock et al., 2014; Trueman & Gagnon, 2016b) and manganese (Trueman, Gregory, et al., 2019) may increase lead release. Decreasing their concentrations throughout the distribution system may be a method for reducing lead corrosion.

3.5.2. Random daytime captured more lead and is more convenient

The need for resident participation in the revised protocols introduces new challenges. Perhaps first among them is the greater inconvenience placed on the homeowner, which may increase the difficulty in recruiting participants for lead monitoring. Random daytime captured more lead, has fewer logistical constraints, and is representative of customer stagnation times (Bailey et al., 1986; van den Hoven, & Slaats, 2006) but exhibits more variability compared to the 30-minute stagnation protocol (Cartier et al., 2011; Riblet et al., 2019; van den Hoven, et al., 1999). Consequently, a greater number of random daytime samples are needed to be representative of a distribution system (Hayes & Croft, 2012). A risk exists that random daytime sampling is not truly random owing to the need for efficient scheduling according to the availability of the resident. Strictly speaking, random daytime samples should be collected at random to better reflect customer water use patterns. Here, sampling was carried out when homeowners were available with no specific instruction on water use before the sampling events issued. This approach may lead to higher than average stagnation times as it avoids periods of frequent water use (e.g. cooking or mealtime). Sample collection by homeowners may have added

quality control aspects but this approach may better capture the random nature of water usage patterns and should be considered. Thirty-minute stagnation sampling sidesteps the issue of user variability, but it is a more involved process (there are more steps) and requires more of the resident's time to complete.

3.6. Conclusions

Health Canada's recommended sampling protocols and MAC have changed significantly to better protect consumers from lead exposure through drinking water. Sampling protocols have shifted from flushed samples in the distribution system to random daytime or 30-minute stagnation samples inside the home to better represent average consumer lead exposure. This study provides insight into the impact of Health Canada's change in sampling protocol and MAC on regulatory compliance, with a data set comprising 147 single family homes in Nova Scotia. Some of the principal limitations of this study are the lack of information on plumbing volumes, configurations, and water usage patterns that limits a mechanistic understanding of the results. The fundamental messages of this study are as follows:

- The reduction in MAC from 10 to 5 μg/L and change in sampling protocol from flushed to random daytime or 30-minute stagnation may increase the rate of non-compliance. This may necessitate more instances of corrective action.

- Flushed samples may fail to identify homes at risk for elevated lead levels.

- Random daytime captured higher lead levels and more frequently exceeded 5 μg/L compared to 30-minute stagnation.

- Homes with lead service lines or systems without corrosion control may experience increased rates of non-compliance. Consistent with previous work, higher lead levels are expected under these conditions.

- More sampling across different distribution systems using random daytime and 30-minute stagnation protocols is needed to provide comprehensive comparisons of protocol performance under varying water qualities. Although water usage was not measured in this study, future lead surveys should make efforts to collect water usage data (e.g. flow rate, stagnation times, volume) to provide a better understanding of lead exposure through drinking water.

4. Chapter 4 Impacts of orthophosphate-polyphosphate blends on the dissolution and transformation of lead (II) carbonate

This chapter is reprinted with permission from the following:

Locsin, J.A., Trueman, B.F., Doré, E., & Gagnon, G.A. Impacts of orthophosphate–polyphosphate blends on the dissolution and transformation of lead (II) carbonate. *Sci Rep* **12**, 17885 (2022).

J.A.L coordinated data collection, analyzed the data, wrote the paper, and prepared the figures.

4.1. Abstract

Orthophosphate-polyphosphate blends are commonly used to control lead release into drinking water, but little is known about how they interact with lead corrosion scale. Conventional corrosion control practice assumes that orthophosphate controls lead release by forming insoluble Pb-phosphate minerals, but this does not always occur, and under certain conditions, phosphate blends may increase lead release.

Continuously-stirred tank reactors were used to compare orthophosphate-polyphosphate blends with orthophosphate on the basis of lead (II) carbonate dissolution and transformation at environmentally relevant phosphate concentrations. Three model polyphosphates—tripoly-, trimeta- and hexametaphosphate— were used. Hexametaphosphate was the strongest

complexing agent (1.60-2.10 $mol_{Pb}/mol_{Polyphosphate}$), followed by tripolyphosphate and trimetaphosphate (1.00 and 0.07 $mol_{Pb}/mol_{Polyphosphate}$, respectively.

At equivalent orthophosphate and polyphosphate concentrations (as P), orthophosphate-trimetaphosphate had minimal impact on lead release, while orthophosphate-tripolyphosphate increased dissolved lead. Orthophosphate-hexametaphosphate also increased dissolved lead, but only over a 24-hr stagnation. Both orthophosphate-tripolyphosphate and orthophosphate-hexametaphosphate increased colloidal lead after 24 hr. Increasing the concentrations of hexameta- and tripoly-phosphate increased dissolved lead release, while all three polyphosphates inhibited the formation of hydroxypyromorphite and reduced the phosphorous content of the resulting lead solids. The impacts of orthophosphate-polyphosphates were attributed to a combination of complexation, adsorption, colloidal dispersion, polyphosphate hydrolysis, and lead mineral precipitation.

4.2. Introduction

While many drinking water utilities add phosphate chemicals for corrosion control or sequestration, revisions to the Lead and Copper Rule (LCR)(US EPA, 2021) will increase the number of utilities evaluating, changing, and implementing phosphate treatment. Utilities may need to provide both adequate sequestration and optimized corrosion control using blends of orthophosphate and polyphosphate. The use of polyphosphate and orthophosphate-polyphosphate blends for corrosion control in drinking water distribution systems is controversial. While polyphosphate is effective for controlling aesthetic water quality issues

(i.e. discoloration, calcium scaling) (Lin & Singer, 2005; Lytle & Snoeyink, 2002b), it increases lead release through aqueous complexation or colloidal dispersion (Edwards & McNeill, 2002b; T. R. Holm & Shock, 1991b; B. Li, Trueman, Locsin, et al., 2021a), and lead-polyphosphate complexes have been observed in tap water (Trueman et al., 2018b).

While the impact of orthophosphate (OrthoP) on lead corrosion is well studied (B. Li, Trueman, Locsin, et al., 2021a; Noel et al., 2014; Zhao et al., 2018b), the mechanisms by which orthophosphate-polyphosphate blends act to limit lead (Pb) release are unclear. One major problem is that the formulation of orthophosphate-polyphosphate blends is generally proprietary, with orthophosphate concentrations ranging between 5 to 70% (US Environmental Protection Agency (USEPA), 2016). Moreover, the precise concentrations of specific polyphosphate species are not always known, even to the manufacturer(Wasserstrom et al., 2017b), and hydrolysis of polyphosphate in the distribution system can result in a variable mixture of OrthoP and smaller polyphosphates, further confounding the effects of each phosphate species.

Individual polyphosphates may differ widely in their effects on water quality: structural differences strongly determine polyphosphate interactions with metal ions. Linear polyphosphates (e.g. tripolyphosphate) are more effective sequestrants than cyclophosphates (e.g. trimetaphosphate, hexametaphosphate) (Gosselin & Coghlan, 1953; Van Wazer & Callis, 1958b). McGaughey(McGaughey, 1983) showed that trimetaphosphate was least effective at preventing calcium precipitation compared to tripolyphosphate or hexametaphosphate and it

inhibited the dissolution of hydroxyapatite, whereas the other two polyphosphates solubilized the mineral. This may be due to steric constraints characteristic of cyclophosphates that can be mitigated by increased chain length (Miyahima et al., 1981). Fundamental polyphosphate chemistry predicts that, at equivalent chain lengths, cyclophosphates will have a smaller effect on lead release than linear polyphosphates and that lead release will increase with polyphosphate chain length.

In addition, theoretical lead solubility predictions with blended phosphates are difficult due to the lack of solubility and formation constants as well as a limited understanding of their effects on lead corrosion scale formation. While the orthoP component is expected to form an insoluble lead-phosphate, this is not always observed in lead pipe scale(Tully et al., 2019b; Wasserstrom et al., 2017b). Instead, field studies have documented complex amorphous layers of phosphorous and co-precipitated metals (e.g. Al, Ca, Fe) forming in orthophosphate-polyphosphate treated systems (Tully et al., 2019b; Wasserstrom et al., 2017b). While corrosion scale plays an important role in lead release, mineral formation due to blended phosphate has not been systematically studied. A limited understanding of orthophosphate-polyphosphate-lead interactions leaves utilities that use these additives vulnerable to lead contamination at consumers' taps.

To address these knowledge gaps, lead carbonate dissolution in the presence of orthophosphate and polyphosphate was studied. The goals of this work were to:

(1) Compare lead release, quantified as the net conversion from suspended lead (II) carbonate to dissolved (<0.2 μm) and small lead colloids (0.2-0.45 μm), in the presence of the three representative polyphosphates: tripolyphosphate (TripolyP), trimetaphosphate (TrimetaP), and hexametaphosphate (HexametaP). Each was tested alone and blended with orthophosphate, using a continuous-flow stirred-tank reactor (CSTR).

(2) Evaluate mineral formation in the presence of OrthoP in combination with TripolyP, TrimetaP, or HexametaP.

4.3. Materials and Methods

4.3.1. Preparation of solutions

Ultrapure water (18.2 MΩ ·cm, TOC < 2 μg L^{-1}) was used to prepare all solutions in this study. Solution composition was chosen to reflect drinking water conditions with low inorganic carbon content. All chemicals were reagent grade or better. Sodium hexametaphosphate ($(NaPO_3)_6$) (Alfa Aesar, Haverhill, MA), sodium trimetaphosphate ($(NaPO_3)_3$) (Alfa Aesar, Haverhill, MA), and sodium tripolyphosphate ($Na_5P_3O_{10}$) (Alfa Aesar, Haverhill, MA) were used to represent different polyphosphate structures. Polyphosphate stock solutions were obtained by dissolving TripolyP, TrimetaP, or HexametaP in 100 mL ultrapure water, before each experiment. All polyphosphate solutions were prepared and used the same day. OrthoP was added as ACS grade phosphoric acid (Fisher Chemical, Fairlawn, NJ). The dissolved inorganic carbon (DIC) concentration of 5 mg C L^{-1} was achieved by dissolving sodium bicarbonate powder (Fisher

Chemical, Fairlawn, NJ) in 20 L of ultrapure water. The pH was adjusted by the addition of 1N trace metal grade nitric acid (Fisher Chemical, Fairlawn, NJ) or freshly prepared 2N sodium hydroxide (Fisher, Fairlawn, NJ).

4.3.2. Flow-through reactor Pb dissolution experiments

Continuously stirred tank reactors (CSTR) made with glass columns (Kimble, Rockwood, TN, 144 mL) were used to evaluate the impacts of phosphate composition, calcium, and pH on lead solubility and mineral formation (Figure 7). Before each experiment, all columns, tubing (Masterflex LS-14, internal diameter = 1.6 mm), stir bars, and glass carboys were immersed in dilute HNO_3 (~ 1.6M) for 24 hours and rinsed at least four times with ultrapure water. Experiments were carried out in duplicate at room temperature (21 ± 2ºC). The CSTRs were fed using peristaltic pumps (Cole Palmer, Montreal, QC) and capped with 0.45 µm cellulose nitrate membranes (Whatman, Maidstone, UK) to prevent the loss of lead solids from the reactor (Figure 7). Using peristaltic pumps, the influent flow rate was maintained at 4.9 mL $min.^{-1}$ providing a hydraulic retention time (HRT) of 30 minutes. This was chosen to reflect current Canadian and European lead sampling guidelines(Health Canada, 2019a; Hoekstra et al., 2009). To ensure saturation, 1 g L^{-1} of lead (II) carbonate powder (Alfa Aesar, Haverhill, MA), composed of a mixture of cerussite and $PbCO_3 \cdot PbO$(B. Li, Trueman, Locsin, et al., 2021b), used as a surrogate of lead corrosion scale, was suspended in the reactors.

Previous studies have noted the high variability in lead release due to labile lead phases in the first 48 HRTs(B. Li, Trueman, Locsin, et al., 2021b; Noel et al., 2014). Based on previous work(B. Li, Trueman, Locsin, et al., 2021b), reactors were considered stable and sampled after 58 HRTs.

At the end of the flow-through experiment, the influent was shut off, reactors were sealed with plastic caps and left to mix for 24 hours (24HS) to evaluate the effect of long stagnation times on lead release.

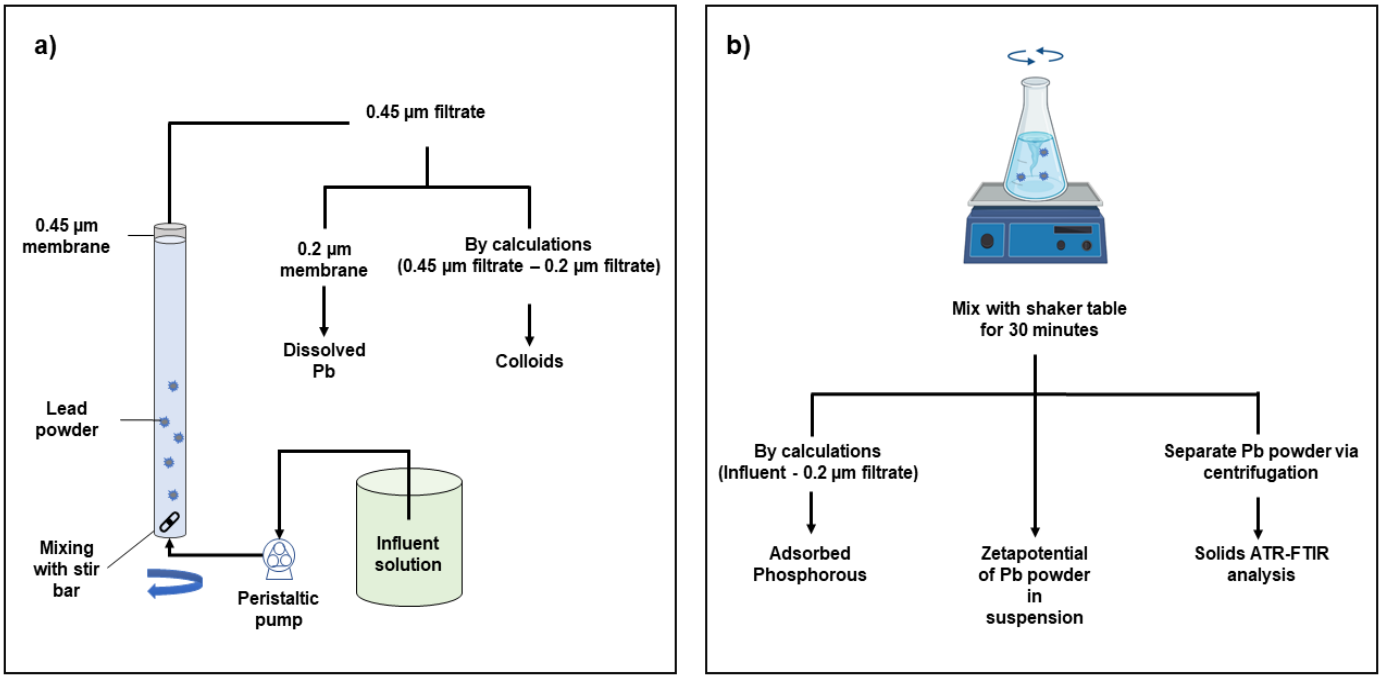

Figure 7 A schematic overview of the (a) CSTR assembly used in dissolution experiments and (b) batch reactor used in the adsorption experiments. Effluent from the CSTR was separated into 0.45 µm filtrate, colloids (0.2-0.45 µm), and dissolved (< 0.2 µm) lead.

Lead release was quantified as mass released per unit surface area under (a) steady-state at a 30-min HRT, or (b) at the end of the 24-hour stagnation. Here, steady-state was defined as less than 30% variation (standard deviation/mean) in lead concentrations over at least four consecutive effluent samples, spanning at least eight HRTs. Once the reactor effluent had stabilized, mass release per unit surface area was calculated according to Equation (1).

Equation 1

$$r_{exp}(\mu g\, m^{-2}) = \frac{Css}{SA * Pbsolid}$$

where r_{exp} is the mass release per unit surface area (SA) (µg m^{-2}), C_{ss} is the effluent lead concentration (µg L^{-1}, SA is the surface area of lead powder determined to be 0.78 m^2 g^{-1}, and Pb_{solid} is the mass of lead powder in g L^{-1}.

The effluent was further filtered through a 0.2 µm polycarbonate membrane (Whatman, Maidstone, UK) to get dissolved lead using a syringe apparatus. The 0.2 µm membranes were decontaminated with dilute nitric acid (~0.16 M), washed with 10mL ultrapure water, then pre-conditioned with 10 mL of sample to minimize losses to adsorption(B. Li, Trueman, Locsin, et al., 2021b).

Since at least 8.6 L of reactor effluent passed through the 0.45 µm cellulose nitrate membrane before sample collection, adsorption losses to that membrane were expected to be minimal(B. Li, Trueman, Locsin, et al., 2021b).

4.3.3. Experiment design

First, the performance of four phosphates at 1000 µg P L^{-1}- OrthoP, TripolyP, TrimetaP, and HexametaP- on lead release in the CSTR at pH 7.5 ± 0.2 were evaluated. The effect on lead release of two factors- orthophosphate-polyphosphate composition (OrthoP-TripolyP, OrthoP-

TrimetaP, or OrthoP-HexametaP), and OrthoP (300 µg P L^{-1}) to polyphosphate (300 (1:1) or 700 (1:2) µg P L^{-1}) concentrations – were evaluated against OrthoP at 300 µg P L^{-1} at pH 7.5 ± 0.2.

4.3.4. Short term phosphorus adsoprtion - batch experiment

To support the CSTR experiment, the effect of OrthoP or polyphosphate on phosphorous adsorption, quantified as the difference between dissolved (<0.2 µm) phosphorous at the beginning and end of the 30 min reaction, was concurrently measured with lead dissolution in a batch reactor. In a 250 mL Erlenmeyer flask, a 1 g L^{-1} dispersion of lead (II) carbonate was prepared in a 5 mg L^{-1} DIC solution. The roles of phosphate composition were explored by adding 1000 µg P L^{-1} of either OrthoP, TripolyP, TrimetaP, or HexametaP at two pH (7 or 9). These pH would represent the upper and lower bound of pH at which phosphate inhibitors are used in drinking water (Bae et al., 2020; Edwards & McNeill, 2002b). The effects of different combinations of OrthoP (1000 µg P L^{-1}) with each of the polyphosphates (500-2000 µg P L^{-1}) were investigated at pH 7. The suspensions were shaken mechanically for 30 mins, at 150 rpm and room temperature (21 ± 2ºC). Thirty minutes was chosen to both mirror stagnation in the CSTR experiment and minimize polyphosphate hydrolysis to OrthoP(T. R. Holm & Edwards, 2003). After 30 minutes, an aliquot was taken from the vessel and filtered through a 0.2 µm polycarbonate membrane. The filtrates were analyzed for dissolved phosphorous and lead via inductively coupled plasma mass spectrometry (ICP-MS).

4.3.5. Effect of phosphates on lead carbonate interparticle forces - batch experiment

The electrophoretic mobility of lead carbonate particles in solution (2 g L^{-1}) was measured as a function of pH (5-9.5) and phosphate type-OrthoP, TripolyP, TrimetaP, and HexametaP- at 1000

μg P L^{-1}. The solution pH was controlled within 0.2 pH units. The solution was initially set to approximately pH 9.5, after which the pH was gradually decreased to 5 via the addition of 1N NaOH. Independent reactors, run in duplicate, were used.

4.3.6. Analytical methods

4.3.6.1. Element quantification

Metals were quantified by ICP-MS (X Series II, Thermo Fisher Scientific, Waltham, MA) using Standard Methods 3125 and 3030 (American Public Health Association, American Water Works Association, Water Environment Federation, 2012). Reporting limits for lead and phosphorous were 0.4 and 4.9 μg L^{-1}, respectively. Filtered effluent was acidified to pH <2 with concentrated trace metal grade HNO_3 and held for a minimum of 24 hours, at room temperature, before analysis (US EPA, 1994a). Dissolved phosphate (PO_4) concentrations were measured using EPA 300.1 (US EPA, 1997) via ion chromatography (Dionex Aquion IC with AS22 column, Thermo Fisher Scientific, MA) with a reporting limit of 10 μg L^{-1} phosphate.

Dissolved metals were defined as lead passing through a 0.2 μm membrane. The colloid (0.2-0.45 μm) fraction was calculated by subtracting dissolved from the 0.45 μm filtrate (Figure 7). Particles smaller than 0.2 μm may be present in the dissolved fraction.

4.3.6.2. Structural characterization of Pb particles

Scanning electron (SEM) (Hitachi S-4700, Tokyo, Japan) microscopy with energy dispersive X-ray spectroscopy (EDS) was used to observe the morphology and analyze elemental composition of

powder surfaces. X-ray diffraction (XRD) (Rigaku Ultima IV X-ray Diffractometer, The Woodlands, TX, copper Kα source) was used to identify crystalline phases. Diffraction patterns were analyzed using Match! 3, version 3.9.0.158 software and Crystallographic Open Database Rev.218120 database. The surface area of the lead (II) carbonate powder was determined via Brunauer-Emmett-Teller analysis (BET-N2) (Nova 4200E, Quantachome, Boynton Beach, FL).

4.3.6.3. Infrared spectroscopy

A single-beam Fourier transform infrared spectroscopy in attenuated total reflectance mode (ATR-FTIR) (Bruker alpha-P, Billerica, MA) was used. Each infrared spectrum (IR) was recorded with the blank cell as the background. Fifty scans at a wavenumber range between 400-4000 cm^{-1} were measured to obtain each spectrum, with a resolution of 4 cm^{-1}. IR spectra of dissolved phosphate species were measured by using a phosphate solution, composed of either OrthoP or polyphosphate in ultrapure water at pH corresponding to the experimental conditions. The pure water IR spectrum was subtracted to produce the spectra of dissolved phosphate species.

At the end of the flow-through experiment, the resulting lead powder was dried in a desiccator for 1 week. Samples were spread evenly across the surface of the ATR crystal using a plastic spatula and their IR spectra were recorded. At the end of the batch adsorption experiment, the spectra of adsorbed phosphate species on the Pb surface were measured using the phosphate solution in the Pb suspension as the sample and the same suspension, without phosphate, as the reference.

4.3.6.4. Zeta potential

Zeta potentials were measured using a Zetasizer Nano ZS (Malvern Panalytical, Malvern, UK). Aliquots of lead (II) carbonate suspension were extracted and measured after a 5 min reaction period at the corresponding pH.

4.3.7. Data analysis

R, along with contributed packages, was used for data analysis and presentation(Team, 2013; Wickham et al., 2019). All experiments were duplicated, with lead concentrations expressed as medians with ranges provided in parenthesis. A Hodges-Lehmann estimate was used to quantify the difference between dosed and recovered phosphorus in the batch experiments (Helsel et al., 2020).

4.4. Results and Discussion

4.4.1. Impacts of orthophosphate or polyphosphate on lead release in CSTR experiments

As expected, OrthoP decreased median lead concentrations compared to the phosphate-free condition. With an HRT of 30 min, OrthoP treatment decreased lead in 0.2 µm filtrate (dissolved) by 98.1 (range = 91.6-99.3) µg $Pb_{0.2\mu m}$ m^{-2}, lead in 0.45 µm filtrate by 99.1 (95.3-104.9) µg $Pb_{0.45\mu m}$ m^{-2}, while colloidal lead—the difference between 0.45 and 0.2 µm filtrate—did not vary significantly. With a 24-hour stagnation period (24HS), OrthoP treatment decreased lead in 0.2 µm filtrate by 139 (130.8-149.0) µg $Pb_{0.2\mu m}$ m^{-2}, lead in 0.45 µm filtrate by 245 ± 16 µg $Pb_{0.45}\mu_m$ m^{-2} (Figure 8).

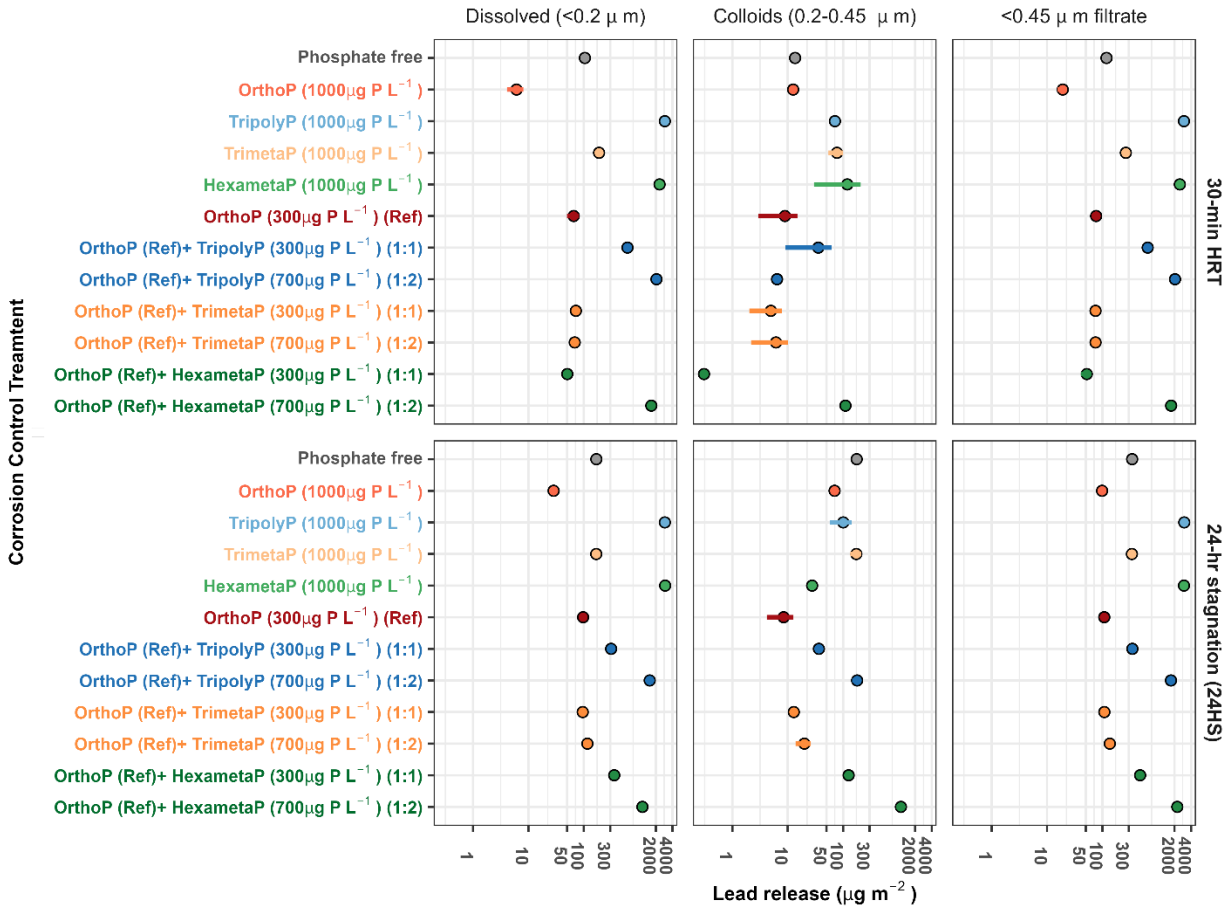

Figure 8 Median mass lead release per unit surface area (log-scale) during reaction at pH 7.5 and DIC 5 mg C L-1 from the CSTR. Lead release from a phosphate free condition was compared with orthophosphate (1000 µg P L^{-1}) and three polyphosphates (1000 µg P L^{-1}). Bends of orthophosphate (300 ug P L^{-1}) and polyphosphates (300 or 700 ug P L^{-1}) were also compared against orthophosphate (300 ug P L^{-1}). Each set represents at least two reactor runs, and error bars span the median absolute deviation of measurements. Tabulated data can be found in Table S1.

TripolyP, the linear polyphosphate, yielded the highest lead concentrations among the polyphosphates, and the dissolved fraction was dominant (>97%) (Figure 8). Compared to the phosphate-free condition, median lead release increased by 2847 (2837-2849) µg $Pb_{0.45\mu m}$ m^{-2} and 2664 (2640-2667) µg $Pb_{0.45\mu m}$ m^{-2} at a 30-min HRT and 24HS, respectively. TripolyP had a

potential complexation capacity—calculated as the molar ratio of median dissolved lead and median residual polyphosphate— of 1.00 $\pm$ 0.01 $mol_{Pb}/mol_{TripolyP}$ (at both a 30-min HRT and 24HS). Moreover, TripolyP achieved apparent equilibrium within 30 minutes. That is, $Pb_{0.45\mu m}$ concentrations between a 30-min HRT and 24HS did not vary by more than 38.5 (2.6 – 84.6) µg $Pb_{0.45\mu m}$ m^{-2}.

TrimetaP, a cyclophosphate with equivalent chain length, had the least impact on lead concentrations among the polyphosphates, with a potential complexation capacity of 0.07 $\pm$ 0.01 $mol_{Pb}/mol_{TrimetaP}$ (at both retention times). Lead release due to TrimetaP was similar to that representing the phosphate-free condition at 24HS. At a 30-min HRT, lead release was higher by 145.7 (141.4-149.7) µg $Pb_{0.45\mu m}$ m^{-2}.

When HexametaP, the larger cyclophosphate, was added instead, lead complexation capacity was greater than TrimetaP: 1.60 to 2.10 $\pm$ 0.01 $mol_{Pb}/mol_{HexametaP}$ (30-min HRT and 24HS). This is consistent with previous work describing lead release from pipes in the presence of HexametaP(Edwards & McNeill, 2002b). Lead release was mostly dissolved (>89%) and exceeded that representing the phosphate-free control by an estimated 2352 (2248-2435) µg $Pb_{0.45\mu m}$ m^{-2} and 2626 (2559-2693) µg $Pb_{0.45\mu m}$ m^{-2} at a 30-min HRT and 24HS, respectively.

OrthoP and cyclophosphates dispersed colloidal lead at a 30-min HRT (Figure 8). OrthoP treatment resulted in a higher proportion of small colloids compared to polyphosphates (65% vs 2.4% vs 29.2% vs 4.8% of $Pb_{0.45\mu m}$ for OrthoP, TriployP, TrimetaP, and HexametaP, respectively). While the proportion of small colloids increased with stagnation time (24HS) for

OrthoP (71.1% of $Pb_{0.45\mu m}$) and TrimetaP (50.8% of $Pb_{0.45\mu m}$) treatment, it was similar with TripolyP and decreased with HexametaP (0.9% of $Pb_{0.45\,\mu m}$). Lead colloids dispersed by HexametaP at the 30-min HRT appeared to dissolve over the extended stagnation (24HS), based on the large decrease in the colloidal fraction with increasing reaction time.

Excess OrthoP is known to promote Pb colloid formation, especially above a P:Pb molar ratio of 1 (Zhao et al., 2018b). At 1000 µg P L^{-1} OrthoP, the P:Pb molar ratio of 302:1 (32.3 µM P: 107 nM Pb) would encourage lead-phosphate precipitation. Polyphosphates also promote colloid formation: TrimetaP can impart a negative surface charge (See Section 4.1: Impacts on electrical double layer and adsorption of orthophosphate or polyphosphate) and has been observed to promote apatite formation even at relatively low pH (Delbem et al., 2014). HexametaP can also stabilize colloids (B. Li, Trueman, Locsin, et al., 2021b).

4.4.2. Combining orthophosphate and polyphosphate

Median lead concentrations in the <0.45 µm filtrate from reactors dosed with OrthoP alone were 77.1 (61.9-96.4) and 108.0 (101.3-113.1) µg $Pb_{0.45\mu m}$ m^{-2} at a 30-min HRT and 24HS, respectively. Dissolved lead concentrations were 65.1 (34.5-83) and 97.1 (94.7-101.1) µg $Pb_{0.2\mu m}$ m^{-2}, while colloidal lead concentrations were 8.90 (6.70-14.5) and 8.40 (4.20-12.2) µg $Pb_{0.2\text{-}0.45\mu m}$ m^{-2} (Figure 8).

Blending either TripolyP or HexametaP with OrthoP increased lead release relative to the OrthoP-only control. Adding TripolyP increased dissolved lead at both doses and stagnation times (1:1 orthophosphate:polyphosphate ratio: 554.0 (540.3-572.8) and 213.5 (191.4-235.5)

μg $Pb_{0.2\mu m}$ m^{-2} at 30-min HRT and 24HS, respectively; 1:2 ratio: 1981 (1936-2005) and 1453 (1445-1459) μg $Pb_{0.2\mu m}$ m^{-2}) (Figure 8). Adding HexametaP increased dissolved lead at 24HS (256.3 (243.1-269.7) vs 1046 (958.7-1134) μg $Pb_{0.2\mu m}$ m^{-2} at 1:1 and 1:2 ratios, respectively).

Both OrthoP-TripolyP and OrthoP-HexametaP increased small colloidal lead concentrations at 24HS. Compared to a 30-min HRT, 700 μg L^{-1} of TripolyP (1:2 ratio) accompanied a decrease in dissolved lead of 502.4 (471.8-510.0) μg $Pb_{0.2\mu m}$ m^{-2} and an increase of 173.7 (144.9-190.8) μg $Pb_{0.2\text{-}0.45\mu m}$ m^{-2} in small colloidal lead. After 24HS, OrthoP-HexametaP treatment increased small colloid concentrations by 124.0 (119.4-131.7) and 980.0 (831.3-1102) μg $Pb_{0.2\text{-}0.45\mu m}$ m^{-2} at the 1:1 and 1:2 ratios, respectively.

Blending TripolyP or HexametaP with OrthoP inhibited the formation of hydroxypyromorphite. At equivalent OrthoP:polyphosphate concentrations (1:1), XRD peaks (Figure 9a,b,c), IR peaks (~540 and 570 cm^{-1}) (Figure 9d,e,f), and rod-like crystals (Bigi et al., 1991) (Figure 10a,e) characteristic of hydroxypyromorphite were observed. At the higher TriployP concentration (1:2), hydroxypyromorphite was no longer observed. Instead, disk-like crystals (Dermatas et al., 2004) and XRD peaks characteristic of hydrocerussite were seen. Furthermore, the proportion of adsorbed phosphorus measured via energy dispersive X-ray spectroscopy (EDS) decreased from 41.69 ± 3.74% to 1.55 ± 1.41% (weight %) as TripolyP was increased from 300 – 700 μg P L^{-1} (OrthoP-TripolyP at 1:1 and 1:2 ratios, respectively). Similarly, increasing the HexametaP concentration by the same mass (1:1 - 1:2) resulted in the disappearance of diffraction peaks characteristic of hydroxypyromorphite (2θ =22, 26.9, 30.5, 32.4, and 58.8°) (Figure 9b). This

result was further supported by a decrease in the proportion of phosphorus on the lead solid from 13.79 $\pm$ 3.46 (1:1) to 0.24 $\pm$ 0.11 wt% (1:2).

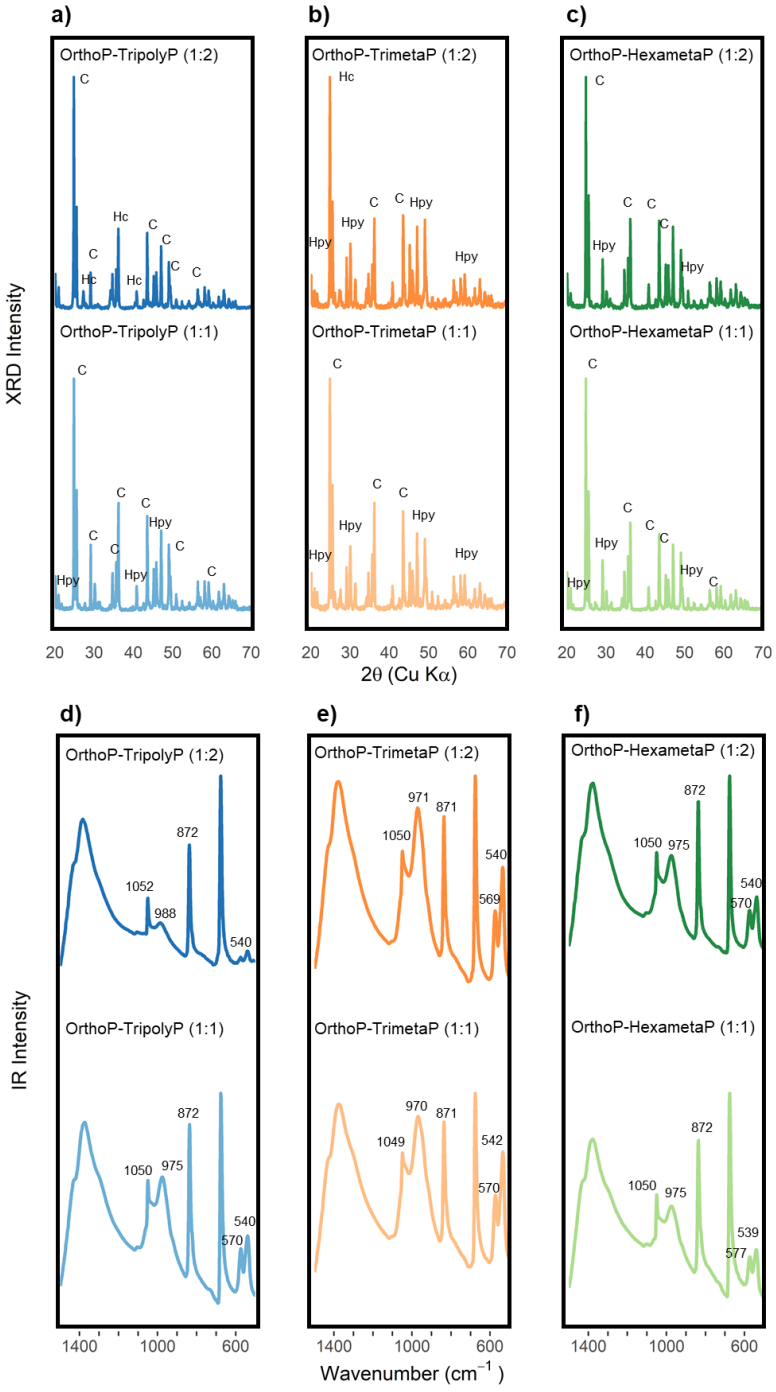

Figure 9 (a-c) XRD and (d-f) FTIR spectra of lead particles from CSTR experiments after reactions with orthophosphate-tripolyphosphate, orthophosphate-trimetaphosphate, and orthophosphate-

hexametaphosphate at pH 7.5 and DIC 5 mg C L^{-1}.Prominent mineral or IR peaks are identified above. XRD lead mineral peaks are identified as follows: C - cerussite, Hc - hydrocerussite, and Hpy - hydroxypyromorphite.

OrthoP-TrimetaP had minimal impact on lead release at both stagnation times (Figure 8). At a 1:1 ratio, median lead release in the presence of OrthoP-TrimetaP differed from OrthoP by just 2.0 and 9.3 µg $Pb_{0.45µm}$ m_{-2} whereas lead release at a 1:2 ratio was greater by just 1.9 and 28.0 µg $Pb_{0.45µm}$ m_{-2} at a 30-min HRT and 24HS, respectively. A 1:1 blend of OrthoP and TrimetaP decreased lead release at 24HS by 239.4 (209.8-269.1) and 372.7 (347.9-395.4) µg $Pb_{0.45µm}$ m^{-2} compared to the equivalent blends with TriployP or HexametaP, respectively. Also, the inhibition of hydroxypyromorphite formation with TrimetaP was not as extreme as with TripolyP or HexametaP. While XRD (Figure 9a,b,c) and IR peaks (539 to 546 and 570 to 577 cm^{-1}) (Figure 9d,e,f) characteristic of hydroxpyromorphite were observed across all OrthoP-polyphosphates at the 1:1 ratio, their intensities were lower with HexametaP or TripolyP compared to TrimetaP. Hydroxypyromorphite was clearly visible (Figure 9b, 10c) with OrthoP-TrimetaP treatment (1:1 ratio) but increasing the TrimetaP concentration (1:2) appeared to inhibit its formation (Figure 10d). Hydroxypyromorphite crystals at the 1:1 ratio presented rod-like particles with sharp, defined edges (Figure 10c), whereas crystals with the 1:2 ratio were still rod-like but presented round edges (Figure 10d). Moreover, phosphorus in the lead solid was reduced from 25.8 ± 7.3% to 6.4 ± 2.4% (weight %) when TrimetaP was increased from 300 (1:1) to 700 (1:2) µg P L^{-1}.

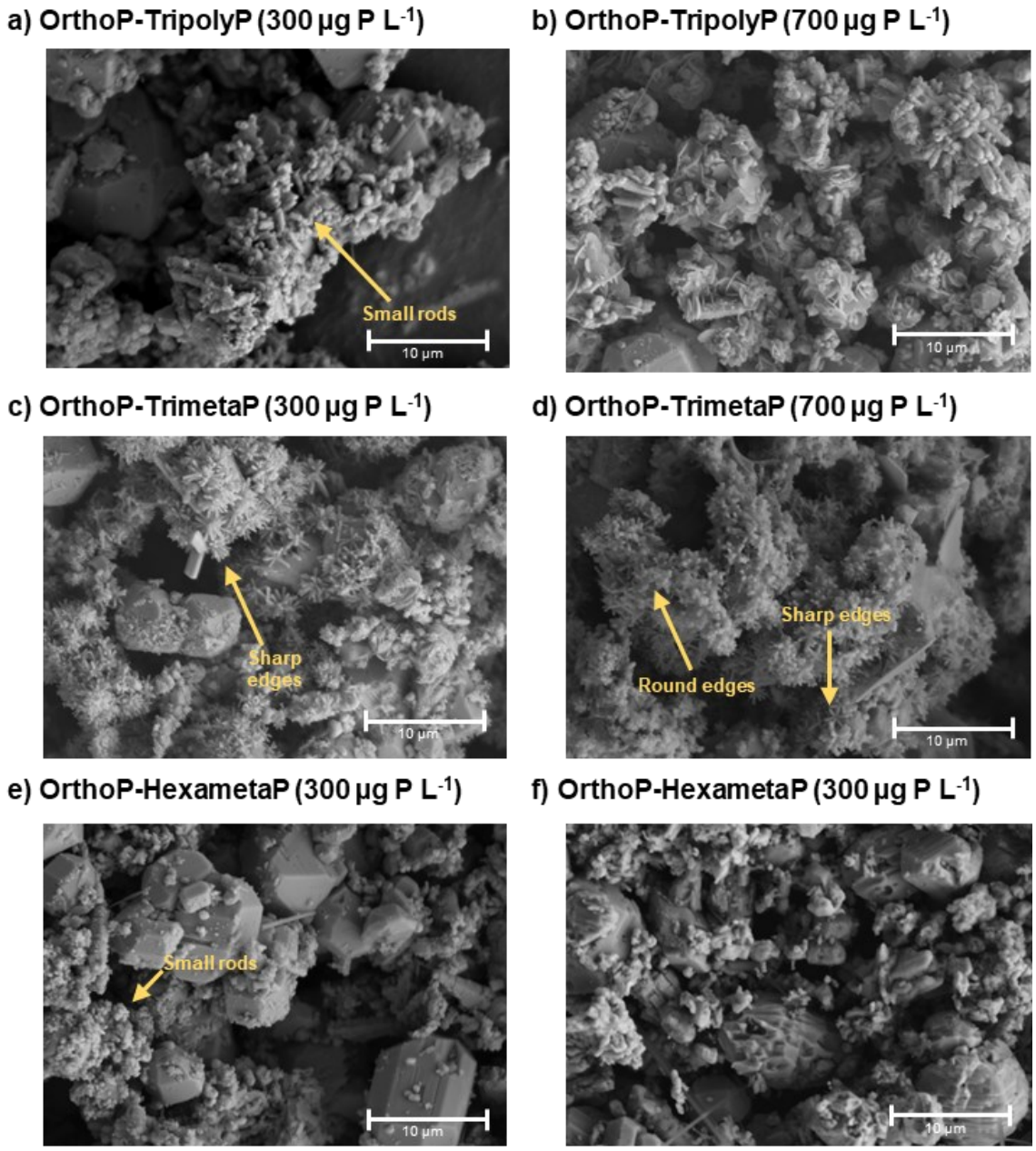

Figure 10 SEM images of lead particles from CSTR experiments after reactions with (a,b) orthophosphate-tripolyphosphate, (c,d) orthophosphate-trimetaphosphate, and (e,f) orthophosphate-hexametaphosphate at pH 7.5 and DIC 5 C L^{-1}.

4.4.3. Exploration of interaction mechanisms for Pb and phosphates

4.4.3.1. Impacts on electrical double layer and adsorption of orthophosphate or polyphosphate

In a batch experiment, the surface charge and adsorption behavior of phosphorous onto lead (II) carbonate was examined at pH 7 (0 ± 0.14 mV) and 9 (-25.2 ± 0.3 mV) to allow for both neutral and negatively charged surfaces, respectively. Of particular interest was the effect of chain length and structure on phosphate adsorbed on the lead surface.

Phosphates shifted the isoelectric potential (pH_{iep}) of lead carbonate. At equivalent chain lengths, TripolyP imparted greater charge reversal than TrimetaP (Figure 11a). Although only present at half the molar concentration, HexametaP imparted more negative charge to the lead surface than TrimetaP, suggesting that chain length is important.

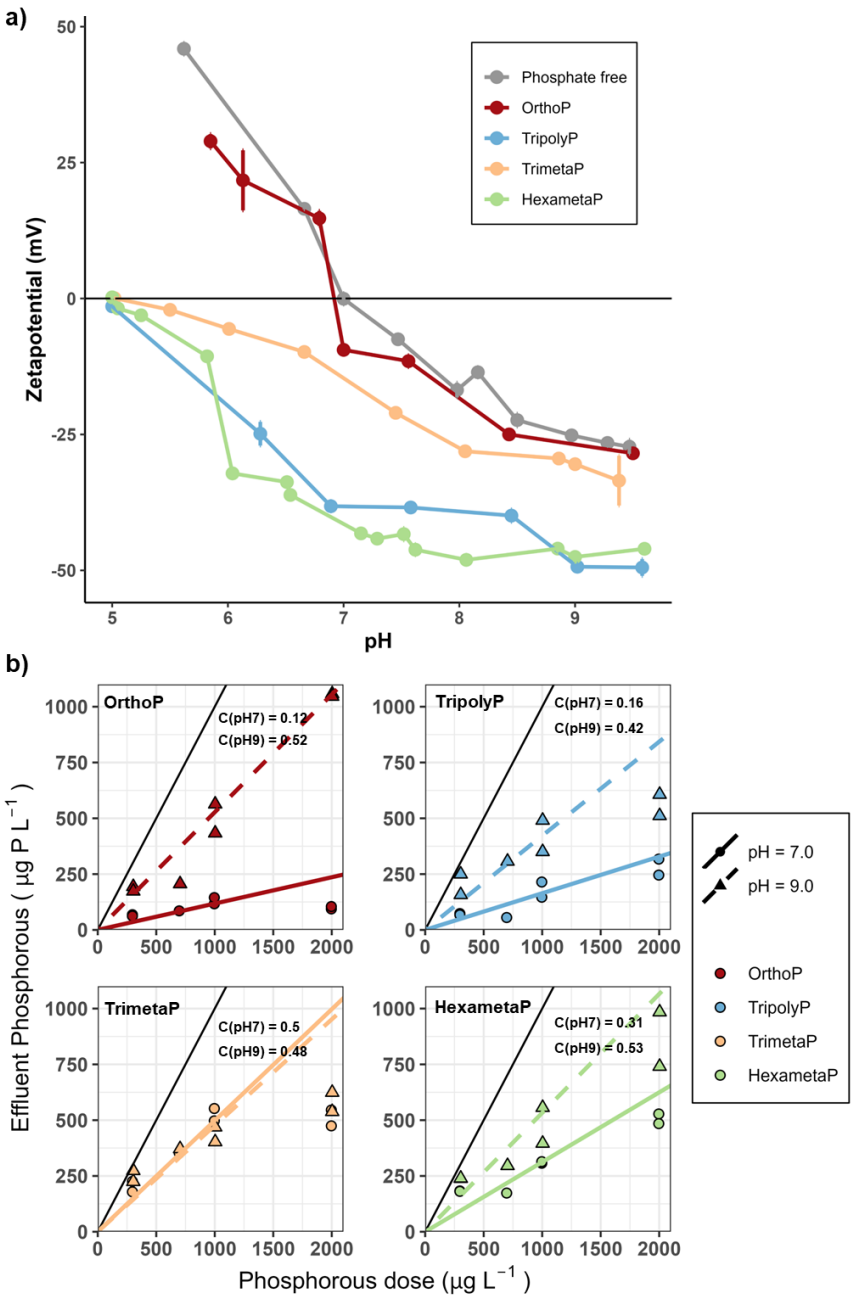

Figure 11 (a) Zetapotential (pH = 5 to 9.5, P = 0 or 1000 µg P L^{-1}), (b) phosphorous adsorption (pH = 7 or 9, P = 0 to 2000 µg P L^{-1}) by lead carbonate as a function of pH and phosphate type (OrthoP, TripolyP, TrimetaP, HexametaP) at DIC 5 mg C L^{-1} from the batch experiment. Each set represents at least two reactor runs, and error bars span the median absolute deviation of measurements. Colored lines (representing y=Cx) are labeled by their corresponding C, where C is the estimated fraction of total phosphorous remaining in solution at the end of 30 minutes. The solid black line represents y=x. The

estimates (C) were obtained by computing a multiplicative difference estimate between the log-transformed influent and effluent phosphorus concentrations.

Similarly, the reduction in effluent dissolved (<0.2µm) phosphorus ($P_{reduction}$), measured as the ratio of effluent to influent phosphorus, presented an apparent dependence on structure and chain length (Figure 11b). The estimates for $P_{reduction}$ were obtained by computing a multiplicative difference estimate between the log-transformed influent and effluent phosphorus concentrations(Helsel et al., 2020). At pH 7.0, $P_{reduction}$ was greatest for OrthoP (0.12, or 12% of initial P remained after reaction (95% confidence interval (CI): 0.05-0.21). At equivalent chain lengths, $P_{reduction}$ was greater with TripolyP (0.16, 95% CI: 0.11-0.23) than TrimetaP (0.50, 95% CI: 0.27-0.64). Increased cyclophosphate chain length resulted in less $P_{reduction}$: HexametaP adsorption by molar basis of polyphosphate was 2.60-fold (95% CI: 1.50-4.50) lower compared to TrimetaP. The similar, albeit reduced, phosphorus adsorption observed at pH 9.0 could be attributed in part to electrostatic repulsion. At pH 7.0, lead (II) carbonate is neutrally charged whereas both lead (II) carbonate and phosphate are negatively charged at pH 9, likely resulting in more adsorption at pH 7 and repulsion at pH 9 (Figure 11a). Moreover, hydroxypyromorphite is more soluble at pH 9. At pH 7.5 at which the CTSR experiment was conducted, phosphate species would be more deprotonated (de Morais et al., 2020; Michelmore et al., 2000), and the lead (II) carbonate would have a slightly more negative surface charge (-7.5 ± 0.65 mV) than at pH 7. For instance, orthophosphate would comprise of 59% $H_2PO_4^-$ and 41% HPO_4^{2-}, and 31% $H_2PO_4^-$ and 69% HPO_4^{2-} at pH 7 and 7.5, respectively. While this may result in reduced phosphorus adsorption in the CSTR, the adsorption trend seen in the

short-term batch experiment can be extended to the CSTR. The apparent independence of trimetaphosphate adsorption from pH may be due to steric constraints, rather than trimetaphosphate species, reducing its ability to interact with the lead (II) carbonate surface (See *Chemical surface interactions between lead and phosphates*).

4.4.3.2. Chemical surface interactions between lead and phosphates

To understand the interactions between phosphates and lead carbonate in the CSTR experiments, a deeper analysis of the surface properties of the lead carbonate after phosphate adsorption in a complementary batch experiment was carried out via ATR-FTIR. IR spectra of free phosphates in solution exhibit several characteristic peaks (Table 7). Following surface adsorption, IR bands experience either shifting or changes in intensity and are discussed below. The peak assignments for the ATR-FTIR spectra of adsorbed phosphates on lead carbonate are extrapolated based on the data of condensed phosphates adsorption on titania, serpentine, and metal (hydr)oxides (Guan et al., 2005; Lu et al., 2019; Michelmore et al., 2000; Socrates, 2004; Wan et al., 2020). A detailed description of the ATR-FTIR analysis can be found in Appendix B.

Table 7 Assignment of ATR-FTIR peaks for phosphates in solution based on Guan et al., 2005, Lu et al., 2019, Michelmore et al., 2000, Socrates, 2004, and Wan et al., 2020.

Phosphate Type	pH	Species	Wavenumber (cm^{-1})	Assignment (free in solution)
Orthophosphate	3.7	$H_2PO_4^-$	1157	v_{as}(P-O)
			1075	v_s(P-O)
			940	v_{as}(P-OH)
			872	v_s(P-OH)
	9.1	HPO_4^{2-}	1075	v_{as}(P-O)
			990	v_s(P-O)
			850	v_s(P-OH)
	12.5	PO_4^{3-}	1008	v_{as}(P-O)
Tripolyphosphate	6-9		1212	v_{as}(P-O)
			1191-1199	v_{as}(P-O in terminal HPO_3 and H_2PO_3)
			1120	v_{as}(P-O) in PO_3
			1101	v_{as}(P-OH in $H_2P_3O_{10}$)
			1060	v_s(P-OH $H_2P_3O_{10}$)
			1029	v_s(P-O in terminal PO_3)
			1002	v_s(P-OH)
			975	v_{as}($P_2O_7^{4-}$)
			905	v_{as}(P-O-P)
Trimetaphosphate	6-9		1260	v_{as}(P-O)
			1150	v_s(P-O)
			1086	v_s(P-O)
			1002	v_b(P-O)
			902	v_{as}(P-O-P)
Hexametaphosphate	6-9		1260	v_{as}(P-O)
			1115	v_s(P-O)
			1090	v_{as}(P-O)
			1030	v_b(P-O)
			1008	v_b(P-O)
			882	v_{as}(P-O-P)
			868	v_s(P-O-P) in long chain

Note: v_{as} – asymmetric stretching vibration

v_s - symmetric stretching vibration

v_b – bending vibration

Lower lead release in the presence of cyclophosphates (TrimetaP and HexametaP) compared to linear polyphosphate (TripolyP) can likely be explained by fundamental chemistry. First, TripolyP (5 oxygens) has more available reactive oxygen sites than TrimetaP (3 oxygens) (Rashchi & Finch, 2000). Although HexametaP (6) has more reactive oxygen sites on a molar basis than TripolyP, at equal mass concentrations, as in our study, TripolyP would supply a greater number of reactive oxygen sites, resulting in the higher lead concentrations observed in the CTSR. Secondly, while TrimetaP would be more ionized than TripolyP (Gosselin & Coghlan, 1953), the greater flexibility (relative freedom of molecules to move, entangle, and disentangle) of TripolyP more easily allows metal ions to be fitted into its structure while cyclophosphates are sterically inhibited from assuming all possible configurations, reducing their interaction with metal ions (Miyahima et al., 1981). Furthermore, longer chains allow for greater flexibility in the polymer bonds and metal incorporation into the polyphosphate structure (Miyahima et al., 1981). The increased lead release with HexametaP compared to TrimetaP may be due to a combination of decreased ring strain and a greater number of reactive oxygen sites.

The interaction between lead carbonate and TripolyP may be regulated by the formation of bidentate or tridentate complexes with ionized terminal PO_3^- or when the middle phosphate group is also bound (Lambert & Watters, 1957; Rashchi & Finch, 2002). This is seen via the vibration bands at 1108-1115 (Michelmore et al., 2000) and 1205 cm^{-1} (Guan et al., 2005) respectively (Figure 12). However, IR spectra suggest that not all phosphate groups were bound to the lead surface, as indicated by the presence of unbound P_2O_7 (967-975 cm^{-1}) (Wan et al., 2020) possibly allowing for further lead complexation.

TrimetaP bonds with lead via OPO_3^- groups, seen in the increased vibration frequency at 1159 (v_s P-O) and 1268 cm^{-1} (v_{as} P-O) (Socrates, 2004). Steric conformation of cyclophosphate is suggested via the shift in vibration bands, indicating the lengthening and shortening of the P-O-P (902 to 874 cm^{-1}) and P-O bonds (1002 to 1010 cm^{-1}), respectively (Figure 6). Compared to TrimetaP in solution, the vibration band at 1088 cm^{-1} (v_s P-O) did not shift positions suggesting that some phosphate groups in TrimetaP are sterically inhibited from interacting with the lead surface. Moreover, the intensity of the bands at 1008 (v_b P-O), 1086-1090 (v_s P-O), and 1268 cm^{-1} (v_{as} P-O) are larger in spectra representing TrimetaP than in those representing HexametaP, possibly caused by the binding of more phosphate groups per polyphosphate molecule with the lead carbonate surface (Figure 12).

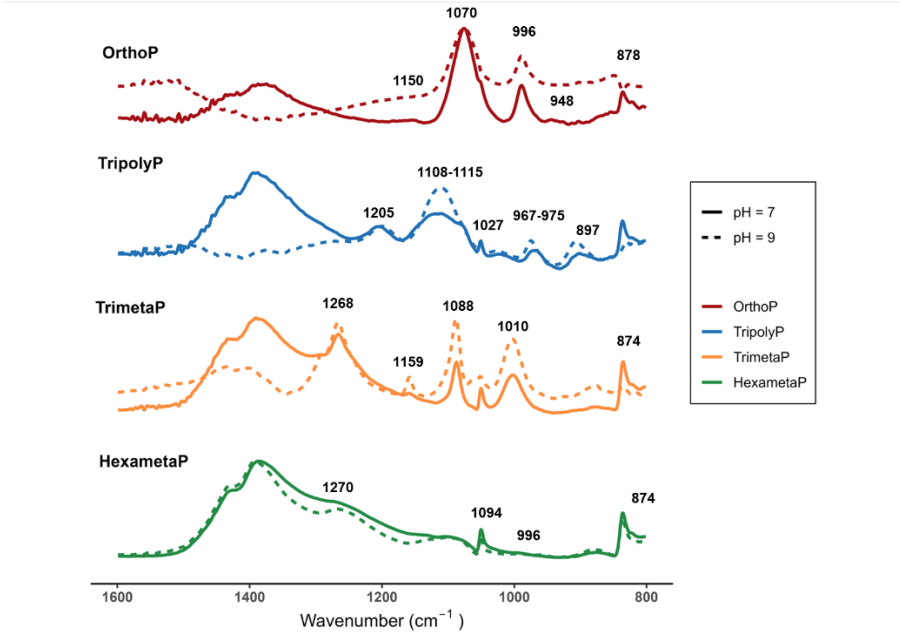

Figure 12 ATR-FTIR spectra of adsorbed phosphates as a function of pH (7 or 9) and phosphate type (OrthoP, TripolyP, TrimetaP, HexametaP) at DIC 5 mg C L^{-1} from the batch experiment. All ATR-FTIR spectra were recorded in a DIC 5 mg C L^{-1} electrolyte solution.

4.4.3.3. Orthophosphate-polyphosphate blends

Using mineral formation and lead dissolution results from the CSTR, along with the zeta potential data and ATR-FTIR spectra from batch experiments, the proposed mechanisms for blended phosphate interactions with lead carbonate are as follows: First, the less pronounced imparted negative charge with orthophosphate-polyphosphates than polyphosphates alone, as well as the presence of IR peaks belonging to both adsorbed OrthoP and polyphosphates, suggests that both phosphate species simultaneously interact with the lead (II) carbonate (Figure 13a,b). Second, the formation of lead-polyphosphate complexes is expected to keep free lead concentrations low, resulting in decreased hydroxypyromorphite formation and increased lead solubility.

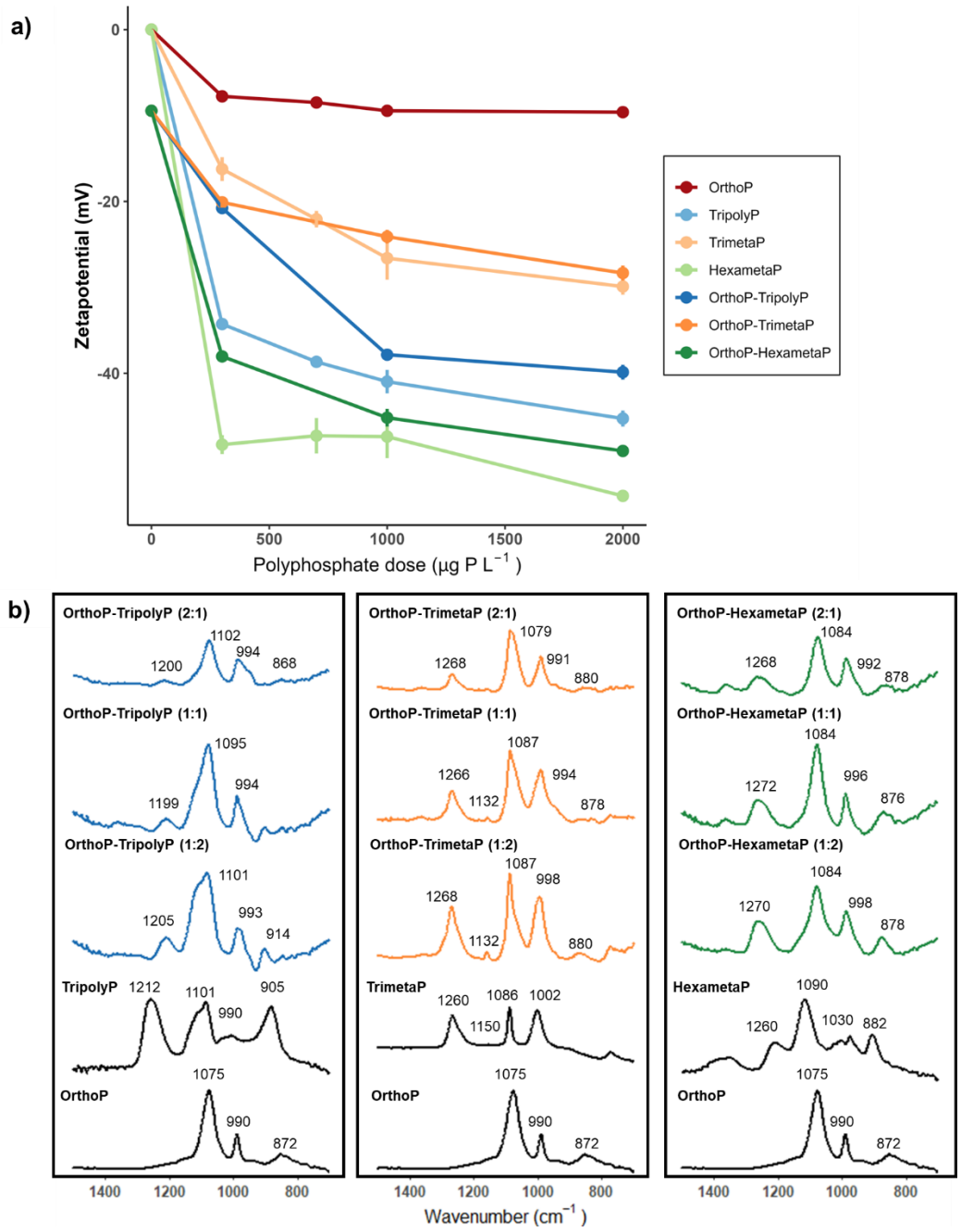

Figure 13 (a) Zetapotential and (b) ATR-FTIR spectra of adsorbed orthophosphate, polyphosphates, and orthophosphate-polyphosphates at pH 7. Orthophosphate:polyphosphate ratios are presented in brackets. Reference ATR-FTIR spectra of free orthophosphate and polyphosphate solutions are presented as solid black lines. All ATR-FTIR spectra were recorded in a DIC 5 mg C L^{-1} electrolyte solution.

FTIR data from the batch experiments suggest that polyphosphates interferes with OrthoP adsorption to the lead carbonate surface. This is supported by a comparison of phosphorous and phosphate adsorption (Figure 14a,b), quantified as the difference between the influent and effluent concentrations. Supplementary experiments (Appendix B) showed that polyphosphate hydrolysis to OrthoP was expected to be less than 10% within the 30 min reaction time in solutions at pH 7.0 and a DIC of *5* mg C L^{-1}. Therefore OrthoP (from phosphoric acid) is the dominant source of PO_4 adsorbed after the 30 min reaction. Polyphosphate loss (adsorption + precipitation) to lead carbonate increased while—in the case of TrimetaP and HexametaP—OrthoP loss decreased with increasing polyphosphate concentrations.

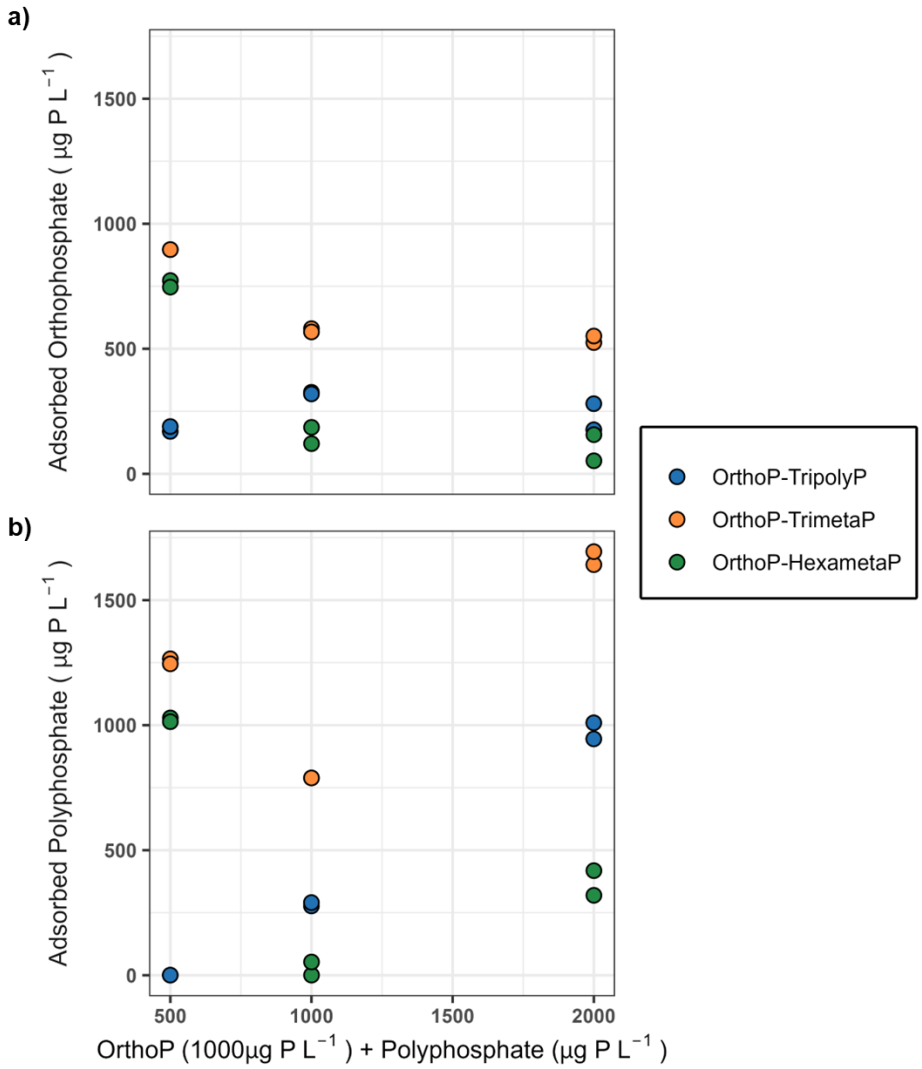

Figure 14 Loss of (a) orthophosphate and (b) polyphosphate at pH 7 from the batch reactors as a function of polyphosphate concentration (500-2000 µg P L^{-1}). The solutions contained 1000 µg P L^{-1} orthophosphate and 5 mg C L^{-1} DIC.

IR spectra suggest that OrthoP (~850-888 and 990-998 cm^{-1}) was adsorbed to lead (II) carbonate in all blends (Figure 14b). In tests with cyclophosphate blends, increases in the peak intensities at 1260-1272 cm^{-1} are consistent with competitive adsorption of cylcophosphates. However, more TrimetaP than HexametaP or TripolyP was lost to the lead (ii) carbonate (Figure 14a).

Moreover, the increase in peak intensities corresponding to TripolyP at 1095-1102 and 1199-1205 cm^{-1} as well as the disappearance of the OrthoP peak at 888 cm^{-1} suggests that more TripolyP than OrthoP was present on the lead (ii) carbonate surface at the 1:2 ratio. This was supported by the 8.8 ± 2.5% decrease in the proportion of adsorbed phosphorous as OrthoP when TripolyP was increased from 1000 (1:1) to 2000 μg P L^{-1}(1:2).

When lead (II) carbonate starts to dissolve, Pb^{2+} is released from the surface into aqueous solution. Pb^{2+} ions may either form complexes with polyphosphate, adsorb to the lead carbonate surface, or precipitate with other anions (e.g., PO_4) at or away from the surface (Figure 15). Precipitation may result in a different surface layer, possibly cerussite, hydrocerussite, or hydroxypyromorphite, forming. While OrthoP is expected to reduce lead release by forming hydroxypyromorphite, polyphosphates compete with OrthoP for lead binding sites. As binding sites on the lead (II) carbonate fill with adsorbed polyphosphates, vacant sites may be more difficult to access by free polyphosphates due to a combination of electric repulsion and structural interference from neighboring phosphate-filled sites. This was reflected by comparing the cyclophosphate blends: There was a -20.7 ± 1.4 mV change in surface charge and a 10.7 to 30.8% decrease in adsorbed phosphorous between blends of OrthoP with TrimetaP than HexametaP. The amount of dissolved lead increased with polyphosphate concentration.

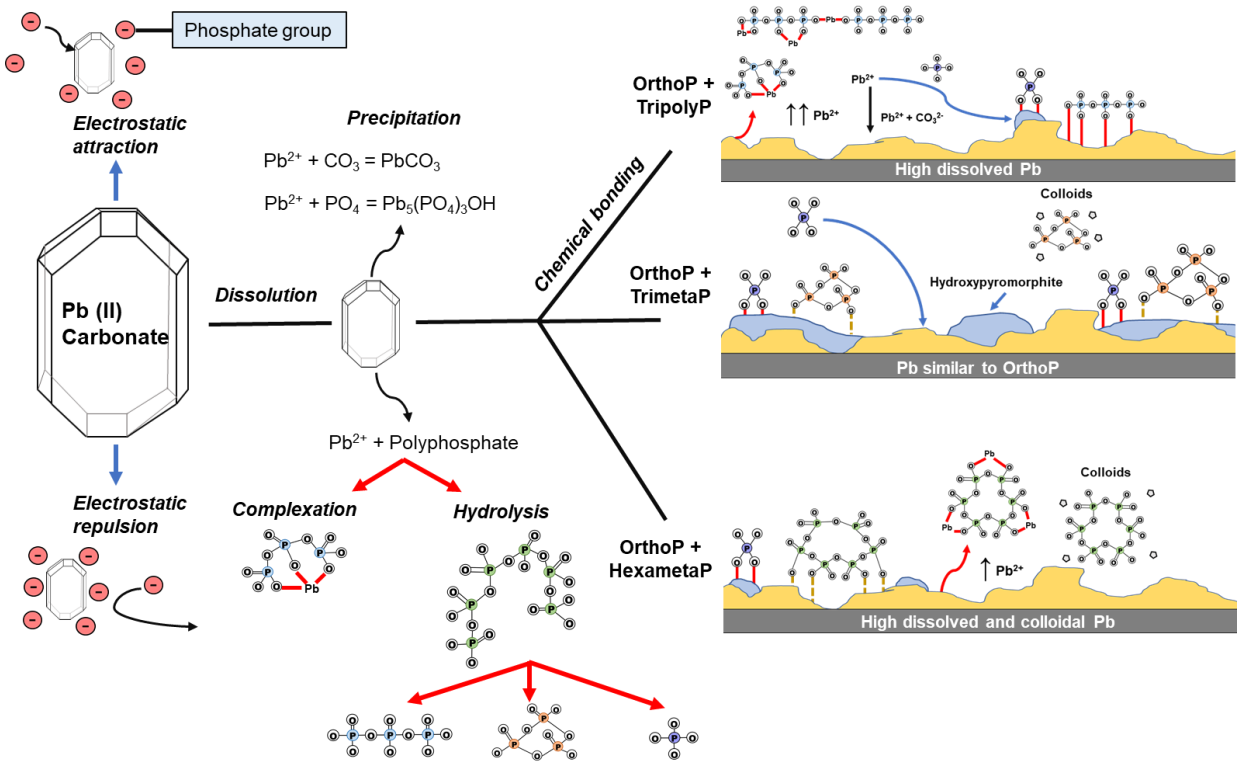

Figure 15 Schematic representation of phosphate-lead interaction mechanisms. Bonding information was sourced from Michelmore et al., 2000, and Rashchi and Finch, 2002.

4.5. Conclusion

Despite decades of use, significant knowledge gaps concerning corrosion control with blended phosphates remain. This study explored the effect of polyphosphate structure —in blended formulations with orthophosphate—on lead release and mineral formation, removing the uncertainties associated with proprietary blend formulations. Orthophosphate-polyphosphate blends made using either linear or cyclophosphates were compared against orthophosphate alone, reaching the following conclusions:

- TripolyP had greater lead-binding capacity than TrimetaP (1.00 vs 0.07 $mol_{Pb}/mol_{polyphosphate}$, respectively). The longer chain length cyclophosphate, HexametaP (1.6.0-2.1.0 $mol_{Pb}/mol_{polyphosphate}$), bound more lead than either TrimetaP or TripolyP.

- Blending OrthoP and TrimetaP resulted in the lowest lead release among the orthophosphate-polyphosphate blends. Blending trimetphosphate with orthophosphate had minimal impact on lead release compared to orthophosphate alone.

- The application of TripolyP or HexametaP exacerbated the amount of dissolved and small colloidal lead. OrthoP-HexametaP treatment increased small colloid concentrations by 124.0 (119.4-131.7) and 980.0 (831.3-1102) µg $Pb_{0.2\text{-}0.45\mu m}$ m^{-2} at the 1:1 and 1:2 ratios, and yielded a high proportion of colloids (26 and 49% for 1:1 and 1:2 ratio, respectively) at 24HS. Whereas OrthoP-TripolyP increased colloidal lead by 173.7 (144.9-190.8) µg $Pb_{0.2\text{-}0.45\mu m}$ m^{-2} only at the1:2 ratio. However, colloidal lead only accounted for 10% of total lead release at 24HS.

- Polyphosphate inhibited formation of hydroxypyromorphite. Lead-polyphosphate complexes may have kept the solution undersaturated with respect to the lead minerals present, resulting in higher lead release. This effect was more pronounced at higher polyphosphate concentrations.

This study provides insight into the interactions and subsequent release of lead associated with blended phosphate treatment. These findings will help us better understand the conditions that might result in higher dissolved or colloidal lead as well as the formation of lead corrosion scale.

OrthoP-TrimetaP blends may be a promising solution for simultaneous corrosion control and sequestration but further investigation on their ability to mitigate aesthetic water quality is needed.

5. Chapter 5 Blending orthophosphate with polyphosphate or sodium silicate: Effects of sequestrant type and polymer structure on iron corrosion and manganese sequestration

5.1. Abstract

Corrosion inhibitors for drinking water usually comprise a blend of orthophosphate—an effective inhibitor of lead and copper corrosion— with polyphosphate or sodium silicate. Polyphosphate and sodium silicate are used widely to prevent water discoloration, but less is known about their impact on iron corrosion. Moreover, the proprietary nature of blended inhibitors makes it difficult to understand their effects on the distribution system.

Here, the effect of orthophosphate, polyphosphate, sodium silicate, and blends of these additives on: (1) discoloration due to iron and manganese precipitation, (2) manganese deposition on iron, and (3) iron release from coupons were investigated.

Compared to orthophosphate alone (710 μg Fe_{Total} L^{-1}), adding 12 mg SiO_2 L^{-1} to orthophosphate was the most effective, decreasing color and iron corrosion by 68 pt-co and 477 μg Fe_{Total} L^{-1}, respectively. When blended with orthophosphate, trimetaphosphate, hexametaphosphate, and tripolyphosphate performed similarly to orthophosphate for reducing color. Orthophosphate- did not increase iron release However, blends with tripolyphosphate or trimetaphosphate increased iron release by 1621 and 1571 μg Fe_{Total} L^{-1}, respectively.

While Mn accumulation on the iron coupon was inhibited by the sequestrants, Mn deposits decreased colloidal (<0.45 μm) iron release by 177 and 83 μg $Fe_{0.45\mu m}$ L^{-1} in hexametaphosphate or silicate blends, respectively. Blends with short chain polyphosphates- tripolyphosphate and trimetaphosphate- were the most effective for sequestering manganese. Both polyphosphates and silicate lost sequestering capacity over time due to depolymerization.

5.2. Introduction

Although water leaving the water treatment plant is typically within the healthy standards for potable water, its quality can deteriorate as it travels through the distribution system (WDS). Therefore, the interaction between the pipe surface and bulk water are crucial to maintaining drinking water quality.

Iron pipes comprise a large proportion, up to 67 %, of distribution systems (American Water Works Service Co, 2004). The corrosion of iron pipes and the subsequent formation of corrosion scale could serve as a sink for organic (e.g biofilm) and inorganic contaminants (e.g. manganese) (Peng et al., 2010, 2012). Inorganic contaminants, present only in trace amount in treated water, can accumulate in pipe scale where their concentration can be several orders of magnitude greater than in bulk water (Peng et al., 2010, 2012). Iron species found in corrosion scale including goethite (α-FeOOH), lepidococite (γ-FeOOH), magnetite (Fe_3O_4), hematite (Fe_2O_3) and ferrihydrrite ($Fe_{10}O_{14}(OH)_2$) (Peng et al., 2010; Sarin P. et al., 2004) can have strong affinity for trace inorganic elements (Nelson et al., 1995; O'Reilly et al., 2001). Manganese oxides are also commonly found in pipe deposits where there is residual

manganese in treated water. The higher surface area and lower isoelectric point of manganese oxides (Trivedi et al., 2001) can result in higher adsorption capacity than iron oxides (Green-Pedersen et al., 1997; McKenzie, 1980).

Corrosion scale rich in iron and manganese can be resuspended by numerous factors, including changes in water chemistry or hydraulic disturbances (Boxall et al., 2003; Polychronopolous et al., 2003; Seth et al., 2004). This may result in aesthetic water quality complaints, such as discoloration, that can be difficult to address and negatively impact consumer confidence in water safety. Colored water can be due to the presence of suspended fine particles (Polychronopolous et al., 2003; Seth et al., 2004).

Sequestrants, like polyphosphates or sodium silicate, can be used to mitigate aesthetic Fe and manganese issues in the distribution system. A major drawback to using polyphosphate or silicate sequestrants is their ability to mobilize regulated heavy metals like lead (B. Li, Trueman, Munoz, et al., 2021a; Trueman et al., 2018b). While sequestration does not reduce iron or manganese concentrations in bulk water, it inhibits their precipitation for a period of time, ideally longer than the retention time in the distribution system. Polyphosphates form complexes with metal ions, the strength of which is dependent on polyphosphate structural properties (Rashchi & Finch, 2000). Most sequestration studies with sodium silicate have predominantly focused on its impact on Fe precipitation (Dart & Foley, 1970; B. Li et al., 2019; Robinson et al., 1992). Sodium silicate inhibits the oxidation of Fe(II) through outer-sphere complexation of Fe(II) to silicate-ferrihydrite and may inhibit the crystallization of iron oxides

(Kinsela et al., 2016; B. Li et al., 2019). However, they may not be as effective for sequestering Mn (Robinson et al., 1992).

Utilities may use blends of orthophosphate and sequestrants to simultaneously manage aesthetic water quality and corrosion control: orthophosphate protects against lead and copper corrosion while the sequestrant prevents iron and manganese precipitation. However, little is known about how they impact concentration and properties of metals released and scarce information is available on multi-contaminant interactions between iron and manganese in the presence of blended phosphates.

Currently there is no simple guidance for the selection of a blended product for a given case, as product formulations are proprietary and dosage choices still are largely based on experience.

The objectives of this study were to

(1) Evaluate the effect of orthophosphate blended with polyphosphate- tripolyphosphate, trimetaphosphate, or hexametaphosphate- or sodium silicate on iron and manganese precipitation;

(2) Identify the impact of sequestrant type on manganese accumulation on corroded iron surfaces;

(3) Investigate the impact of orthophosphate-polyphosphate and orthophosphate-silicate blends on iron release from coupons.

5.3. Materials and Methods

5.3.1. Preparation of solutions

Ultrapure water (18.2 MΩcm, TOC < 2 μg L^{-1}) was used to prepare all solutions in this study. Solution composition was chosen to reflect drinking water conditions with low inorganic carbon content. All chemicals were reagent grade. Sodium hexametaphosphate ($(NaPO_3)_6$) (Alfa Aesar, Haverhill, MA), sodium trimetaphosphate ($(NaPO_3)_3$) (Alfa Aesar, Haverhill, MA), and sodium tripolyphosphate ($Na_5P_3O_{10}$) (Alfa Aesar, Haverhill, MA) were used to represent different polyphosphate structures. Polyphosphate or sodium silicate (3.22:1 NaO:SiO_2,PQ, USA) stock solutions were obtained by dissolving tripolyphosphate, trimetaphosphate, hexametaphosphate, or silicate in 100 mL ultrapure water, before each experiment. Orthophosphate was added as ACS grade phosphoric acid (Fisher Chemical, Fairlawn, NJ). The dissolved inorganic carbon was added as sodium bicarbonate powder (Fisher Chemical, Fairlawn, NJ). The pH was adjusted by the addition of 1N trace metal grade nitric acid (Fisher Chemical, Fairlawn, NJ) or freshly prepared 2N sodium hydroxide (Fisher, Fairlawn, NJ). Sodium hypochlorite (NaOCl) was used to provide a free chlorine residual of 1 mg L^{-1}. Iron (II) and manganese (II) were added as $FeSO_47H_2O$ (Fisher Chemical, Fairlawn, NJ) and $MnSO_4H_2O$ (Fisher Chemical, Fairlawn, NJ), respectively. All solutions were freshly prepared and used immediately.

5.3.2. Precipitation experiments

The intent was to simulate conditions similar to the distribution system wherein Fe(II) is released from pipe wall or Mn(II) from source water is oxidized. The particle formation approach used in this study is also representative of drinking water conditions wherein a chemical sequestrant is added to prevent particle precipitation. A diagram of the experimental set-up can be found in Appendix C. Experiments were performed in 500 ml Erlenmeyer flasks (Figure 25a). A background solution containing 5 mg C L^{-1} (0.42 mM) DIC were prepared at pH either 7.5 or 8.5 and 21 $\pm$ 2 ∘C. Freshly prepared iron (II) and manganese (II) sulfate solutions were added to achieve the target concentrations of each experiment. Iron and manganese particles were generated by reacting Fe(II) and Mn(II) with dissolved oxygen (~9 mg O_2 L^{-1}) and NaOCl to a target free chlorine residual, after 24 h, of 1 mg Cl_2 L^{-1}. Samples were mixed at 150 rpm and kept in the dark for 24 or 120 h. The pH was measured and adjusted to the target pH every 15 minutes for the first 4 h. Each run was duplicated at a minimum.

5.3.2.1. Iron or Manganese precipitation

The ability of sodium silicate (5-120 mg SiO_2 L^{-1}, 80-1920 μM) and three polyphosphates (5-20 mg P L^{-1}, 160-640 μM) to reduce iron and manganese precipitation at pH 7.5 was evaluated with a batch experiment. Manganese or Iron were added at 1 mg L^{-1} (18 μM). At the end of the 24 h hydraulic retention time (HRT), aliquots were extracted and sampled for true and apparent color, and phosphate. The reactors were re-sealed and set to mix for 120 h then re-sampled to determine the long-term effect of the sequestrants.

5.3.2.2. Iron and Manganese co-precipitation

Iron (II) and manganese (II) were added at 5000 μg Fe L^{-1} (90 μM) and 500 μg Mn L^{-1} (9 μM), respectively. Total concentrations are on the higher end of measured concentrations in some waters (Ahmad et al., 2019) but were chosen to enable sufficient particle generation to allow for measurements of different size fractions. Using a full factorial (2^2) design with centre points, the formation of colloidal iron and manganese in the presence of three polyphosphate blends at equivalent orthophosphate to polyphosphate concentrations (orthophosphate = 300 μg P L^{-1}, polyphosphate = 300 μg P L^{-1})- orthophosphate-tripolyphosphate, orthophosphate-trimetaphosphate, and orthophosphate-hexametaphosphate- and an orthophosphate-silicate blend (Orthophosphate = 300 μg P L^{-1}, silicate = 12 mg SiO_2 L^{-1}) were evaluated against orthophosphate (300 μg P L^{-1}) alone at two pH (7.5 or 8.5). Samples were collected for analysis at the end of the 24 h reaction period.

5.3.3. Iron corrosion cells

A diagram of the experimental set-up can be found in Appendix C. New iron coupons (76 × 13 × 1.5 mm^3, BioSurface Technologies Corp.) were polished with 400 grit sandpaper (3M Pro grade Precision) then soaked in a pH <2 HNO_3 solution for 1 h. They were re-polished then hung vertically in a 240 mL Polyphenylene Ether (PPE) bottle at a depth of 40 mm from the water surface (Figure 25b). The coupons were immediately immersed in 200 mL solutions at varying water quality to simulate the exposure of iron pipes at relevant drinking water conditions. Iron corrosion was evaluated in the presence of in the presence of three polyphosphate blends at equivalent orthophosphate to polyphosphate concentrations (orthophosphate = 300 μg P L^{-1},

polyphosphate = 300 μg P L^{-1})- Orthophosphate-tripolyphosphate , orthophosphate-trimetaphosphate , and orthophosphate-hexametaphosphate- and an orthophosphate-silicate blend (orthophosphate = 300 μg P L^{-1}, silicate = 12 mg SiO_2 L^{-1}) against orthophosphate (300 μg P L^{-1}) alone at pH 7.5. All solutions contained 0.42 mM DIC, with a free chlorine residual at the end of 24 hrs of 1 mg L^{-1} and temperature of 21 $\pm$ 2 ∘C. Solutions were replaced daily. Prior to sampling, solutions were left to stagnate for 24 h. The pH, dissolved oxygen, free chlorine did not vary by more than 0.23, 0.07 mg L^{-1}, and 0.18 mg L^{-1}, respectively. All experiments were duplicated. Coupons were conditioned for 70 hydraulic retention times (HRT) prior to obtaining a baseline iron measurement (HRT 80-140). Manganese (1000 μg L^{-1}) was then added and the coupons were conditioned between HRT's of 140-230.

To examine the impact of blended phosphates on small colloid formation and mobility, stagnated suspensions were passed through a 0.45 μm cellulose nitrate membrane prior to analysis with asymmetrical flow filed flow fractionation (A4F). To minimize adsorption, the first 10 mL of each aliquot was filtered to waste, then next 10 mL was collected into a polypropylene tube.

5.3.4. Analytical Methods

Turbidity was measured with a TL2350 turbidity meter (Hach, Loveland, CO). Color was measured using the platinum cobalt method (DR 5000, Hach, Loveland, CO). True color was measured on 0.1 µm filtrate. Free chlorine was measured using the N, N-diethyl-p-

phenylenediamine method (DR 5000, Hach, Loveland, CO). Dissolved oxygen was measured with a dissolved oxygen meter (Thermo Orion, UK).

Metals were quantified by inductively coupled plasma-mass-spectrometry (ICP-MS, iCAP-RQ, Thermo Fisher Scientific, Waltham, MA) using Standard Methods 3125 and 3030(American Public Health Association, American Water Works Association, Water Environment Federation, 2012). Reporting limits for iron, manganese, silica, and phosphorous were 7, 0.8, 18, and 4.9 μg L^{-1}, respectively. Small colloidal metals were defined as passing through 0.45 μm membrane. Filter membranes were decontaminated with dilute HNO_3, washed with 10 mL of ultrapure water, then 10 mL of sample was passed through to waste to minimize adsorption. Samples were acidified to pH <2 with concentrated trace metal grade HNO_3 and held for a minimum of 24 h, at room temperature, before analysis. Dissolved phosphate (PO_4) concentrations were measured using EPA 300.1 (US EPA, 1997) via Ion Chromatography (Dionex Aquion IC with AS22 column, Thermo Fisher Scientific, MA) with a reporting limit of 10 μg L^{-1} phosphate.

For examination by transmission electron microscopy (JOEL 1230 TEM), 50 μL of sample was deposited in 10μL increments on a TEM grid (Formvar/Carbon FCF200) and drawn through the grid with filter paper. TEM grids were stored in a desiccator until analysis. Particle sizes were measured via dynamic light scattering (Zetasizer NS, Malvern Instruments, Worcestershire, UK).

Colloidal metals in the iron coupon effluent were characterized via A4F (Post Nova AF2000 Multiflow, Germany) with a 300 Da poly(ethersolfone) membrane described in Trueman *et al.*

(2022). The system was coupled sequentially with a UV absorbance detector at 254 nm, and an ICP-MS. The details of the A4F method are summarized in Appendix C.

5.3.5. Data Analysis

R version 4.2 (R Core Team, 2022) and a collection of contributed packages (Allaire et al., 2022; Trueman, 2022; Wickham et al., 2019) was used for data analysis and graphical representation. Effect sizes of experimental factors were calculated as described by MacBerthouex and Brown (1996).

5.4. Results and Discussion

5.4.1. Particle aggregation and sequestration

The effect of sequestrants without orthophosphate on color due to iron or manganese was evaluated in $NaHCO_3$ buffered water with a free chlorine residual of 1 mg L^{-1} (Figure 16). At an approximate sequestrant to analyte molar ratio of 3:1 (P/Fe or P/Mn), polyphosphates were effective for reducing the average apparent color after 24 h, with a greater reduction in manganese (by 46-60 pt-co) than iron (by 23-37 pt-co).

At equivalent chain lengths, tripolyphosphate, the linear polyphosphate, was more effective than trimetaphosphate (cyclophosphate) for reducing color – average color due to iron or manganese was lower by 14 and 7.5 pt-co with tripolyphosphate than trimetaphopshate, respectively. Hexametaphophate, the larger cyclophosphate, was the most effective for both iron and manganese, reducing color by 60 and 37 pt-co, respectively. Aside from

hexametaphosphate, polyphosphates typically experienced increased color over longer retention times, possibly due to depolymerization (See Section 5.4.2).

Similar to previous studies (Robinson & Ronk, 1987), sodium silicate was more effective for reducing color due to Fe than Mn. Silicate at an approximate sequestrant to analyte molar ratio (SiO_2/Fe or SiO_2/Mn) of 3:1 reduced color in iron and manganese suspensions by 24 and 63 pt-co, respectively. Apparent color did not increase in iron suspensions after 120 h, that is color did not vary by more than 2.6 $\pm$ 2.1 pt-co between 24 and 120 h. However, the 42.6 $\pm$ 4 pt-co increase in apparent color but 25.8 $\pm$ 4 pt-co decrease in true color in manganese suspensions suggests that silicate may stabilize colloids rather than form dissolved complexes with manganese.

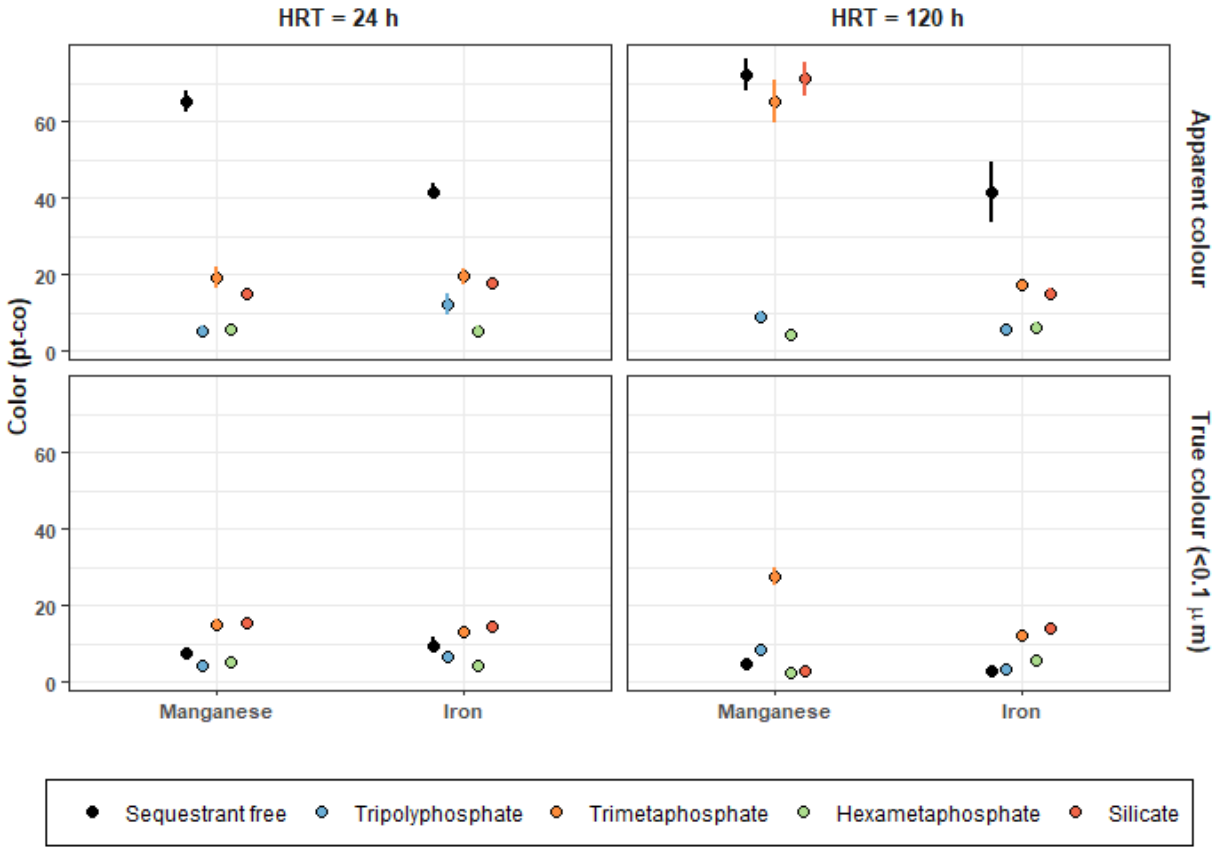

Figure 16 Effect of sequestrants- tripolyphosphate, trimetaphosphate, hexametaphosphate, and sodium silicate at an approximate sequestrant (P or SiO_2) to analyte (Fe or Mn) molar ratio of 3:1 - on true (<0.1µm) and apparent color due to iron or manganese (1 mg L^{-1}, 18 µM) after 24 and 120 h. The background electrolyte solution was buffered with $NaHCO_3$ (5 mg C L^{-1}) at a free chlorine residual of 1 mg L^{-1} and pH 7.5.

5.4.2. Loss of sequestration capacity due to depolymerization

The increase in color over time may be attributed to Fe and Mn catalyzed polyphosphate hydrolysis or the depolymerization of silicate. Increased polyphosphate hydrolysis may have resulted in the formation of iron or manganese-phosphate precipitates and the reduced amount of polyphosphate available for complexation. The hydrolysis of linear (i.e. tripolyphosphate) or longer chains (i.e. hexametaphosphate) is greater than that of cyclic or shorter chains (i.e. trimetaphosphate) (Wan et al., 2019, 2021). While hexametaphosphate

did partially hydrolyze into orthophosphate, it did not exhibit an increase in color after 120 h. Hexametaphosphate contains more reactive oxygen sites for binding with metal ions, which could explain lower color observations. This result highlights that polyphosphate structure, more than concentration may be a strong determinant for successful sequestration.

The relatively poor performance of silicate may be due to a combination of its loss of effectiveness due to depolymerization as well as the slow oxidation of manganese by chlorine (Robinson & Ronk, 1987). Silicate can depolymerize and lose its effectiveness within 24 h (Robinson & Ronk, 1987) leading to the worse results after 120 h. Additionally, manganese precipitates would be negatively charged at pH 7(Gray et al., 1978) and hinder its interaction with anionic silicate.

5.4.3. Co-precipitation of Iron and Manganese

An extended study was conducted to investigate the impacts of blending orthophosphate with polyphosphate or silicate on the precipitation of Fe(II) and Mn(II). Orthophosphate treatment (OP = 300 μg P L^{-1}) at pH 7.5 was used as the reference condition, which produced an apparent color of 200.3 $\pm$ 17.8 pt-co. At pH 7.5, blending orthophosphate with silicate reduced apparent color by -68 pt-co (95% CI: -49 to -76 pt-co), the largest reduction among all the blends (Figure 17). Meanwhile, blends of orthophosphate and hexametaphosphate (by -25 pt-co, 95% CI: -15 to -34 pt-co), trimetaphosphate (by -18 pt-co, 95% CI: -13 to -22 pt-co), or tripolyphosphate (by -21 pt-co, 95% CI: -12 to -30 pt-co) produced similar reductions in color. Increasing pH to 8.5 did

not have significant impacts on apparent color, varying by only 2.3 pt-co (95% CI: -2.1 to 2.8 pt-co) from pH 7.5.

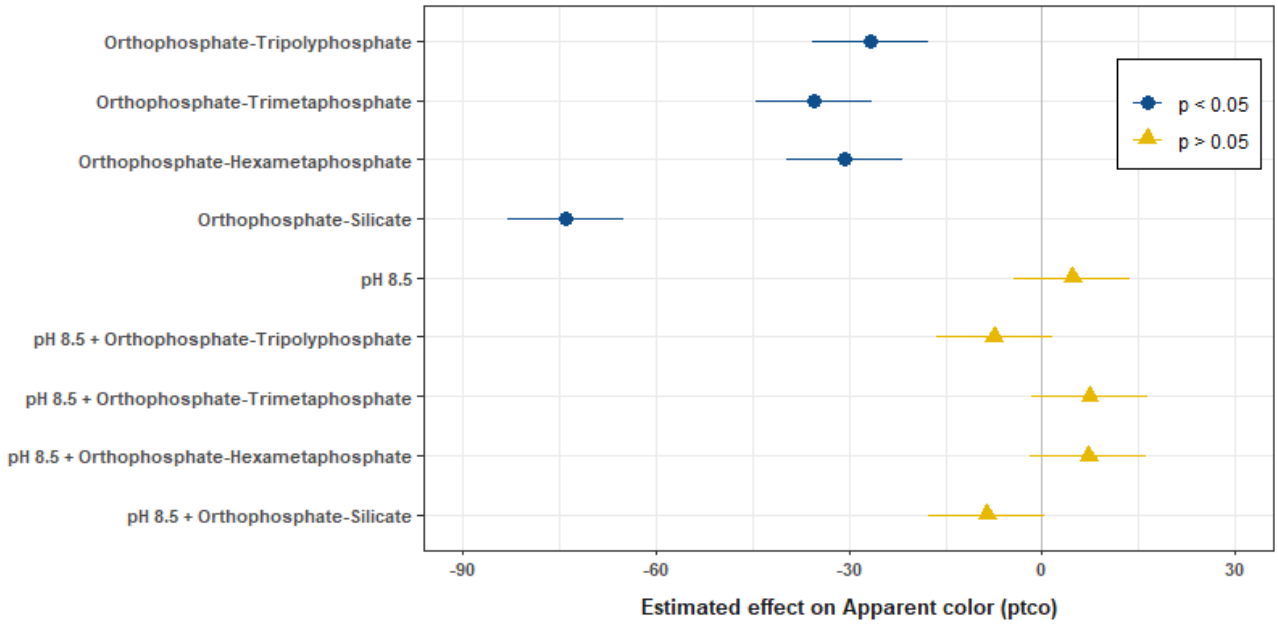

Figure 17 Estimated effects of sequestrants and pH on color. Points indicate the effect sizes and error bars span the 95% confidence interval.

5.4.3.1. Particle size and composition

Orthophosphate treatment was not effective as sequestering Fe or Mn (87.8% and 93.5% removal of Fe and Mn from solution, respectively) at this concentration and produced large particles with a fraction of solid-phase manganese to iron (Mn_{mol}/Fe_{mol}) of 0.112 mol/mol (Table 8). Adding a sequestrant produced smaller colloids (0.1-0.45 μm) in suspension and reduced the amount of phosphorous present in the precipitate (Table 8).

Orthophosphate-tripolyphosphate produced smaller colloids (169.6 nm, 0.126 mol/mol) with a higher solid-phase Mn/Fe than orthophosphate-trimetaphosphate (345 nm, 0.107 mol/mol).

While orthophosphate-hexametaphosphate was not effective at preventing their precipitation, it was effective at reducing particle size (252 nm). Hexametaphosphate molar concentrations were only half of tripolyphosphate or trimetaphosphate which may have resulted in its poorer performance for preventing precipitation. In contrast to silicates alone, orthophosphate-silicate was the most effective for sequestring manganese. Orthophosphate-silicate treatment resulted in both the smallest particles and lowest solid-phase ratio (112.5 nm, 0.07 mol/mol).

The larger surface area of smaller iron colloids available for manganese adsorption should have resulted in higher manganese residuals with orthophosphate-silicate suspensions. However, the species of iron oxides formed may influence metals adsorption. The formation of poorly ordered Fe(III) precipitates via the oxidation of Fe(II) by HOCl or through the inhibition of crystal formation with phosphates and silicates seen here are concurrent with other studies (Ahmad et al., 2019; Jones et al., 2014; Kandori et al., 1992) (Figure 18). Needlelike particles were observed in the orthophosphate and orthophosphate-polyphosphate experiments. In orthophosphate-silicate systems, small spherical particles with low apparent crystallinity were seen instead. While, previous work has reported the enhancement of Mn(II) adsorption by phosphate or silicate, the pronounced effect with polyphosphates may be due to the formation of direct Mn(II)-O-P bonds on the iron oxide surfaces (Ahmad et al., 2019).

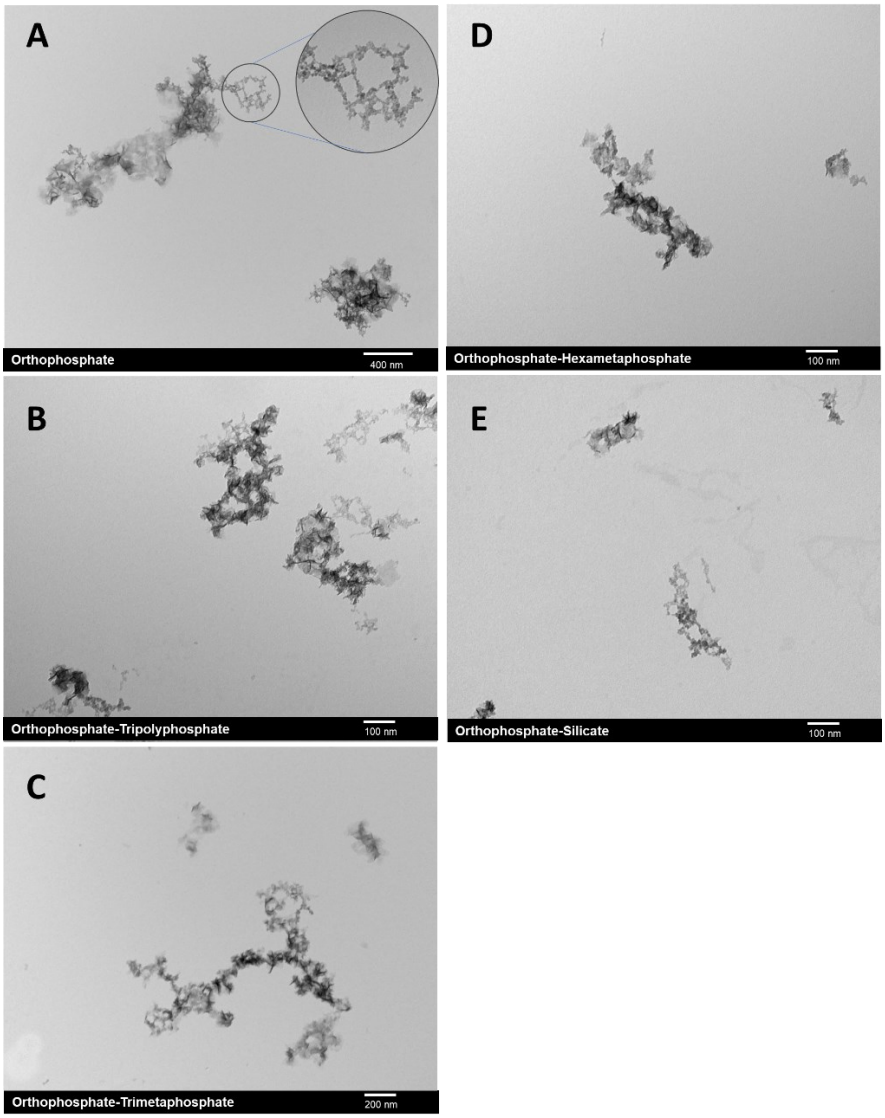

Figure 18 Transmission electron micrographs of iron (5 mg L^{-1}, 90 µM) and manganese (500 µg L^{-1}, 9 µM) particles formed after 24 h in NaHCO3 (5 mg C L^{-1}) buffered pure water systems at pH 7.5, free chlorine residual of 1 mg L^{-1}, and temperature of 21 ± 1 °C. (A) the reference system with orthophosphate (300 µg P L^{-1}, ~10 µM), (B) orthophosphate (300 µg P L^{-1}, ~10 µM) - tripolyphosphate (300 µg P L^{-1}, ~10 µM), (C) orthophosphate (300 µg P L^{-1}, ~10 µM) - trimetaphosphate (300 µg P L^{-1}, ~10 µM), (D) orthophosphate (300 µg P L^{-1}, ~10 µM) - hexametaphosphate (300 µg P L^{-1}, ~10 µM), and (E) orthophosphate (300 µg P L^{-1}, ~10 µM) - sodium silicate (12 mg SiO_2 L^{-1}, ~200 µM).

Table 8 Initial composition, Fe and Mn removed by filtration and solids ratio in co-oxidation experiment.

Experiment ID	**Initial solution composition**							**Hydrodynamic diameter (nm)**	**Fe and Mn removed by 0.45 µm filtration**				**Fe and Mn removed by 0.1 µm filtration**				**Solids Ratio**
	Fe	Mn	OP	TP	TM	HM	PS		Fe	Mn	P	Si	Fe	Mn	P	Si	>0.1 µm
	µmol L^{-1}								%				%				Mn/Fe
Orthophosphate (Ref)	90	9	10	0	0	0	0	953±88	87.8±24.2	90.9±26	70.5±19.2	NA	87.8±22.3	93.5±20.7	72.5±15.9	NA	0.112±0.006
Orthophosphate-Tripolyphosphate	90	9	10	10	0	0	0	169.6±15.7	29.3±12.1	49.3±9.6	24.3±1.2	NA	74.1±21	86.8±15.3	59.9±1	NA	0.126±0.007
Orthophosphate-Trimetaphosphate	90	9	10	0	10	0	0	345.1±25.3	74±1.4	75.5±0.8	20.4±1.7	NA	85.2±16.2	96.5±11.2	21.4±1.8	NA	0.107±0.003
Orthphosphate-Hexametaphosphate	90	9	10	0	0	10	0	252.33±6.7	59.4±17.2	85.7±2.5	37.1±3.6	NA	99.2±2.3	99.9±3	55.8±0.9	NA	0.122±0.002
Orthophosphate-Silicate	90	9	10	0	0	0	200	112.5±7.6	71±10	14.3±1.6	11.8±4.4	2.31±1.16	81.5±11	56.3±10.2	55.7±3	4.27±2.75	0.070±0.006

Table 9 Composition of corrosion scale from coupons.

Treatment	Cell 1								Cell 2							
	Fe		Mn		P		Si		Fe		Mn		P		Si	
	µg per g of scale	% by mass	µg per g of scale	% by mass	µg per g of scale	% by mass	µg per g of scale	% by mass	µg per g of scale	% by mass	µg per g of scale	% by mass	µg per g of scale	% by mass	µg per g of scale	% by mass
Orthophosphate (Ref)	909677	99.6	2594	0.28	1109	0.12	NA	NA	885143	99.6	2203	0.25	1246	0.14	NA	NA
Orthophosphate-Tripolyphosphate	690352	99.4	1942	0.28	2040	0.29	NA	NA	756104	99.5	2295	0.3	1660	0.21	NA	NA
Orthophosphate-Trimetaphosphate	627635	99.3	2006	0.32	2311	0.37	NA	NA	872008	99.3	3545	0.4	2921	0.33	NA	NA
Orthphosphate-Hexametaphosphate	870868	99.6	1831	0.21	1760	0.2	NA	NA	879232	99.3	2233	0.25	3800	0.43	NA	NA
Orthophosphate-Silicate	769215	99.1	2624	0.34	1053	0.14	7788	0.49	781440	98.8	3224	0.41	1322	0.17	9765	0.59

5.4.4. Phosphorus accumulation on Fe coupons in Mn-free systems

Although there was a decrease in total effluent phosphorous concentrations compared to the initial phosphorus dose in the iron corrosion cells (Figure 19), the discrepancy in phosphorus consumption behavior may be attributed to phosphate structural characteristics that impact their complexation with free iron ions or adsorption to the coupon surface.

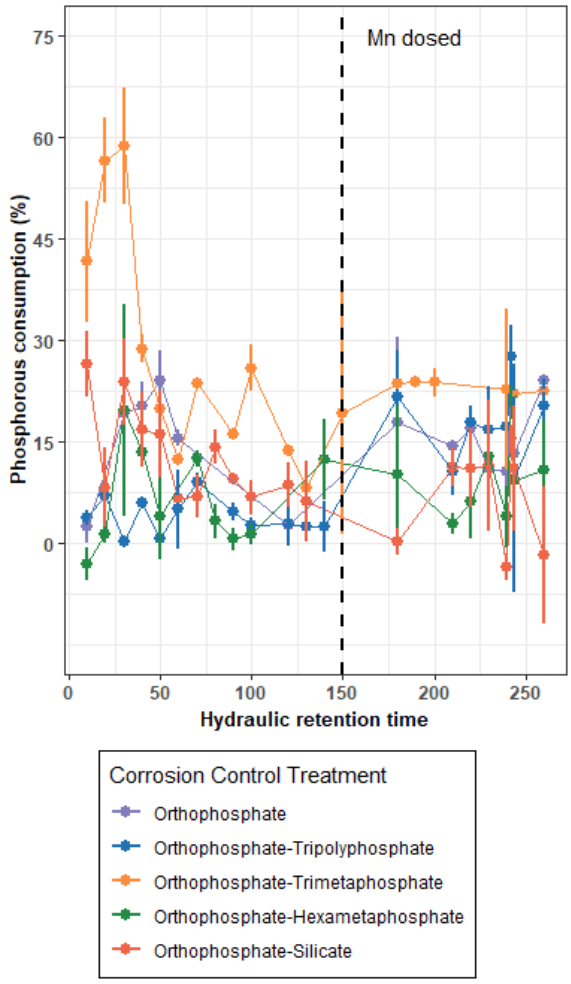

Figure 19 Residual phosphorous from the corrosion cells after 24 h in $NaHCO_3$ (5 mg C L^{-1}) buffered pure water systems at pH 7.5, free chlorine residual of 1 mg L^{-1}, and temperature of 21 ± 1 °C.): the reference system with orthophosphate (300 µg P L^{-1}, ~10 µM), orthophosphate (300 µg P L^{-1}, ~10 µM) - tripolyphosphate (300 µg P L^{-1}, ~10 µM), orthophosphate (300 µg P L^{-1}, ~10 µM) - trimetaphosphate (300

µg P L^{-1}, ~10 µM), orthophosphate (300 µg P L^{-1}, ~10 µM) - hexametaphosphate (300 µg P L^{-1}, ~10 µM), and orthophosphate (300 µg P L^{-1}, ~10 µM) - sodium silicate (12 mg SiO_2 L^{-1}, ~200 µM).

While most of the orthophosphate-tripolyphosphate remained in solution, phosphorus loss from solution with the other treatments increased until HRT 60 then began to decrease. Iron oxide corrosion products may have facilitated the initial accumulation of phosphorus on the coupon surface via their high sorption capacities (Herndon et al., 2019; Weng et al., 2012). In the case of orthophosphate-tripolyphosphate, tripolyphosphate's strong complexing ability may have, instead, produced soluble iron-phosphate complexes. This is supported by high concentrations of iron and phosphorus present in the 0.45 μm filtrate (Figure 20a).

With blends of orthophosphate and cyclophosphate, polymer chain length appeared to determine phosphorus adsorption by the iron coupon. The structural constraints associated with longer ring chains, may have limited hexametaphosphate's ability to conform around the corroded iron surface (Miyajima et al., 1981).

5.4.5. Mn accumulation on Fe coupons

Compared to the initial Mn dose (1000 μg Mn L^{-1}), the decrease of total Mn in solution reveals that it accumulates on the coupon surface (Figure 20b). Acid digestion of corrosion scale estimated the amount of Mn accumulation during the experiment (Table 9). Orthophosphate was predicted to accumulate 2.7 $\pm$ 0.25 mg Mn per g of scale. Compared to orthophosphate alone, blends with silicate or trimetaphosphate were predicted to increase Mn accumulation by 1 and 0.9 mg Mn per g of scale, respectively. However, it was not detected on the corroded iron surface via SEM-EDS.

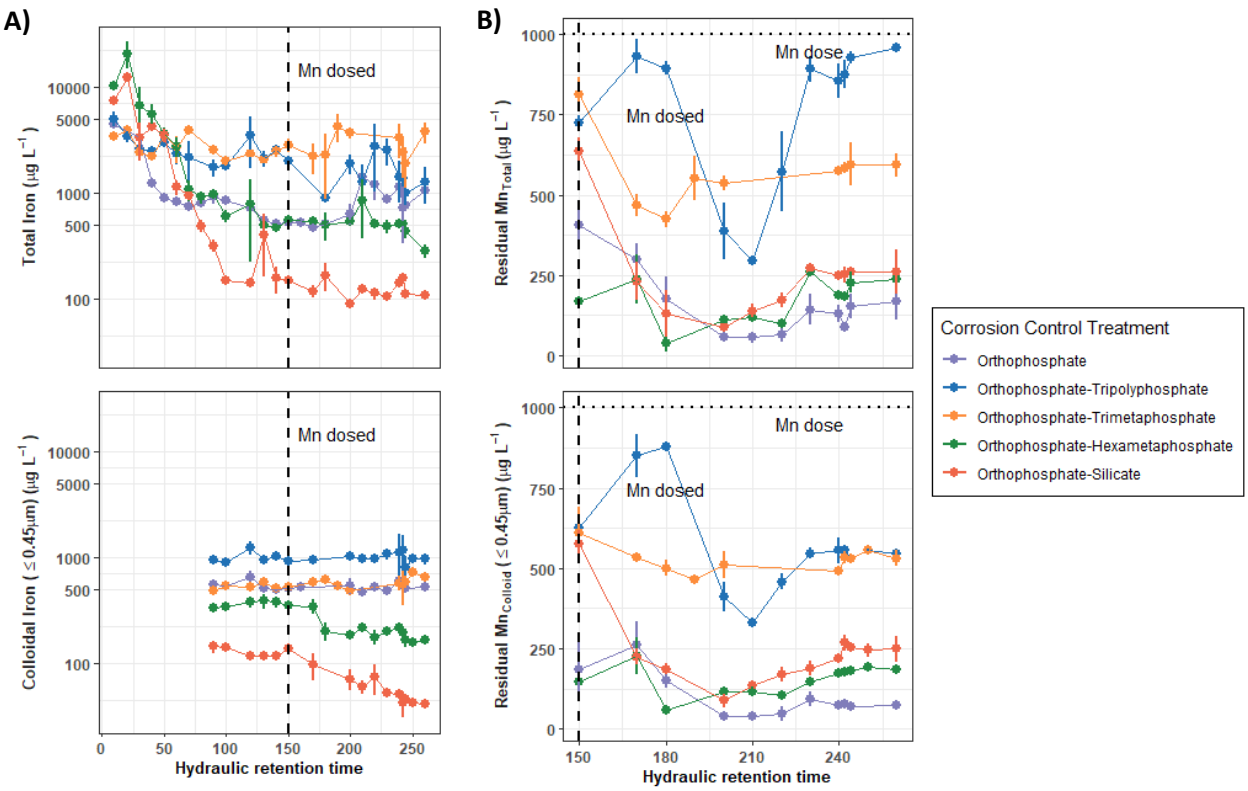

Figure 20 : Iron released (A) and residual manganese (B) from the corrosion cells after 24 h in $NaHCO_3$ (5 mg C L^{-1}) buffered pure water systems at pH 7.5, free chlorine residual of 1 mg L^{-1}, and temperature of 21 ± 1 °C. Manganese was added at 1 mg L^{-1} (18 µM): the reference system with orthophosphate (300 µg P L^{-1}, ~10 µM), orthophosphate (300 µg P L^{-1}, ~10 µM) - tripolyphosphate (300 µg P L^{-1}, ~10 µM), orthophosphate (300 µg P L^{-1}, ~10 µM) - trimetaphosphate (300 µg P L^{-1}, ~10 µM), orthophosphate (300 µg P L^{-1}, ~10 µM) - hexametaphosphate (300 µg P L^{-1}, ~10 µM), and orthophosphate (300 µg P L^{-1}, ~10 µM) - sodium silicate (12 mg SiO_2 L^{-1}, ~200 µM).

The lack of Mn accumulation on the surface may be due to its incorporation into layers of iron scale as it forms which is consistent with field observations (Cerrato et al., 2006). Iron corrosion products could facilitate manganese accumulation, possibly by enhancing the autocatalysis of adsorbed Mn^{2+} to form Mn oxides (Junta & Hochella, 1994). However, the rate of manganese adsorption declines after the initial phase (HRT = 190-220), likely due to the saturation of, or a

localized pH drop at the adsorption sites on iron corrosion scale due to Mn (II) adsorption (Buamah et al., 2008).

Here, orthophosphate was not effective for sequestring manganese. Between HRTs 240-260, 92.0 $\pm$ 1.2% of influent Mn was retained in orthophosphate treated reactors. Blends with hexametaphosphate or silicate showed limited effectiveness, with 17.9 $\pm$ 0.7% and 24.8 $\pm$ 6.8% of Mn remaining in the <0.45 μm filtrate, respectively. Blends with short chain polyphosphates were more effective and resulted in the highest Mn residuals in the <0.45 μm filtrate: 56 $\pm$ 5% and 54 $\pm$ 3.3% for tripolyphosphate and trimetaphosphate, respectively. However, the highest particulate Mn (357 $\pm$ 56 μg $Mn_{Particulate}$ L^{-1}) concentration was seen with orthophosphate-tripolyphosphate. This may be due to Mn adsorption to Fe particles, as seen via the high co-occurring Fe and Mn particulate concentrations (Figure 20a,b).

5.4.6. Ability of blends to control iron corrosion

The ability of blends to inhibit iron release had apparent dependence on sequestrant type (i.e. silicate vs polyphosphate) or polyphosphate structure. Orthophosphate-silicate was more effective than polyphosphate blends at reducing iron release. Compared to orthophosphate alone, adding 12 mg SiO_2 L^{-1} exhibited the lowest iron concentrations, reducing total and colloidal (<0.45μm) iron concentrations by 477.2 μg Fe_{Total} $L^{-1}$and 407.4 μg $Fe_{0.45\mu m}$ L^{-1}, respectively. Salasi *et al*. (2007) showed that combining phosphorous and silicates provide synergistic effects for reducing the corrosion of carbon steel, providing a more compact, homogeneous corrosion layer compared to diphosphonate or silicate treatment alone.

In contrast, blending orthophosphate with 300 µg P L^{-1} short chain polyphosphates-tripolyphosphate and trimetaphosphate- increased iron release by 1621 and 1571 μg Fe_{Total} L^{-1}, respectively. Adding tripolyphosphate also resulted in a 490 μg $Fe_{0.45\mu m}$ L^{-1} increase in colloidal iron as well as a high particulate fraction (56 $\pm$ 33%). Meanwhile, adding trimetaphosphate resulted in mostly particulate iron (76 $\pm$ 13%) with similar colloidal iron compared to orthophopshate alone (538.1 $\pm$ 48.4 vs 561.4 $\pm$ 68.9 μg $Fe_{0.45\mu m}$ L^{-1}, respectively). In contrast, orthophosphate-hexametaphosphate, the blend with the longer cyclophosphate, reduced iron release by 171 μg $Fe_{0.45\mu m}$ L^{-1}, respectively. It was unclear if particulate iron was a product of weak scale layers dislodging during sampling or from precipitation in solution. In distribution systems, the mobilization of particulate iron may be unpredictable, but is acknowledged to be occurring (Liu et al., 2016; Vreeburg & Boxall, 2007). The physical and chemical properties of the corrosion scale may provide protection from further corrosion or may detach into the water.

The adsorption of Mn onto corrosion scale appeared to benefit blends with silicate or hexametaphosphate. While the addition of Mn (HRT >150) did not impact iron release with orthophosphate or blends with tripolyphosphate or trimetaphosphate, colloidal iron concentrations in blends with hexametaphosphate or silicate decreased by 173 and 73.2 μg $Fe_{0.45\mu m}$ L^{-1}. While no manganese minerals were observed via XRD (Figure 21), the adsorption of Mn(II) could have provided a barrier reducing iron corrosion with these treatments. High manganese residuals seen with blends with tripolyphosphate or trimetaphosphate could have inhibited manganese accumulation on the scale surface.

5.4.6.1. Scale morphology, structure, and elemental composition

Iron scale with orthophosphate or orthophosphate-polyphosphate blends developed scale that was mostly uniform in structure and color (Figure 27). Similar to field studies, iron scale was a combination of lepidocrocite, goethite, and magnetite (M. Li et al., 2016; Yang et al., 2012) as seen via XRD and SEM (Figure 21, 28). Tall tubercles were developed in samples with orthophosphate or orthophosphate-trimetaphosphate, a characteristic not observed with other samples. Corrosion scale in orthophosphate-silicate systems were dominated by goethite, magnetite, and silica minerals. The absence of lepidocrocite can be attributed to its inhibition by silica.

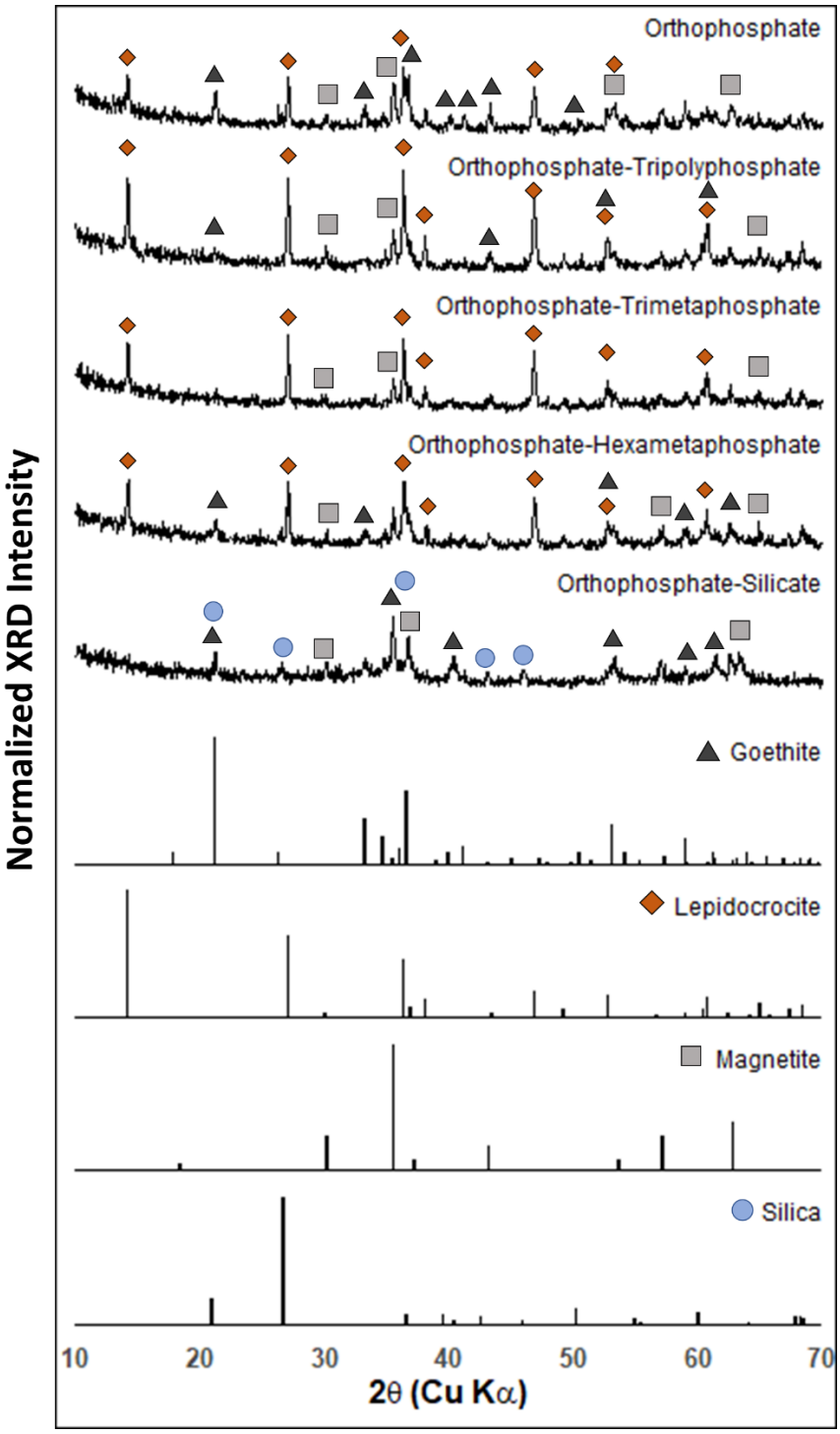

Figure 21 X-ray diffraction patterns of corrosion scale from iron coupons. The characteristic peaks of goethite (PDF: 96-100-8767), lepidocrocite (PDF: 96-901-5232), magnetite (PDF: 96-722-8111), and silica (PDF: 96-152-6861) are shown for reference.

Differences in scale formations are likely due to the incorporation of phosphorus and silica within the scale and the amount of iron released into the solution as the reaction progresses (Table 9). Here, orthophosphate was accumulated at 1.3 $\pm$ 0.13 mg P per g of scale. The addition of polyphosphate increased phosphorous in scale by 2.6 $\pm$ 0.53, 3.5 $\pm$ 0.24, and 3.2 $\pm$ 1.6 mg P per g of scale with tripolyphosphate, trimetaphosphate, and hexametaphosphate respectively. The lower phosphorous concentration with tripolyphosphate addition is due to the inefficient adsorption of phosphorous (Figure 19). The greater iron release followed by deposition may be responsible for the tubercle generation with orthophosphate-trimetaphosphate.

The durability of scale formed might be important- scale that readily flakes off is more likely to cause water discoloration or act as a transport vector for regulated contaminants (e.x. Mn, Pb) while tougher scale may provide a protective barrier to prevent further iron corrosion. Although no quantitative measurements were made, corrosion scale with silica was observed to be difficult to remove from the coupons compared to the others.

5.4.7. Dispersion of colloids

Recent evidence suggests that, other than form soluble complexes, sequestrants can also stabilize colloids in suspension (B. Li, Trueman, Munoz, et al., 2021a; Trueman et al., 2018b). To understand the impact of blends on dissolved and small colloid release, colloidal interactions between 300 Da-0.45 μm in the 0.45 μm filtrate were analyzed via A4F (Figure 22).

Among the polyphosphate blends, only orthophosphate-trimetaphosphate did not exhibit any colloids. The lack of distinct colloidal peaks past the void peak, and low analyte recoveries (<1%) suggests that the analytes (i.e., Fe, Mn, and P) are in species smaller than 300 Da and would pass through to waste (Table 10).

Manganese partitioned to phosphorus stabilized iron colloids at approximate molecular weights of 1000 and 1000-2000 kDa in both orthophosphate-tripolyphosphate and orthophosphate-hexametaphosphate suspensions. This is consistent with previous research describing adsorption or incorporation (Ahmad et al., 2019) of Mn into Fe particles and their co-transport through the distribution system (Barkatt et al., 2009; Gora et al., 2020; Trueman, Anaviapik-Soucie, et al., 2019).

Orthophosphate-tripolyphosphate was the most effective at generating colloids among the blends. Iron concentrations in the 0.45 µm filtrate were highest at 992.56 μg $Fe_{0.45\ \mu m}$ L^{-1} with 69% (685.57 μg $Fe_{0.45\ \mu m}$ L^{-1}) being colloidal. Here, manganese was mostly dissolved with only 0.44% present in the colloidal fraction. This suggests that manganese may preferentially partition to dissolved phosphorous than colloidal iron. However, smaller iron colloids may increase manganese adsorption -57% (1.14 μg $Mn_{0.45\ \mu m}$ L^{-1}) of colloidal manganese was associated with iron colloids at 1000 kDa. This may be due to the greater surface area available with smaller colloids.

A third peak corresponding to colloids approximately 100 kDa was only present with orthophosphate-hexametaphosphate. This difference can be attributed to the stabilization of

iron-manganese nanoparticles by hexametaphosphate. The presence of hexametaphosphate (~100-1000 kDa) is seen via the principal phosphorous peak in orthophosphate-hexametaphosphate suspensions corresponds to the retention time of pure hexametaphosphate in $NaHCO_3$ buffered water (Trueman et al., 2022). While the A4F recovered all of the phosphorous with the hexametaphosphate standard ($P_{Recovery}$ = 111%), the partial recovery of phosphorous, iron, and manganese from orthophosphate-hexametaphosphate suspensions suggests that hexamataphosphate hydrolysis species, such as orthophosphate, trimetaphosphate, and tripolyphosphate (McCullough et al., 1956), may have chelated iron (Rasmussen & Toftlund, 1986) and manganese (Bull, 1977), which would pass through the membrane to waste. The chelation of iron and manganese by phosphates can also explain the low recovery with orthophosphate-trimetaphosphate and orthophosphate-tripolyphosphate. Even in a simple system, polyphosphate hydrolysis occurs within 24 h (Figure 26c,d). In distribution systems, polyphosphate hydrolysis is expected to be more significant (T. R. Holm & Edwards, 2003), especially in systems with older pipes or greater concentrations of iron and manganese in bulk water.

Table 10 Estimated analyte recovery by treatment.

Treatment	Analyte	A4F (µg L^{-1})	0.45 µm filtrate (µg L^{-1})	Recovery (%)
Orthophosphate-Tripolyphosphate	31P	144.85	683.38	21.20
Orthophosphate-Tripolyphosphate	55Mn	2.04	459.19	0.44
Orthophosphate-Tripolyphosphate	57Fe	685.57	992.56	69.07
Orthophosphate-Trimetaphosphate	31P	38.43	542.69	7.08
Orthophosphate-Trimetaphosphate	55Mn	0.31	581.78	0.05
Orthophosphate-Trimetaphosphate	57Fe	3.54	515.86	0.69
Orthophosphate-Hexametaphosphate	31P	94.55	674.95	14.01
Orthophosphate-Hexametaphosphate	55Mn	2.10	170.30	1.23
Orthophosphate-Hexametaphosphate	57Fe	153.23	313.03	48.95
Orthophosphate-Silicate	31P	23.32	291.19	8.01
Orthophosphate-Silicate	55Mn	3.80	558.52	0.68
Orthophosphate-Silicate	57Fe	19.44	46.45	41.86

Silicate stabilized iron colloids at ~100 kDa. Moreover, larger iron-manganese colloids were also present at 1000-2000 kDa. Complexation of iron and the inhibition of manganese oxidation (Ju et al., 1999) by silicates may be responsible for the partial recovery of iron ($Fe_{Recovery}$ = 41.9%) and low recovery of manganese ($Mn_{Recovery}$ = 0.68%) suggesting the presence of iron chelates or soluble manganese (<300Da).

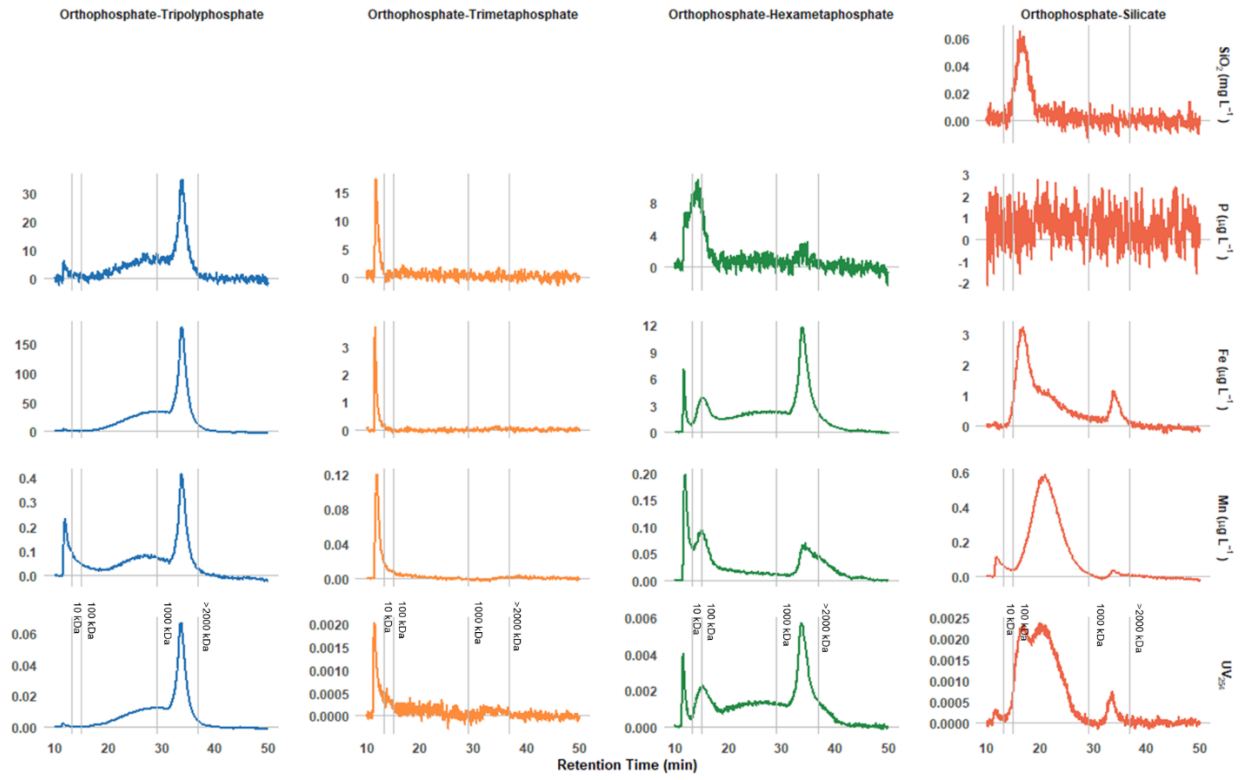

Figure 22 Fractograms representing colloidal iron and manganese from corrosion cells after 24 h in $NaHCO_3$ (5 mg C L^{-1}) buffered pure water systems at pH 7.5, free chlorine residual of 1 mg L^{-1}, and temperature of 21 ± 1 °C.

5.5. Conclusion

This work identified key factors affecting iron release and manganese sequestration with blends of orthophosphate and polyphosphates or silicate. Orthophosphate-silicate and orthophosphate-polyphosphate blends, made using either linear or cyclophosphates, were compared against orthophosphate alone, reaching the following conclusions:

1. Sequestrants impacted discoloration by decreasing precipitate particle sizes and maintaining suspended colloids or metal complexes in solution. However, they may lose effectiveness over time due to depolymerization.

2. Blending orthophosphate with short chain polyphosphates, tripolyphosphate or trimetaphosphate, increased iron release and resulted in high particulate iron concentrations but were most effective for sequestring manganese. Orthophosphate-tripolyphosphate (linear polyphosphate) increased colloids concentrations while Orthophosphate-trimetaphosphate (cyclophosphate) did not. Orthophosphate-hexametaphosphate was effective for reducing iron release but was the least effective orthophosphate-polyphosphate blend for Mn sequestration. Orthophosphate-silicate resulted in the lowest iron release among the blends and had limited effectiveness for Mn sequestration.

3. With blends, manganese was mostly dissolved (<300 Da), as seen via the low A4F recoveries. However, a fraction of manganese was either bound to colloidal iron stabilized by either phosphorous or silica or formed small colloids on their own.

These findings have important implication for drinking water. When sequestrants are added to minimize the aesthetic effects of iron and manganese, they may increase iron release. Heightened iron corrosion may result in the premature failure of distribution mains or disperse manganese bearing colloids. Recent work has shown that iron colloids can act as transport vectors for manganese and other heavy metals (i.e. lead) with sodium silicate treatment.

6. Chapter 6 Conclusions and Recommendations

6.1. Conclusions

This work identified key factors affecting the corrosion of lead and iron as well as the sequestration of manganese. A brief summary of the key findings follows.

Small colloids present unique challenges for maintaining drinking water quality. Techniques used for sampling and colloids characterization can shape corrosion control decisions. While most published literature has adopted a threshold for soluble lead of < 0.45 µm, strong evidence of lead colloids occurring below this threshold has been reported across North America and Europe. This thesis provides information on the qualitative and quantitative analysis of colloidal lead in a literature review (Chapter 2). Moreover, sampling techniques vary between studies and can have a large impact on measured lead concentrations at the tap. Chapter 3 provided a comparison of two new regulatory sampling techniques –random day time and 30-minute stagnation – taken from a survey of seven drinking water distribution systems in Nova Scotia. At the time of publication, data reported here represented – to my knowledge – the first and largest study comparing random daytime and 30-minutes stagnation sampling in Nova Scotia. These data show that random daytime captured an estimated 45% more lead and more frequently exceeded 5 μg/L compared to 30-minute stagnation (7.5% vs 5.4%). The information from Chapters 2 & 3 helped shape the experimental design and interpretation of results in the subsequent chapters.

Polyphosphate structure was a significant predictor of lead and iron release and the explanatory mechanism may be more complex than previously thought. Orthophosphate is often applied along with polyphosphate in practice with little understanding of the reactions that may be occurring within the distribution system. This thesis (Chapters 4 & 5) offers new insights into these interactions via experimental chemical data and the characterization of colloid from bench scale studies. Experiments showed that the amplified release of iron and lead with a short chain linear polyphosphate, tripolyphosphate, could be significant. In contrast, blends with trimetaphosphate, a short chain cyclophosphate, did not significantly impact dissolved lead and dissolved iron concentrations. However, blends with hexametaphosphate, a long chain cyclophosphate, reduced iron and lead release in certain cases. These phenomena may be linked to a combination of complexation, adsorption, colloidal dispersion, polyphosphate hydrolysis, and mineral precipitation: to our knowledge, the potential of lead and iron release via these mechanisms in drinking water has not been acknowledged previously.

When iron or lead dissolves, Fe^{2+} or Pb^{2+} ions are released form the surface into aqueous solution. Metal ions may either form complexes with polyphosphate or precipitate at or away from the pipe surface. Experiments showed that the strong interactions between linear polyphosphates and metal ions were due to their greater number of reactive oxygen sites as well as their structural flexibility more easily allowing metal ions to be fitted into its structure (Chapters 4 & 5). Whereas cyclophosphates are sterically inhibited, having a lower relative freedom of molecules to move, entangle, and disentangle around metal ions, reducing their

interactions. Moreover, longer chains allow for greater flexibility in the polymer bonds and metal incorporation into the polyphosphate structure. Compared to the 30 minute retention time, an increase in suspended colloidal lead was observed at 24 h with orthophosphate-polyphosphate blends. This effect was more pronounced with in cyclophosphate treated experiments. This may be attributed to the loss of polyphosphate chelation capacity due to its depolymerization into orthophosphate. Polyphosphate species and concentration could be crucial for inhibiting lead phosphate mineral formation. Recent observations showing the lack of lead phosphate minerals on lead service lines from distribution systems treated with orthophosphate-polyphosphate blends provide an instructive analogue. This appears to occur when polyphosphate competes with orthophosphate for metal binding sites on the mineral surface (Chapter 4). As the binding sites fill with adsorbed polyphosphates, vacant sites may be more difficult to access by free phosphates due to a combination of electrical repulsion and structural interference from neighboring filled binding sites. This effect was more pronounced with increased polyphosphate concentration (Chapter 4). This information could inform corrosion control programs in selecting orthophosphate-polyphosphate formulations that minimize the risk exacerbating iron and lead water issues.

The use of sequestrants entails considerable risk and may be counterproductive to minimizing consumer exposure to lead and manganese. While the use of sequestrants are widely and controversially practiced, little research is available on their effects on lead release and manganese behavior under drinking water conditions. The dispersive properties of sequestrants resulted in the mobilization of manganese via its attachment to iron colloids or

maintain dissolved metals in solution. Polyphosphates and silicates reduced the size of iron colloids and inhibited their crystallization. Increased adsorptive capacity of smaller colloids or amorphous iron have been reported in other studies and could potentially transport regulated metals, such as lead and manganese, to the tap. In the experiments described here, orthophosphate-polyphosphates tended to increase lead and iron release but were effective for sequestering manganese (Chapter 5). Combining orthophosphate and sodium silicate reduced iron corrosion and sequestered manganese but it was not as effective as blends with polyphosphate.

6.2. Recommendations

Several recommendations follow from these key findings

Given the risk of heightened lead and manganese concentrations in drinking water, the use of sequestrants should be used with caution. Polyphosphate species have the potential to increase lead and iron solubility via complexation reactions, but the extent of species dependent interactions is unclear. Data presented here shows that sequestrants represent a manganese and lead exposure risk. Other than metal complexation and the stabilization of colloids, the loss of sequestering capacity over time may result in the deposition and concentration of contaminant metals on pipe scale. This in conjunction with the formation of amorphous layers rather than crystalline mineral phases with sequestrants pose a potential health risk. These deposits may slough off during hydraulic disturbances and be transported to

the tap. While removal of manganese and lead at the source may be capital intensive, that would be the optimal option to reduce health impacts related with these contaminants.

A better understanding of the practical relevance and optimization of polyphosphate use for blends is needed. Drinking water guidelines and regulations across North America, strongly advise against the use of polyphosphate for corrosion control but regard orthophosphate-polyphosphate blends as a legitimate alternative. Given the wide-spread use of orthophosphate-polyphosphates, potential interactions between polyphosphates, lead, iron, and manganese have received little attention. While these documents point out the limited availability of information on the interactions and fate of orthophosphate-polyphosphate blends in distribution systems, but the lack of clarity on specific corrosion protection mechanisms, such as the possible formation of a protective phosphorous barrier, may result the sub-optimal application of blended phosphates. The significance of polyphosphate as a chelator is supported by theoretical and experimental work but understanding the extent of lead exposure risk due to different polyphosphate species would inform both corrosion control strategies and health risk assessments. Analytical methods to characterize metal complexation could be applied to identify corrosion issues related to polyphosphate use and could lead to a better understanding of the role of polyphosphates in metals mobility and corrosion throughout the distribution system.

Sodium silicate combined with orthophosphate may be a possible alternative for simultaneous corrosion control and sequestration. Phosphorous use is heavily tied to, not only

the water treatment industry, but to agriculture as well. Moreover, it is a regulated contaminant in wase water effluent. Although phosphate use has been effective for corrosion control, the development of a more environmentally friendly chemical would be beneficial- either through dose optimization or blend formulation. Unlike some polyphosphates, sodium silicates have minimal impact on lead solubility. However, the limited amount of peer-reviewed work on phosphate-silicate blends focused mainly on cast iron corrosion. The long-term impacts as well as a more comprehensive investigation on corrosion inhibition and sequestration with orthophosphate-silicates is worth investigating.

References

Abokifa, A. A., & Biswas, P. (2017). Modeling Soluble and Particulate Lead Release into Drinking Water from Full and Partially Replaced Lead Service Lines. *Environmental Science & Technology*, *51*(6), 3318–3326. https://doi.org/10.1021/acs.est.6b04994

Aghasadeghi, K., Peldszus, S., Trueman, B. F., Mishrra, A., Cooke, M. G., Slawson, R. M., Giammar, D. E., Gagnon, G. A., & Huck, P. M. (2021). Pilot-scale comparison of sodium silicates, orthophosphate and pH adjustment to reduce lead release from lead service lines. *Water Research*, *195*, 116955. https://doi.org/10.1016/j.watres.2021.116955

Ahmad, A., van der Wal, A., Bhattacharya, P., & van Genuchten, C. M. (2019). Characteristics of Fe and Mn bearing precipitates generated by Fe(II) and Mn(II) co-oxidation with O2, MnO4 and HOCl in the presence of groundwater ions. *Water Research*, *161*, 505–516. https://doi.org/10.1016/j.watres.2019.06.036

Alam, S. B., Panciera, F., Hansen, O., Mølhave, K., & Ross, F. M. (2015). Creating New VLS Silicon Nanowire Contact Geometries by Controlling Catalyst Migration. *Nano Letters*, *15*(10), 6535–6541. https://doi.org/10.1021/acs.nanolett.5b02178

Allaire, J., Xie, Y., McPherson, J., Luraschi, J., Ushey, K., Atkins, A., Wickham, H., Cheng, J., Chang, W., & Iannoe, R. (n.d.). *R. Rmarkdown: Dynamic documents for r*. https://github.com/rstudio/rmarkdown.

Alp, E., Mini, S., & Ramanathan, M. (1990). *X-ray absorption spectroscopy: EXAFS and XANES-A versatile tool to study the atomic and electronic structure of materials*.

American Public Health Association, American Water Works Association, Water Environment Federation. (2012). *Standard methods for examination of water and wastewater* (22nd ed.). American Water Works Association.

American Water Works Service Co. (2004). *I. Water://Stats 2002 Distribution Survey*. AWWA.

Anderson, L. E., Krkošek, W. H., Stoddart, A. K., Trueman, B. F., & Gagnon, G. A. (2017). Lake Recovery Through Reduced Sulfate Deposition: A New Paradigm for Drinking Water Treatment. *Environmental Science & Technology*, *51*(3), 1414–1422. https://doi.org/10.1021/acs.est.6b04889

Anderson, L. E., Trueman, B. F., Dunnington, D. W., & Gagnon, G. A. (2021). Relative importance of organic- and iron-based colloids in six Nova Scotian lakes. *Npj Clean Water*, *4*(1), 26. https://doi.org/10.1038/s41545-021-00115-4

Baalousha, M., & Lead, J. (2013). Characterization of natural and manufactured nanoparticles by atomic force microscopy: Effect of analysis mode, environment and sample preparation. *Colloids and Surfaces A: Physicochemical and Engineering Aspects*, *419*, 238–247. https://doi.org/10.1016/j.colsurfa.2012.12.004

Baalousha, M., Manciulea, A., Cumberland, S., Kendall, K., & Lead, J. R. (2008). Aggregation and surface properties of iron oxide nanoparticles: Influence of ph and natural organic matter. *Environmental Toxicology and Chemistry*, *27*(9), 1875–1882. https://doi.org/10.1897/07-559.1

Baalousha, M., Stolpe, B., & Lead, J. R. (2011). Flow field-flow fractionation for the analysis and characterization of natural colloids and manufactured nanoparticles in environmental systems: A critical review. *Journal of Chromatography A*, *1218*(27), 4078–4103. https://doi.org/10.1016/j.chroma.2011.04.063

Bae, Y., Pasteris, J. D., & Giammar, D. E. (2020). Impact of orthophosphate on lead release from pipe scale in high pH, low alkalinity water. *Water Research*, *177*, 115764. https://doi.org/10.1016/j.watres.2020.115764

Bailey, R., Holmes, D., Jolly, P., & Lacey, R. (1986). *Lead concentration and stagnation time in water drawn through lead domestic pipes* (Environment Report TR 243). Water Research Centre.

Baird, R. B. (2017). *Standard methods for the examination of water and wastewater, 23rd*. American Public Health Association.

Balnois, E., Papastavrou, G., & Wilkinson, K. J. (2007). Force microscopy and force measurements of environmental colloids. *IUPAC Series on Analytical and Physical Chemistry of Environmental Systems*, *10*, 405.

Bargar, J. R., Brown, G. E., & Parks, G. A. (1997). Surface complexation of Pb(II) at oxide-water interfaces: II. XAFS and bond-valence determination of mononuclear Pb(II) sorption products and surface functional groups on iron oxides. *Geochimica et Cosmochimica Acta*, *61*(13), 2639–2652. https://doi.org/10.1016/S0016-7037(97)00125-7

Barkatt, A., Pulvirenti, A. L., Adel-Hadadi, M. A., Viragh, C., Senftle, F. E., Thorpe, A. N., & Grant, J. R. (2009). Composition and particle size of superparamagnetic corrosion products in tap water. *Water Research*, *43*(13), 3319–3325. https://doi.org/10.1016/j.watres.2009.04.048

Baron, J. (2001). Monitoring strategy for lead in drinking water at consumer's tap: Field experiments in France. *Water Supply*, *1*(4), 193–200. https://doi.org/10.2166/ws.2001.0084

Bigi, A., Gandolfi, M., Gazzano, M., Ripamonti, A., Roveri, N., & Thomas, S. A. (1991). Structural modifications of hydroxyapatite induced by lead substitution for calcium. *Journal of the Chemical Society, Dalton Transactions*, *11*, 2883–2886. https://doi.org/10.1039/DT9910002883

Bouchard, M. F., Surette, C., Cormier, P., & Foucher, D. (2018). Low level exposure to manganese from drinking water and cognition in school-age children. *Manganese Health Effects on Neurodevelopment and Neurodegenerative Diseases*, *64*, 110–117. https://doi.org/10.1016/j.neuro.2017.07.024

Boxall, J. B., Skipworth, P. J., & Saul, A. J. (2003). Aggressive flushing for discolouration event mitigation in water distribution networks. *Water Supply*, *3*(1–2), 179–186. https://doi.org/10.2166/ws.2003.0101

Boyd, R. D., Pichaimuthu, S. K., & Cuenat, A. (2011). New approach to inter-technique comparisons for nanoparticle size measurements; using atomic force microscopy, nanoparticle tracking analysis and dynamic light scattering. *Colloids and Surfaces A: Physicochemical and Engineering Aspects*, *387*(1), 35–42. https://doi.org/10.1016/j.colsurfa.2011.07.020

Brewer, A. K., & Striegel, A. M. (2008). Particle size characterization by quadruple-detector hydrodynamic chromatography. *Analytical and Bioanalytical Chemistry*, *393*(1), 295. https://doi.org/10.1007/s00216-008-2319-y

Brewer, A. K., & Striegel, A. M. (2010). Hydrodynamic chromatography of latex blends. *Journal of Separation Science*, *33*(22), 3555–3563. https://doi.org/10.1002/jssc.201000565

Brownie, C., & Boos, D. D. (1994). Type I Error Robustness of ANOVA and ANOVA on Ranks When the Number of Treatments is Large. *Biometrics*, *50*(2), 542–549. JSTOR. https://doi.org/10.2307/2533399

Buamah, R., Petrusevski, B., & Schippers, J. C. (2008). Adsorptive removal of manganese(II) from the aqueous phase using iron oxide coated sand. *Journal of Water Supply: Research and Technology-Aqua*, *57*(1), 1–11. https://doi.org/10.2166/aqua.2008.078

Bull, R. J. (1977). *Effects of Manganese and Their Modification by Hexametaphosphate*. Health Effects Research Laboratory, Office of Research and Development.

Canfield, R. L., Henderson, C. R., Cory-Slechta, D. A., Cox, C., Jusko, T. A., & Lanphear, B. P. (2003). Intellectual Impairment in Children with Blood Lead Concentrations below 10 µg per Deciliter. *New England Journal of Medicine*, *348*(16), 1517–1526. https://doi.org/10.1056/NEJMoa022848

Cantor, A. F. (2017). *Optimization of phosphorus-based corrosion control chemicals using a comprehensive perspective of water quality*. Water Research Foundation.

Cardew, P. (2009). Measuring the Benefit of Orthophosphate Treatment on Lead in Drinking Water. *Journal of Water and Health*, *7*, 123–131. https://doi.org/10.2166/wh.2009.015

Cardew, P. T. (2000). Simulation of lead compliance data. *Water Research*, *34*(8), 2241–2252. https://doi.org/10.1016/S0043-1354(99)00411-X

Cardew, P. T. (2003). A method for assessing the effect of water quality changes on plumbosolvency using random daytime sampling. *Water Research*, *37*(12), 2821–2832. https://doi.org/10.1016/S0043-1354(03)00120-9

Cartier, C., Arnold, R. B., Triantafyllidou, S., Prévost, M., & Edwards, M. (2012). Effect of flow rate and lead/copper pipe sequence on lead release from service lines. *Water Research*, *46*(13), 4142–4152. https://doi.org/10.1016/j.watres.2012.05.010

Cartier, C., Doré, E., Laroche, L., Nour, S., Edwards, M., & Prévost, M. (2013). Impact of treatment on Pb release from full and partially replaced harvested lead service lines (LSLs). *Water Research*, *47*(2), 661–671. https://doi.org/10.1016/j.watres.2012.10.033

Cartier, C., Laroche, L., Deshommes, E., Nour, S., Richard, G., Edwards, M., & Prévost, M. (2011). Investigating dissolved lead at the tap using various sampling protocols. *Journal-American Water Works Association*, *103*(3), 55–67. https://doi.org/10.1002/j.1551-8833.2011.tb11420.x

Cerrato, J. M., Reyes, L. P., Alvarado, C. N., & Dietrich, A. M. (2006). Effect of PVC and iron materials on Mn(II) deposition in drinking water distribution systems. *Water Research*, *40*(14), 2720–2726. https://doi.org/10.1016/j.watres.2006.04.035

Chen, Q., Cho, H., Manthiram, K., Yoshida, M., Ye, X., & Alivisatos, A. P. (2015). Interaction Potentials of Anisotropic Nanocrystals from the Trajectory Sampling of Particle Motion using in Situ Liquid Phase Transmission Electron Microscopy. *ACS Central Science*, *1*(1), 33–39. https://doi.org/10.1021/acscentsci.5b00001

Christl, I., Milne, C. J., Kinniburgh, D. G., & Kretzschmar, R. (2001). Relating ion binding by fulvic and humic acids to chemical composition and molecular size. 2. Metal binding. *Environmental Science & Technology*, *35*(12), 2512–2517. https://doi.org/10.1021/es0002520

Chun, K.-H., Zhang, H., & Chan, W.-T. (2018). Double-viewing-position single-particle inductively coupled plasma–atomic emission spectrometry for the selection of ICP sampling position in SP-ICP measurements. *Analytical Sciences*, *34*(6), 711–717. https://doi.org/10.2116/analsci.18SBP11

City of Toronto. (2018). *Annual report—Lead in drinking water mitigation strategy*. Toronto, Ontario, Canada.

City of Winnipeg. (2019). *2019 Annual Water Quality Report.* City of Winnipeg Water Supply System.

Clark, B. N., Masters, S. V., & Edwards, M. A. (2015). Lead Release to Drinking Water from Galvanized Steel Pipe Coatings. *Environmental Engineering Science*, *32*(8), 713–721. https://doi.org/10.1089/ees.2015.0073

Conover, W. J., & Iman, R. L. (1981). Rank Transformations as a Bridge between Parametric and Nonparametric Statistics. *The American Statistician*, *35*(3), 124–129. https://doi.org/10.1080/00031305.1981.10479327

Dai, C., Zhao, J., Giammar, D. E., Pasteris, J. D., Zuo, X., & Hu, Y. (2018). Heterogeneous lead phosphate nucleation at organic–water interfaces: Implications for lead immobilization. *ACS Earth and Space Chemistry*, *2*(9), 869–877. https://doi.org/10.1021/acsearthspacechem.8b00040

Dart, F. J., & Foley, P. D. (1970). Preventing Iron Deposition with Sodium SIlicate. *Journal AWWA*, *62*(10), 663–668. https://doi.org/10.1002/j.1551-8833.1970.tb03987.x

Das, N. C., & Misra, P. K. (1972). Diamagnetic Susceptibility of Lead. *Physical Review B*, *5*(8), 3369.

Daulton, T. L., Little, B. J., Lowe, K., & Jones-Meehan, J. (2001). In Situ Environmental Cell–Transmission Electron Microscopy Study of Microbial Reduction of Chromium(VI) Using Electron Energy Loss Spectroscopy. *Microscopy and Microanalysis*, *7*(6), 470–485. https://doi.org/10.1007/S10005-001-0021-3

Daye, M., Klepac-Ceraj, V., Pajusalu, M., Rowland, S., Farrell-Sherman, A., Beukes, N., Tamura, N., Fournier, G., & Bosak, T. (2019). Light-driven anaerobic microbial oxidation of manganese. *Nature*, *576*(7786), 311–314. https://doi.org/10.1038/s41586-019-1804-0

De Cicco, L. (2017). *SmwrQW: Tools for censored data analysis*.

de Mora, S. J., & Harrison, R. M. (1983). The use of physical separation techniques in trace metal speciation studies. *Water Research*, *17*(7), 723–733. https://doi.org/10.1016/0043-1354(83)90066-0

de Mora, S. J., Harrison, R. M., & Wilson, S. (1987). The effect of water treatment on the speciation and concentration of lead in domestic tap water derived from a soft upland source. *Water Research*, *21*(1), 83–94. https://doi.org/10.1016/0043-1354(87)90102-3

de Morais, S. C., de Lima, D. F., Ferreira, T. M., Domingos, J. B., de Souza, M. A. F., Castro, B. B., & Balaban, R. de C. (2020). Effect of pH on the efficiency of sodium hexametaphosphate as calcium

carbonate scale inhibitor at high temperature and high pressure. *Desalination*, *491*, 114548. https://doi.org/10.1016/j.desal.2020.114548

De Rosa, S., & Williams, S. (1992). *Particulate Lead in Water Supplies-Final Report to the Department of the Environment-May 1987 to December 1991*. Department of the Environment, WRc Swidon, Wiltshire.

Del Toral, M. A., Porter, A., & Schock, M. R. (2013). Detection and Evaluation of Elevated Lead Release from Service Lines: A Field Study. *Environmental Science & Technology*, *47*(16), 9300–9307. https://doi.org/10.1021/es4003636

Delbem, A. C. B., Souza, J. A. S., Zaze, A. C. S. F., Takeshita, E. M., Sassaki, K. T., & Moraes, J. C. S. (2014). Effect of trimetaphosphate and fluoride association on hydroxyapatite dissolution and precipitation in vitro. *Brazilian Dental Journal*, *25*, 479–484. https://doi.org/10.1590/0103-6440201300174

Demangeat, E., Pédrot, M., Dia, A., Bouhnik-le-Coz, M., Grasset, F., Hanna, K., Kamagate, M., & Cabello-Hurtado, F. (2018). Colloidal and chemical stabilities of iron oxide nanoparticles in aqueous solutions: The interplay of structural, chemical and environmental drivers. *Environmental Science: Nano*, *5*(4), 992–1001. https://doi.org/10.1039/C7EN01159H

Dermatas, D., Dadachov, M., Dutko, P., Menounou, N., Arienti, P., & Shen, G. (2004). Weathering of lead in Fort Irwin firing range soils. *Global Nest*, *6*(2), 167–175.

Deshommes, E., Bannier, A., Laroche, L., Nour, S., & Prévost, M. (2016). Monitoring-Based Framework to Detect and Manage Lead Water Service Lines. *Journal AWWA*, *108*(11), E555–E570. https://doi.org/10.5942/jawwa.2016.108.0167

Deshommes, E., Laroche, L., Nour, S., Cartier, C., & Prévost, M. (2010). Source and occurrence of particulate lead in tap water. *Water Research*, *44*(12), 3734–3744. https://doi.org/10.1016/j.watres.2010.04.019

Deshommes, E., Prévost, M., Levallois, P., Lemieux, F., & Nour, S. (2013). Application of lead monitoring results to predict 0–7 year old children's exposure at the tap. *Water Research*, *47*(7), 2409–2420. https://doi.org/10.1016/j.watres.2013.02.010

Deshommes, E., Trueman, B., Douglas, I., Huggins, D., Laroche, L., Swertfeger, J., Spielmacher, A., Gagnon, G. A., & Prévost, M. (2018). Lead Levels at the Tap and Consumer Exposure from Legacy and Recent Lead Service Line Replacements in Six Utilities. *Environmental Science & Technology*, *52*(16), 9451–9459. https://doi.org/10.1021/acs.est.8b02388

Dion, L.-A., Saint-Amour, D., Sauvé, S., Barbeau, B., Mergler, D., & Bouchard, M. F. (2018). Changes in water manganese levels and longitudinal assessment of intellectual function in children exposed through drinking water. *Manganese Health Effects on Neurodevelopment and Neurodegenerative Diseases*, *64*, 118–125. https://doi.org/10.1016/j.neuro.2017.08.015

Dodrill, D. M., & Edwards, M. (1995). Corrosion control on the basis of utility experience. *Journal - AWWA*, *87*(7), 74–85. https://doi.org/10.1002/j.1551-8833.1995.tb06395.x

Domingos, R. F., Baalousha, M. A., Ju-Nam, Y., Reid, M. M., Tufenkji, N., Lead, J. R., Leppard, G. G., & Wilkinson, K. J. (2009). Characterizing manufactured nanoparticles in the environment: Multimethod

determination of particle sizes. *Environmental Science & Technology*, *43*(19), 7277–7284. https://doi.org/10.1021/es900249m

Donald, A. M. (2003). The use of environmental scanning electron microscopy for imaging wet and insulating materials. *Nature Materials*, *2*(8), 511–516. https://doi.org/10.1038/nmat898

Dong, D., Liu, L., Hua, X., & Lu, Y. (2007). Comparison of lead, cadmium, copper and cobalt adsorption onto metal oxides and organic materials in natural surface coatings. *Microchemical Journal*, *85*(2), 270–275. https://doi.org/10.1016/j.microc.2006.06.015

Doré, E., Deshommes, E., Laroche, L., Nour, S., & Prévost, M. (2019). Study of the long-term impacts of treatments on lead release from full and partially replaced harvested lead service lines. *Water Research*, *149*, 566–577. https://doi.org/10.1016/j.watres.2018.11.037

Doré, E., Formal, C., Muhlen, C., Williams, D., Harmon, S. M., Pham, M., Triantafyllidou, S., & Lytle, D. A. (2021). Effectiveness of point-of-use and pitcher filters at removing lead phosphate nanoparticles from drinking water. *Water Research*, 117285. https://doi.org/10.1016/j.watres.2021.117285

Dryer, D. J., & Korshin, G. V. (2007). Investigation of the reduction of lead dioxide by natural organic matter. *Environmental Science & Technology*, *41*(15), 5510–5514. https://doi.org/10.1021/es070596r

Dubascoux, S., Le Hécho, I., Hassellöv, M., Von Der Kammer, F., Potin Gautier, M., & Lespes, G. (2010). Field-flow fractionation and inductively coupled plasma mass spectrometer coupling: History, development and applications. *Journal of Analytical Atomic Spectrometry*, *25*(5), 613. https://doi.org/10.1039/b927500b

Edwards, M., & McNeill, L. S. (2002a). Effect of PHOSPHATE inhibitors on lead release from pipes. *Journal AWWA*, *94*(1), 79–90. https://doi.org/10.1002/j.1551-8833.2002.tb09383.x

Edwards, M., & McNeill, L. S. (2002b). Effect of phosphate inhibitors on lead release from pipes. *Journal AWWA*, *94*(1), 79–90. https://doi.org/10.1002/j.1551-8833.2002.tb09383.x

Egerton, R. (2011). *Physical principles of electron microscopy: An introduction to TEM, SEM, and AEM* (Vol. 56). Springer US. https://books.google.ca/books?id=t6TTgqp3O5MC

Elfland, C., Scardina, P., & Edwards, M. (2010). Lead-contaminated water from brass plumbing devices in new buildings. *Journal AWWA*, *102*(11), 66–76. https://doi.org/10.1002/j.1551-8833.2010.tb11340.x

Elzinga, E., Peak, D., & Sparks, D. (2001). Spectroscopic studies of Pb (II)-sulfate interactions at the goethite-water interface. *Geochimica et Cosmochimica Acta*, *65*(14), 2219–2230. https://doi.org/10.1016/S0016-7037(01)00595-6

European Commission. (2018). *Proposal for a directive of the European parliament and of the council on the quality of water intended for human consumption (recast)*.

Filipe, V., Hawe, A., & Jiskoot, W. (2010). Critical Evaluation of Nanoparticle Tracking Analysis (NTA) by NanoSight for the Measurement of Nanoparticles and Protein Aggregates. *Pharmaceutical Research*, *27*(5), 796–810. https://doi.org/10.1007/s11095-010-0073-2

Furusawa, K., Shou, Z., & Nagahashi, N. (1992). Polymer adsorption on fine particles; the effects of particle size and its stability. *Colloid & Polymer Science*, *270*(3), 212–218. https://doi.org/10.1007/BF00655472

Geckeis, H., Rabung, Th., Manh, T. N., Kim, J. I., & Beck, H. P. (2002). Humic colloid-borne natural polyvalent metal ions: Dissociation experiment. *Environmental Science & Technology*, *36*(13), 2946–2952. https://doi.org/10.1021/es010326n

Gerke, T. L., Little, B. J., & Barry Maynard, J. (2016). Manganese deposition in drinking water distribution systems. *Science of The Total Environment*, *541*, 184–193. https://doi.org/10.1016/j.scitotenv.2015.09.054

Giddings, J. C. (1993). Field-flow fractionation: Analysis of macromolecular, colloidal, and particulate materials. *Science (New York, N.Y.)*, *260*(5113), 1456–1465. https://doi.org/10.1126/science.8502990

Glover, L. J., Eick, M. J., & Brady, P. V. (2002). Desorption kinetics of cadmium2+ and lead2+ from goethite: Influence of time and organic acids. *Soil Science Society of America Journal*, *66*(3), 797–804.

Goldstein, J. I., Newbury, D. E., Michael, J. R., Ritchie, N. W. M., Scott, J. H. J., & Joy, D. C. (2017). *Scanning Electron Microscopy and X-Ray Microanalysis*. Springer New York. https://books.google.ca/books?id=D0I_DwAAQBAJ

Gora, S. L., Trueman, B. F., Anaviapik-Soucie, T., Gavin, M. K., Ontiveros, C. C., Campbell, J., L'Hérault, V., Stoddart, A. K., & Gagnon, G. A. (2020). Source water characteristics and building-specific factors influence corrosion and point of use water quality in a decentralized Arctic drinking water system. *Environmental Science & Technology*, *54*(4), 2192–2201. https://doi.org/10.1021/acs.est.9b04691

Gosselin, R. E., & Coghlan, E. R. (1953). The stability of complexes between calcium and orthophosphate, polymeric phosphate, and phytate. *Archives of Biochemistry and Biophysics*, *45*(2), 301–311. https://doi.org/10.1016/S0003-9861(53)80007-X

Government of Alberta. (2022). Potable Water Regulation, Alberta Regulation 277/2003. *Alberta, Canada*.

Government of Ontario. (2002). *Safe Drinking Water Act, 2002, Ontario Regulation 170/03*.

Government of Quebec. (2021). *Assessment and Response Guide for Monitoring Lead nd Copper in Drinking Water*. https://www.environnement.gouv.qc.ca/eau/potable/plomb/guide-evaluation-intervention.htm

Gray, M. J., Malati, M. A., & rophael, M. W. (1978). The point of zero charge of manganese dioxides. *Journal of Electroanalytical Chemistry and Interfacial Electrochemistry*, *89*(1), 135–140. https://doi.org/10.1016/S0022-0728(78)80038-2

Green-Pedersen, H., Jensen, B. T., & Pind, N. (1997). Nickel Adsorption on MnO2, Fe(OH)3, Montmorillonite, Humic Acid and Calcite: A Comparative Study. *Environmental Technology*, *18*(8), 807–815. https://doi.org/10.1080/09593331808616599

Guan, X.-H., Liu, Q., Chen, G.-H., & Shang, C. (2005). Surface complexation of condensed phosphate to aluminum hydroxide: An ATR-FTIR spectroscopic investigation. *Journal of Colloid and Interface Science*, *289*(2), 319–327. https://doi.org/10.1016/j.jcis.2004.08.041

Harmon, S. M., Lytle, D. A., Formal, C., & Doré, E. (2020). *Analysis of particulate and nanoparticles in drinking waters: Analytical techniques, interpretations and considerations*. https://cfpub.epa.gov/si/si_public_record_Report.cfm?dirEntryId=350495&Lab=CESER

Harrison, R. M., & Laxen, D. P. (1980). Physicochemical speciation of lead in drinking water. *Nature*, *286*(5775), 791–793. https://doi.org/DOI: 10.1038/286791a0

Hassan, P. A., Rana, S., & Verma, G. (2015). Making sense of Brownian motion: Colloid characterization by dynamic light scattering. *Langmuir*, *31*(1), 3–12. https://doi.org/10.1021/la501789z

Hayes, C. R. (2009). Computational modelling to investigate the sampling of lead in drinking water. *Water Research*, *43*(10), 2647–2656. https://doi.org/10.1016/j.watres.2009.03.023

Hayes, C. R., Croft, N., Phillips, E., Craik, S., & Schock, M. (2016). An evaluation of sampling methods and supporting techniques for tackling lead in drinking water in Alberta Province. *Journal of Water Supply: Research and Technology-Aqua*, *65*(5), 373–383. https://doi.org/10.2166/aqua.2016.117

Hayes, C. R., & Croft, T. N. (2012). An investigation into the representativeness of random daytime sampling for lead in drinking water, using computational modelling. *Journal of Water Supply: Research and Technology-Aqua*, *61*(3), 142–152. https://doi.org/10.2166/aqua.2012.092

Hayes, C. R., Incledion, S., & Balch, M. (2008). Experience in Wales (UK) of the optimisation of ortho-phosphate dosing for controlling lead in drinking water. *Journal of Water and Health*, *6*(2), 177–185. https://doi.org/10.2166/wh.2008.044

Hazen and Sawyer. (2019). *Corrosion Control: Results from a National Survey*. Hazen and Sawyer. https://www.hazenandsawyer.com/publications/evolving-utility-practices-and-experiences-with-corrosion-control-results-f/

Health Canada. (1992). *Guidelines for Canadian drinking water quality: Guideline technical document – lead*.

Health Canada. (2009). *Guidance on controlling corrosion in drinking water distribution systems*.

Health Canada. (2019a). *Guidelines for Canadian Drinking Water Quality: Guideline Technical Document – Lead*. https://www.canada.ca/en/health-canada/services/publications/healthy-living/guidelines-canadian-drinking-water-quality-guideline-technical-document-lead.html

Health Canada. (2019b). *Guidelines for Canadian Drinking Water Quality: Guideline Technical Document – Manganese*. https://www.canada.ca/en/health-canada/services/publications/healthy-living/guidelines-canadian-drinking-water-quality-guideline-technical-document-manganese.html

Helsel, D. R., Hirsch, R. M., Ryberg, K. R., Archfield, S. A., & Gilroy, E. J. (2020). *Statistical methods in water resources* (Report No. 4-A3; Techniques and Methods, p. 484). USGS Publications Warehouse. https://doi.org/10.3133/tm4A3

Herndon, E. M., Kinsman-Costello, L., Duroe, K. A., Mills, J., Kane, E. S., Sebestyen, S. D., Thompson, A. A., & Wullschleger, S. D. (2019). Iron (Oxyhydr)Oxides Serve as Phosphate Traps in Tundra and Boreal Peat Soils. *Journal of Geophysical Research: Biogeosciences*, *124*(2), 227–246. https://doi.org/10.1029/2018JG004776

Ho, K.-S., Lui, K.-O., Lee, K.-H., & Chan, W.-T. (2013). Considerations of particle vaporization and analyte diffusion in single-particle inductively coupled plasma-mass spectrometry. *Spectrochimica Acta Part B: Atomic Spectroscopy*, *89*, 30–39. https://doi.org/10.1016/j.sab.2013.08.012

Hochberg, Y. (1988). A sharper Bonferroni procedure for multiple tests of significance. *Biometrika*, *75*(4), 800–802. https://doi.org/10.1093/biomet/75.4.800

Hoekstra, E., Hayes, C., Aertgeerts, R., Becker, A., Jung, M., Postawa, A., Russell, L., & Witczak, S. (2009). Guidance on sampling and monitoring for lead in drinking water. *JRC Scientific and Technical Reports*.

Holm, S. (1979). A Simple Sequentially Rejective Multiple Test Procedure. *Scandinavian Journal of Statistics*, *6*(2), 65–70. JSTOR.

Holm, T. R., & Edwards, M. (2003). Metaphosphate reversion in Laboratory and Pipe-Rig Experiments. *Journal AWWA*, *95*(4), 172–178. https://doi.org/10.1002/j.1551-8833.2003.tb10343.x

Holm, T. R., & Shock, M. R. (1991a). Potential effects of polyphosphate products on lead solubility in plumbing systems. *Journal - American Water Works Association*, *83*(7), 76–82. https://doi.org/10.1002/j.1551-8833.1991.tb07182.x

Holm, T. R., & Shock, M. R. (1991b). Potential Effects of Polyphosphate Products on Lead Solubility in Plumbing Systems. *Journal AWWA*, *83*(7), 76–82. https://doi.org/10.1002/j.1551-8833.1991.tb07182.x

Hülsey, M. J., Zhang, B., Ma, Z., Asakura, H., Do, D. A., Chen, W., Tanaka, T., Zhang, P., Wu, Z., & Yan, N. (2019). In situ spectroscopy-guided engineering of rhodium single-atom catalysts for CO oxidation. *Nature Communications*, *10*(1), 1330. https://doi.org/10.1038/s41467-019-09188-9

Hulsmann, A. D. (1990). Particulate lead in water supplies. *Water and Environment Journal*, *4*(1), 19–25. https://doi.org/10.1111/j.1747-6593.1990.tb01553.x

Iler, K. R. (1979). The chemistry of silica. *Solubility, Polymerization, Colloid and Surface Properties and Biochemistry of Silica*.

Jackson, B. P., Ranville, J. F., Bertsch, P. M., & Sowder, A. G. (2005). Characterization of colloidal and humic-bound Ni and U in the “dissolved” fraction of contaminated sediment extracts. *Environmental Science & Technology*, *39*(8), 2478–2485. https://doi.org/10.1021/es0485208

Jones, A. M., Griffin, P. J., Collins, R. N., & Waite, T. D. (2014). Ferrous iron oxidation under acidic conditions – The effect of ferric oxide surfaces. *Geochimica et Cosmochimica Acta*, *145*, 1–12. https://doi.org/10.1016/j.gca.2014.09.020

Ju, Y., Ni, Y., & Ohi, H. (1999). Improving Peroxide Bleaching of Chemical Pulps by Stabilizing Manganese. *Journal of Wood Chemistry and Technology*, *19*(4), 323–334. https://doi.org/10.1080/02773819909349615

Junta, J. L., & Hochella, M. F. (1994). Manganese (II) oxidation at mineral surfaces: A microscopic and spectroscopic study. *Geochimica et Cosmochimica Acta*, *58*(22), 4985–4999. https://doi.org/10.1016/0016-7037(94)90226-7

Kálomista, I., Kéri, A., & Galbács, G. (2017). Optimization of plasma sampling depth and aerosol gas flow rates for single particle inductively coupled plasma mass spectrometry analysis. *Talanta*, *172*, 147–154. https://doi.org/10.1016/j.talanta.2017.05.051

Kammer, F. v. d., Baborowski, M., & Friese, K. (2005). Field-flow fractionation coupled to multi-angle laser light scattering detectors: Applicability and analytical benefits for the analysis of environmental colloids. *Analytica Chimica Acta*, *552*(1–2), 166–174. https://doi.org/10.1016/j.aca.2005.07.049

Kandori, K., Uchida, S., Kataoka, S., & Ishikawa, T. (1992). Effects of silicate and phosphate ions on the formation of ferric oxide hydroxide particles. *Journal of Materials Science*, *27*(3), 719–728. https://doi.org/10.1007/PL00020655

Kim, A., Ng, W. B., Bernt, W., & Cho, N.-J. (2019). Validation of Size Estimation of Nanoparticle Tracking Analysis on Polydisperse Macromolecule Assembly. *Scientific Reports*, *9*(1), 2639. https://doi.org/10.1038/s41598-019-38915-x

Kimbrough, D. E. (2001). Brass Corrosion and The LCR Monitoring Program. *Journal AWWA*, *93*(2), 81–91. https://doi.org/10.1002/j.1551-8833.2001.tb09128.x

Kinsela, A. S., Jones, A. M., Bligh, M. W., Pham, A. N., Collins, R. N., Harrison, J. J., Wilsher, K. L., Payne, T. E., & Waite, T. D. (2016). Influence of Dissolved Silicate on Rates of Fe(II) Oxidation. *Environmental Science & Technology*, *50*(21), 11663–11671. https://doi.org/10.1021/acs.est.6b03015

Kogo, A., Payne, S. J., & Andrews, R. C. (2017). Comparison of three corrosion inhibitors in simulated partial lead service line replacements. *Journal of Hazardous Materials*, *329*, 211–221. https://doi.org/10.1016/j.jhazmat.2017.01.039

Korshin, G. V., Ferguson, J. F., & Lancaster, A. N. (2000). Influence of natural organic matter on the corrosion of leaded brass in potable water. *Corrosion Science*, *42*(1), 53–66. https://doi.org/10.1016/S0010-938X(99)00055-4

Korshin, G. V., Ferguson, J. F., & Lancaster, A. N. (2005). Influence of natural organic matter on the morphology of corroding lead surfaces and behavior of lead-containing particles. *Water Research*, *39*(5), 811–818. https://doi.org/10.1016/j.watres.2004.12.009

Korshin, G. V., & Liu, H. (2019). Preventing the colloidal dispersion of Pb(iv) corrosion scales and lead release in drinking water distribution systems. *Environmental Science: Water Research & Technology*, *5*(7), 1262–1269. https://doi.org/10.1039/C9EW00231F

Kuch, A., & Wagner, I. (1983). A mass transfer model to describe lead concentrations in drinking water. *Water Research*, *17*(10), 1303–1307. https://doi.org/10.1016/0043-1354(83)90256-7

Lambert, S. M., & Watters, J. I. (1957). The complexes of pyrophosphate ion with alkali metal ions. *Journal of the American Chemical Society*, *79*(16), 4262–4265.

Lang, F., & Kaupenjohann, M. (2003). Effect of dissolved organic matter on the precipitation and mobility of the lead compound chloropyromorphite in solution: Precipitation of chloropyromorphite from soil solution. *European Journal of Soil Science*, *54*(1), 139–148. https://doi.org/10.1046/j.1365-2389.2003.00505.x

Langevin, D., Raspaud, E., Mariot, S., Knyazev, A., Stocco, A., Salonen, A., Luch, A., Haase, A., Trouiller, B., Relier, C., Lozano, O., Thomas, S., Salvati, A., & Dawson, K. (2018). Towards reproducible measurement of nanoparticle size using dynamic light scattering: Important controls and considerations. *NanoImpact*, *10*, 161–167. https://doi.org/10.1016/j.impact.2018.04.002

Lead, J. R., & Wilkinson, K. J. (2007). Environmental colloids and particles: Current knowledge and future developments. *IUPAC Series on Analytical and Physical Chemistry of Environmental Systems*, *10*, 1.

Leung, K., & Criscenti, L. J. (2017). Lead and selenite adsorption at water–goethite interfaces from first principles. *Journal of Physics: Condensed Matter*, *29*(36), 365101. https://doi.org/10.1088/1361-648X/aa7e4f

Levallois, P., St-Laurent, J., Gauvin, D., Courteau, M., Prévost, M., Campagna, C., Lemieux, F., Nour, S., D'Amour, M., & Rasmussen, P. E. (2014). The impact of drinking water, indoor dust and paint on blood lead levels of children aged 1–5 years in Montréal (Québec, Canada). *Journal of Exposure Science & Environmental Epidemiology*, *24*(2), 185–191. https://doi.org/10.1038/jes.2012.129

Li, B., Trueman, B. F., Locsin, J. M., Gao, Y., Rahman, M. S., Park, Y., & Gagnon, G. A. (2021a). Impact of sodium silicate on lead release from lead(II) carbonate. *Environmental Science: Water Research & Technology*, *7*(3), 599–609. https://doi.org/10.1039/D0EW00886A

Li, B., Trueman, B. F., Locsin, J. M., Gao, Y., Rahman, M. S., Park, Y., & Gagnon, G. A. (2021b). Impact of sodium silicate on lead release from lead(ii) carbonate. *Environmental Science: Water Research & Technology*, *7*(3), 599–609. https://doi.org/10.1039/D0EW00886A

Li, B., Trueman, B. F., Munoz, S., Locsin, J. M., & Gagnon, G. A. (2021a). Impact of sodium silicate on lead release and colloid size distributions in drinking water. *Water Research*, *190*, 116709. https://doi.org/10.1016/j.watres.2020.116709

Li, B., Trueman, B. F., Munoz, S., Locsin, J. M., & Gagnon, G. A. (2021b). Impact of sodium silicate on lead release and colloid size distributions in drinking water. *Water Research*, *190*, 116709. https://doi.org/10.1016/j.watres.2020.116709

Li, B., Trueman, B. F., Rahman, M. S., Gao, Y., Park, Y., & Gagnon, G. A. (2019). Understanding the impacts of sodium silicate on water quality and iron oxide particles. *Environmental Science: Water Research & Technology*, *5*(8), 1360–1370. https://doi.org/10.1039/C9EW00257J

Li, M., Liu, Z., Chen, Y., & Hai, Y. (2016). Characteristics of iron corrosion scales and water quality variations in drinking water distribution systems of different pipe materials. *Water Research*, *106*, 593–603. https://doi.org/10.1016/j.watres.2016.10.044

Lin, Y.-P., & Singer, P. C. (2005). Inhibition of calcite crystal growth by polyphosphates. *Water Research*, *39*(19), 4835–4843. https://doi.org/10.1016/j.watres.2005.10.003

Lin, Y.-P., & Valentine, R. L. (2008). The Release of Lead from the Reduction of Lead Oxide (PbO2) by Natural Organic Matter. *Environmental Science & Technology*, *42*(3), 760–765. https://doi.org/10.1021/es071984w

Lishtvan, I., Dudarchik, V., Kovrik, S., Smychnik, T., & Strigutskii, V. (2005). Peculiarities of the formation of supramolecular structures of copper-and lead-humic acid complexes in aqueous solutions. *Colloid Journal*, *67*(6), 741.

Liu, G., Ling, F. Q., van der Mark, E. J., Zhang, X. D., Knezev, A., Verberk, J. Q. J. C., van der Meer, W. G. J., Medema, G. J., Liu, W. T., & van Dijk, J. C. (2016). Comparison of Particle-Associated Bacteria from a Drinking Water Treatment Plant and Distribution Reservoirs with Different Water Sources. *Scientific Reports*, *6*(1), 20367. https://doi.org/10.1038/srep20367

Locsin, J. M., Trueman, B. F., Serracin-Pitti, D., Stanton, G. M., & Gagnon, G. A. (2020). Potential regulatory implications of Health Canada's new lead guideline. *AWWA Water Science*, *2*(4), e1182. https://doi.org/10.1002/aws2.1182

Loghman-Adham, M. (1997). Renal effects of environmental and occupational lead exposure. *Environmental Health Perspectives*, *105*(9), 928–939. https://doi.org/10.1289/ehp.97105928

Lu, J., Sun, M., Yuan, Z., Qi, S., Tong, Z., Li, L., & Meng, Q. (2019). Innovative insight for sodium hexametaphosphate interaction with serpentine. *Colloids and Surfaces A: Physicochemical and Engineering Aspects*, *560*, 35–41. https://doi.org/10.1016/j.colsurfa.2018.09.076

Lytle, D. A., Formal, C., Cahalan, K., Muhlen, C., & Triantafyllidou, S. (2021). The impact of sampling approach and daily water usage on lead levels measured at the tap. *Water Research*, *197*, 117071. https://doi.org/10.1016/j.watres.2021.117071

Lytle, D. A., Formal, C., Doré, E., Muhlen, C., Harmon, S., Williams, D., Triantafyllidou, S., & Pham, M. (2020). Synthesis and characterization of stable lead (II) orthophosphate nanoparticle suspensions. *Journal of Environmental Science and Health, Part A*, *55*(13), 1504–1512. https://doi.org/10.1080/10934529.2020.1810498

Lytle, D. A., & Schock, M. R. (2000). Impact of stagnation time on metal dissolution from plumbing materials in drinking water. *Journal of Water Supply: Research and Technology-Aqua*, *49*(5), 243–257. https://doi.org/10.2166/aqua.2000.0021

Lytle, D. A., Schock, M. R., Formal, C., Bennett-Stamper, C., Harmon, S., Nadagouda, M. N., Williams, D., DeSantis, M. K., Tully, J., & Pham, M. (2020). Lead particle size fractionation and identification in Newark, New Jersey's drinking water. *Environmental Science & Technology*, *54*(21), 13672–13679. https://doi.org/10.1021/acs.est.0c03797

Lytle, D. A., Schock, M. R., Wait, K., Cahalan, K., Bosscher, V., Porter, A., & Del Toral, M. (2019). Sequential drinking water sampling as a tool for evaluating lead in flint, Michigan. *Water Research*, *157*, 40–54. https://doi.org/10.1016/j.watres.2019.03.042

Lytle, D. A., & Snoeyink, V. L. (2002a). Effect of ortho-and polyphosphates on the properties of iron particles and suspensions. *Journal - American Water Works Association*, *94*(10), 87–99. https://doi.org/10.1002/j.1551-8833.2002.tb09560.x

Lytle, D. A., & Snoeyink, V. L. (2002b). Effect of ortho-and polyphosphates on the properties of Iron particles and suspensions. *Journal AWWA*, *94*(10), 87–99. https://doi.org/10.1002/j.1551-8833.2002.tb09560.x

Lyvén, B., Hassellöv, M., Haraldsson, C., & Turner, D. (1997). Optimisation of on-channel preconcentration in flow field-flow fractionation for the determination of size distributions of low molecular weight colloidal material in natural waters. *Analytica Chimica Acta*, *357*(3), 187–196. https://doi.org/10.1016/S0003-2670(97)00565-5

MacBerthouex, P., & Brown, L. C. (1996). *Statistics for Environmental Engineers*. Lewis Publishers.

Masters, S. V., & Edwards, M. (2015). Increased lead in water associated with iron corrosion. *Environmental Engineering Science*, *32*(5), 361–369. https://doi.org/10.1089/ees.2014.0400

Masters, S. V., Parks, J., Atassi, A., & Edwards, M. A. (2016). Inherent variability in lead and copper collected during standardized sampling. *Environmental Monitoring and Assessment*, *188*(3), 177. https://doi.org/10.1007/s10661-016-5182-x

Masters, S. V., Welter, G. J., & Edwards, M. (2016). Seasonal Variations in Lead Release to Potable Water. *Environmental Science & Technology*, *50*(10), 5269–5277. https://doi.org/10.1021/acs.est.5b05060

McCullough, J. F., Van Wazer, J. R., & Griffith, E. J. (1956). Structure and Properties of the Condensed Phosphates. XI. Hydrolytic Degradation of Graham's Salt. *Journal of the American Chemical Society*, *78*(18), 4528–4533. https://doi.org/10.1021/ja01599a006

McFadden, M., Giani, R., Kwan, P., & Reiber, S. H. (2011). Contributions to drinking water lead from galvanized iron corrosion scales. *Journal - AWWA*, *103*(4), 76–89. https://doi.org/10.1002/j.1551-8833.2011.tb11437.x

McGaughey, C. (1983). Binding of Polyphosphates and Phosphonates to Hydroxyapatite, Subsequent Hydrolysis, Phosphate Exchange and Effects on Demineralization, Mineralization and Microcrystal Aggregation. *Caries Research*, *17*(3), 229–241. https://doi.org/10.1159/000260671

McKenzie, R. (1980). The adsorption of lead and other heavy metals on oxides of manganese and iron. *Soil Research*, *18*(1), 61–73.

McNeill, L., & Edwards, M. (2002). Phosphate inhibitor use at US utilities. *J. Am. Water Works Assoc*, *94*(7), 57–63.

McNeill, L. S., & Edwards, M. (2002). Phosphate inhibitor use at US utilities. *Journal AWWA*, *94*(7), 57–63. https://doi.org/10.1002/j.1551-8833.2002.tb09506.x

Michelmore, A., Gong, W., Jenkins, P., & Ralston, J. (2000). The interaction of linear polyphosphates with titanium dioxide surfaces. *Physical Chemistry Chemical Physics*, *2*(13), 2985–2992.

Mitrano, D. M., Barber, A., Bednar, A., Westerhoff, P., Higgins, C. P., & Ranville, J. F. (2012). Silver nanoparticle characterization using single particle ICP-MS (SP-ICP-MS) and asymmetrical flow field flow fractionation ICP-MS (AF4-ICP-MS). *Journal of Analytical Atomic Spectrometry*, *27*(7), 1131–1142. https://doi.org/10.1039/C2JA30021D

Miyahima, T., Onaka, T., & Ohashi, S. (1981). A Gel Chromatographic Study on the Interactions of Long-Chain Polyphosphate Anions with Magnesium Ions. In *Phosphorus Chemistry* (Vol. 171, pp. 377–380). AMERICAN CHEMICAL SOCIETY. https://doi.org/10.1021/bk-1981-0171.ch078

Miyajima, T., Onaka, T., & Ohashi, S. (1981). A Gel Chromatographic Study on the Interactions of Long-Chain Polyphosphate Anions with Magnesium Ions. In *Phosphorus Chemistry* (Vol. 171, pp. 377–380). AMERICAN CHEMICAL SOCIETY. https://doi.org/10.1021/bk-1981-0171.ch078

Montaño, M. D., Badiei, H. R., Bazargan, S., & Ranville, J. F. (2014). Improvements in the detection and characterization of engineered nanoparticles using spICP-MS with microsecond dwell times. *Environmental Science: Nano*, *1*(4), 338–346. https://doi.org/10.1039/C4EN00058G

Montaño, M. D., Olesik, J. W., Barber, A. G., Challis, K., & Ranville, J. F. (2016). Single Particle ICP-MS: Advances toward routine analysis of nanomaterials. *Analytical and Bioanalytical Chemistry*, *408*(19), 5053–5074. https://doi.org/10.1007/s00216-016-9676-8

Moore, J., & Cerasoli, E. (2017). Particle light scattering methods and applications. In *Encyclopedia of Spectroscopy and Spectrometry* (pp. 543–553). Elsevier. https://doi.org/10.1016/B978-0-12-803224-4.00040-6

Mosley, L. M., Hunter, K. A., & Ducker, W. A. (2003). Forces between Colloid Particles in Natural Waters. *Environmental Science & Technology*, *37*(15), 3303–3308. https://doi.org/10.1021/es026216d

Mourdikoudis, S., M. Pallares, R., & K. Thanh, N. T. (2018). Characterization techniques for nanoparticles: Comparison and complementarity upon studying nanoparticle properties. *Nanoscale*, *10*(27), 12871–12934. https://doi.org/10.1039/C8NR02278J

Naderi, R., Arman, S. Y., & Fouladvand, Sh. (2014). Investigation on the inhibition synergism of new generations of phosphate-based anticorrosion pigments. *Dyes and Pigments*, *105*, 23–33. https://doi.org/10.1016/j.dyepig.2014.01.015

Napper, D. H. (1970). Colloid stability. *Industrial & Engineering Chemistry Product Research and Development*, *9*(4), 467–477.

Nelson, Y. M., Lo, W., Lion, L. W., Shuler, M. L., & Ghiorse, W. C. (1995). Lead distribution in a simulated aquatic environment: Effects of bacterial biofilms and iron oxide. *Water Research*, *29*(8), 1934–1944. https://doi.org/10.1016/0043-1354(94)00351-7

Nic, M., Jirat, J., & Kosata, B. (2019). *The IUPAC Compendium of Chemical Terminology: The Gold Book* (V. Gold, Ed.; 4th ed.). International Union of Pure and Applied Chemistry (IUPAC). https://doi.org/10.1351/goldbook

Nigg, J. T., Knottnerus, G. M., Martel, M. M., Nikolas, M., Cavanagh, K., Karmaus, W., & Rappley, M. D. (2008). Low Blood Lead Levels Associated with Clinically Diagnosed Attention-Deficit/Hyperactivity Disorder and Mediated by Weak Cognitive Control. *Impulse Control: Aggression, Addiction, and Attention Deficits*, *63*(3), 325–331. https://doi.org/10.1016/j.biopsych.2007.07.013

Noel, J. D., Wang, Y., & Giammar, D. E. (2014). Effect of water chemistry on the dissolution rate of the lead corrosion product hydrocerussite. *Water Research*, *54*, 237–246. https://doi.org/10.1016/j.watres.2014.02.004

Nova Scotia Environment. (2010). A guide to assist nova scotia municipal water works prepare annual sampling plans. In *A Guide to Assist Nova Scotia Municipal Water Works Prepare Annual Sampling Plans*.

NSF International. (2015). *NSF/ANSI 53: Drinking Water Treatment Units–Health Effects*.

NSF International. (2019). *NSF/ANSI 53: Drinking Water Treatment Units–Health Effects*.

O'Reilly, S. E., & Hochella Jr, M. F. (2003). Lead sorption efficiencies of natural and synthetic Mn and Fe-oxides. *Geochimica et Cosmochimica Acta*, *67*(23), 4471–4487. https://doi.org/10.1016/S0016-7037(03)00413-7

O'Reilly, S. E., Strawn, D. G., & Sparks, D. L. (2001). Residence Time Effects on Arsenate Adsorption/Desorption Mechanisms on Goethite. *Soil Science Society of America Journal*, *65*(1), 67–77. https://doi.org/10.2136/sssaj2001.65167x

Ostergren, J. D., Trainor, T. P., Bargar, J. R., Brown Jr, G. E., & Parks, G. A. (2000). Inorganic ligand effects on Pb (II) sorption to goethite (α-FeOOH): I. Carbonate. *Journal of Colloid and Interface Science*, *225*(2), 466–482.

Pace, H. E., Rogers, N. J., Jarolimek, C., Coleman, V. A., Gray, E. P., Higgins, C. P., & Ranville, J. F. (2012). Single particle inductively coupled plasma-mass spectrometry: A performance evaluation and method comparison in the determination of nanoparticle size. *Environmental Science & Technology*, *46*(22), 12272–12280. https://doi.org/10.1021/es301787d

Pan, W., Johnson, E. R., & Giammar, D. E. (2021). Lead phosphate particles in tap water: Challenges for point-of-use filters. *Environmental Science & Technology Letters*, *8*(3), 244–249. https://doi.org/10.1021/acs.estlett.1c00055

Patterson, A. (1939). The Scherrer formula for X-ray particle size determination. *Physical Review*, *56*(10), 978.

Peckys, D. B., & de Jonge, N. (2011). Visualizing Gold Nanoparticle Uptake in Live Cells with Liquid Scanning Transmission Electron Microscopy. *Nano Letters*, *11*(4), 1733–1738. https://doi.org/10.1021/nl200285r

Peng, C.-Y., Hill, A. S., Friedman, M. J., Valentine, R. L., Larson, G. S., Romero, A. M. Y., Reiber, S. H., & Korshin, G. V. (2012). Occurrence of trace inorganic contaminants in drinking water distribution systems. *Journal AWWA*, *104*(3), E181–E193. https://doi.org/10.5942/jawwa.2012.104.0042

Peng, C.-Y., Korshin, G. V., Valentine, R. L., Hill, A. S., Friedman, M. J., & Reiber, S. H. (2010). Characterization of elemental and structural composition of corrosion scales and deposits formed in drinking water distribution systems. *Water Research*, *44*(15), 4570–4580. https://doi.org/10.1016/j.watres.2010.05.043

Pieper, K. J., Martin, R., Tang, M., Walters, L., Parks, J., Roy, S., Devine, C., & Edwards, M. A. (2018). Evaluating Water Lead Levels During the Flint Water Crisis. *Environmental Science & Technology*, *52*(15), 8124–8132. https://doi.org/10.1021/acs.est.8b00791

Pinto, J. A., McAnally, A. S., & Flora, J. R. V. (1997). Evaluation of lead and copper corrosion control techniques. *Journal of Environmental Science and Health . Part A: Environmental Science and Engineering and Toxicology*, *32*(1), 31–53. https://doi.org/10.1080/10934529709376526

Polychronopolous, M., Dudley, K., Ryan, G., & Hearn, J. (2003). Investigation of factors contributing to dirty water events in reticulation systems and evaluation of flushing methods to remove deposited particles. *Water Supply*, *3*(1–2), 295–306. https://doi.org/10.2166/ws.2003.0117

Prazeres, D. M. F. (1997). A theoretical analogy between multistage ultrafiltration and size-exclusion chromatography. *Chemical Engineering Science*, *52*(6), 953–960. https://doi.org/10.1016/S0009-2509(96)00467-8

Purchase, J. M., Rouillier, R., Pieper, K. J., & Edwards, M. (2021). Understanding failure modes of NSF/ANSI 53 lead-certified point-of-use pitcher and faucet filters. *Environmental Science & Technology Letters*, *8*(2), 155–160. https://doi.org/10.1021/acs.estlett.0c00709

Quevauviller, Ph., & Donard, O. F. X. (1991). Organotin stability during storage of marine waters and sediments. *Fresenius' Journal of Analytical Chemistry*, *339*(1), 6–14. https://doi.org/10.1007/BF00324751

R Core Team. (2022). *R: A language and environment for statistical computing*. https://www.R-project.org/

Rahman, S. M., Kippler, M., Ahmed, S., Palm, B., El Arifeen, S., & Vahter, M. (2015). Manganese exposure through drinking water during pregnancy and size at birth: A prospective cohort study. *Reproductive Toxicology*, *53*, 68–74. https://doi.org/10.1016/j.reprotox.2015.03.008

Rashchi, F., & Finch, J. A. (2000). Polyphosphates: A review their chemistry and application with particular reference to mineral processing. *Minerals Engineering*, *13*(10), 1019–1035. https://doi.org/10.1016/S0892-6875(00)00087-X

Rashchi, F., & Finch, J. A. (2002). Lead-Polyphosphate Complexes. *Canadian Metallurgical Quarterly*, *41*(1), 1–6. https://doi.org/10.1179/cmq.2002.41.1.1

Rasmussen, L., & Toftlund, H. (1986). Phosphate compounds as iron chelators in animal cell cultures. *In Vitro Cellular & Developmental Biology*, *22*(4), 177–179. https://doi.org/10.1007/BF02623301

Reuben, A., Caspi, A., Belsky, D. W., Broadbent, J., Harrington, H., Sugden, K., Houts, R. M., Ramrakha, S., Poulton, R., & Moffitt, T. E. (2017). Association of Childhood Blood Lead Levels With Cognitive Function and Socioeconomic Status at Age 38 Years and With IQ Change and Socioeconomic Mobility Between Childhood and Adulthood. *JAMA*, *317*(12), 1244–1251. https://doi.org/10.1001/jama.2017.1712

Riblet, C., Deshommes, E., Laroche, L., & Prévost, M. (2019). True exposure to lead at the tap: Insights from proportional sampling, regulated sampling and water use monitoring. *Water Research*, *156*, 327–336. https://doi.org/10.1016/j.watres.2019.03.005

Robinson, R. B., Reed, G. D., & Frazier, B. (1992). Iron and Manganese Sequestration Facilities Using Sodium Silicate. *Journal AWWA*, *84*(2), 77–82. https://doi.org/10.1002/j.1551-8833.1992.tb07307.x

Robinson, R. B., & Ronk, S. K. (1987). The Treatability of Manganese by Sodium Silicate and Chlorine. *Journal AWWA*, *79*(11), 64–70. https://doi.org/10.1002/j.1551-8833.1987.tb02945.x

Salasi, M., Shahrabi, T., Roayaei, E., & Aliofkhazraei, M. (2007). The electrochemical behaviour of environment-friendly inhibitors of silicate and phosphonate in corrosion control of carbon steel in soft water media. *Materials Chemistry and Physics*, *104*(1), 183–190. https://doi.org/10.1016/j.matchemphys.2007.03.008

Sandvig, A., Kwan, P., Kirmeyer, G., Maynard, B., Mast, D., Trussell, R. R., Trussell, S., Cantor, A., & Prescott, A. (2009). *Contribution of service line and plumbing fixtures to lead and copper rule compliance issues*. Water Environment Research Foundation Alexandria, VA.

Santucci, R. J., & Scully, J. R. (2020). The pervasive threat of lead (Pb) in drinking water: Unmasking and pursuing scientific factors that govern lead release. *Proceedings of the National Academy of Sciences*. https://doi.org/10.1073/pnas.1913749117

Sarin P., Snoeyink V. L., Lytle D. A., & Kriven W. M. (2004). Iron Corrosion Scales: Model for Scale Growth, Iron Release, and Colored Water Formation. *Journal of Environmental Engineering*, *130*(4), 364–373. https://doi.org/10.1061/(ASCE)0733-9372(2004)130:4(364)

Schock, M. R. (1989). Understanding corrosion control strategies for lead. *Journal - American Water Works Association*, *81*(7), 88–100. https://doi.org/10.1002/j.1551-8833.1989.tb03244.x

Schock, M. R., Cantor, A. F., Triantafyllidou, S., Desantis, M. K., & Scheckel, K. G. (2014). Importance of pipe deposits to Lead and Copper Rule compliance. *Journal AWWA*, *106*(7). https://doi.org/10.5942/jawwa.2014.106.0064

Schock, M. R., & Lemieux, F. G. (2010). Challenges in addressing variability of lead in domestic plumbing. *Water Supply*, *10*(5), 793–799. https://doi.org/10.2166/ws.2010.173

Schock, M. R., Lytle, D. A., Sandvig, A. M., Clement, J., & Harmon, S. M. (2005). Replacing polyphosphate with silicate to solve lead, copper, and source water iron problems. *Journal - American Water Works Association*, *97*(11), 84–93. https://doi.org/10.1002/j.1551-8833.2005.tb07521.x

Schock, M. R., & Oliphant, R. J. (1996). Corrosion and Solubility of Lead in Drinking Water. In *Internal Corrosion of Water Distribution Systems* (p. 131−230). AWWA Research Foundation.

Senftle, F. E., Thorpe, A. N., Grant, J. R., & Barkatt, A. (2007). Superparamagnetic nanoparticles in tap water. *Water Research*, *41*(13), 3005–3011. https://doi.org/10.1016/j.watres.2007.03.035

Seth, A., Bachmann, R., Boxall, J., Saul, A., & Edyvean, R. (2004). Characterisation of materials causing discolouration in potable water systems. *Water Science and Technology*, *49*(2), 27–32. https://doi.org/10.2166/wst.2004.0080

Shi, Q., Zhang, S., Ge, J., Wei, J., Christodoulatos, C., Korfiatis, G. P., & Meng, X. (2020). Lead immobilization by phosphate in the presence of iron oxides: Adsorption versus precipitation. *Water Research*, *179*, 115853. https://doi.org/10.1016/j.watres.2020.115853

Shi, Z., & Stone, A. T. (2009). PbO2(s, Plattnerite) Reductive Dissolution by Natural Organic Matter: Reductant and Inhibitory Subfractions. *Environmental Science & Technology*, *43*(10), 3604–3611. https://doi.org/10.1021/es802441g

Shih, R. A., Hu, H., Weisskopf, M. G., & Schwartz, B. S. (2007). Cumulative Lead Dose and Cognitive Function in Adults: A Review of Studies That Measured Both Blood Lead and Bone Lead. *Environmental Health Perspectives*, *115*(3), 483–492. https://doi.org/10.1289/ehp.9786

Singh, B., & Grafe, M. (2010). *Synchrotron-based techniques in soils and sediments*. Elsevier.

Singh, R., & Hankins, N. (2016). *Emerging membrane technology for sustainable water treatment*. Elsevier.

Sly, L. I., Hodgkinson, M. C., & Arunpairojana, V. (1990). Deposition of manganese in a drinking water distribution system. *Applied and Environmental Microbiology*, *56*(3), 628–639. https://doi.org/10.1128/aem.56.3.628-639.1990

Socrates, G. (2004). *Infrared and Raman characteristic group frequencies: Tables and charts*. John Wiley & Sons.

Stetefeld, J., McKenna, S. A., & Patel, T. R. (2016). Dynamic light scattering: A practical guide and applications in biomedical sciences. *Biophysical Reviews*, *8*(4), 409–427. https://doi.org/10.1007/s12551-016-0218-6

Striegel, A. M., & Brewer, A. K. (2012). Hydrodynamic Chromatography. *Annual Review of Analytical Chemistry*, *5*(1), 15–34. https://doi.org/10.1146/annurev-anchem-062011-143107

Štulík, K., Pacáková, V., & Tichá, M. (2003). Some potentialities and drawbacks of contemporary size-exclusion chromatography. *Journal of Biochemical and Biophysical Methods*, *56*(1–3), 1–13. https://doi.org/10.1016/S0165-022X(03)00053-8

Sundberg, R., Holm, R., Hertzman, S. N., Hutchinson, B., & Lindh-Ulmgren, E. (2003). Dezincification (da) and intergranular corrosion (iga) of brass-influence of composition and heat treatment. *Metall*, *57*(11), 721–731.

Team, R. C. (2013). *R: A language and environment for statistical computing*.

Triantafyllidou, S., & Edwards, M. (2012). Lead (Pb) in Tap Water and in Blood: Implications for Lead Exposure in the United States. *Critical Reviews in Environmental Science and Technology*, *42*(13), 1297–1352. https://doi.org/10.1080/10643389.2011.556556

Triantafyllidou, S., Parks, J., & Edwards, M. (2007). Lead Particles in Potable Water. *Journal AWWA*, *99*(6), 107–117. https://doi.org/10.1002/j.1551-8833.2007.tb07959.x

Trivedi, P., Axe, L., & Tyson, T. A. (2001). XAS Studies of Ni and Zn Sorbed to Hydrous Manganese Oxide. *Environmental Science & Technology*, *35*(22), 4515–4521. https://doi.org/10.1021/es0109848

Trivedi, P., Dyer, J. A., & Sparks, D. L. (2003). Lead sorption onto ferrihydrite. 1. A macroscopic and spectroscopic assessment. *Environmental Science & Technology*, *37*(5), 908–914. https://doi.org/10.1021/es0257927

Trueman, B. F. (n.d.). *fffprocessr: Process FFF-UV-MALS-ICP-MS data*. https://github.com/bentrueman/fffprocessr.

Trueman, B. F., Anaviapik-Soucie, T., L'Hérault, V., & Gagnon, G. A. (2019). Characterizing colloidal metals in drinking water by field flow fractionation. *Environmental Science: Water Research & Technology*, *5*(12), 2202–2209. https://doi.org/10.1039/C9EW00560A

Trueman, B. F., Camara, E., & Gagnon, G. A. (2016). Evaluating the Effects of Full and Partial Lead Service Line Replacement on Lead Levels in Drinking Water. *Environmental Science & Technology*, *50*(14), 7389–7396. https://doi.org/10.1021/acs.est.6b01912

Trueman, B. F., & Gagnon, G. A. (2016a). A new analytical approach to understanding nanoscale lead-iron interactions in drinking water distribution systems. *Journal of Hazardous Materials*, *311*, 151–157. https://doi.org/10.1016/j.jhazmat.2016.03.001

Trueman, B. F., & Gagnon, G. A. (2016b). Understanding the role of particulate iron in lead release to drinking water. *Environmental Science & Technology*, *50*(17), 9053–9060. https://doi.org/10.1021/acs.est.6b01153

Trueman, B. F., Gregory, B. S., McCormick, N. E., Gao, Y., Gora, S., Anaviapik-Soucie, T., L'Hérault, V., & Gagnon, G. A. (2019). Manganese increases lead release to drinking water. *Environmental Science & Technology*, *53*(9), 4803–4812. https://doi.org/10.1021/acs.est.9b00317

Trueman, B. F., Krkošek, W. H., & Gagnon, G. A. (2018a). Effects of ortho- and polyphosphates on lead speciation in drinking water. *Environmental Science: Water Research & Technology*, *4*(4), 505–512. https://doi.org/10.1039/C7EW00521K

Trueman, B. F., Krkošek, W. H., & Gagnon, G. A. (2018b). Effects of ortho-and polyphosphates on lead speciation in drinking water. *Environmental Science: Water Research & Technology*, *4*(4), 505–512.

Trueman, B. F., Locsin, J. A., Doré, E., & Hood, K. M. (2022). *Sodium silicate and hexametaphosphate promote the release of (oxyhydr)oxide nanoparticles from corroding iron.* ChemRxiv. https://doi.org/10.26434/chemrxiv-2022-rtzqm

Trueman, B. F., Sweet, G. A., Harding, M. D., Estabrook, H., Bishop, D. P., & Gagnon, G. A. (2017). Galvanic corrosion of lead by iron (oxyhydr)oxides: Potential impacts on drinking water quality. *Environmental Science & Technology*, *51*(12), 6812–6820. https://doi.org/10.1021/acs.est.7b01671

Tso, C., Zhung, C., Shih, Y., Tseng, Y.-M., Wu, S., & Doong, R. (2010). Stability of metal oxide nanoparticles in aqueous solutions. *Water Science and Technology*, *61*(1), 127–133. https://doi.org/10.2166/wst.2010.787

Tully, J., DeSantis, M. K., & Schock, M. R. (2019a). Water quality–pipe deposit relationships in Midwestern lead pipes. *AWWA Water Science*, *1*(2), e1127. https://doi.org/10.1002/aws2.1127

Tully, J., DeSantis, M. K., & Schock, M. R. (2019b). Water quality–pipe deposit relationships in Midwestern lead pipes. *AWWA Water Science*, *1*(2), e1127. https://doi.org/10.1002/aws2.1127

US Environmental Protection Agency (USEPA). (2016). Optimal Corrosion Control Treatment Evaluation Technical Recommendations for Primacy Agencies and Public Water Systems. *EPA 816-B-16-003*.

US EPA. (1991). *Maximum contaminant level goals and national primary drinking water regulations for lead and copper. Final rule* (Vol. 56).

US EPA. (1994a). *EPA Method 200.8, Revision 5.4: Determination of trace elements in waters and wastes by inductively coupled plasma-mass spectrometry* (p. 58). Office of Research and Development, Cincinnati, OH, United States. https://www.epa.gov/esam/epa-method-2008-determination-trace-elements-waters-and-wastes-inductively-coupled-plasma-mass

US EPA. (1994b). *Method 200.7, Revision 4.4: Determination of metals and trace elements in water and wastes by inductively coupled plasma-atomic emission spectrometry*. Office of Research and Development,Cincinnati, OH, United States. https://www.epa.gov/esam/method-2007-determination-metals-and-trace-elements-water-and-wastes-inductively-coupled-plasma

US EPA. (1997). Method 300.1 Determination of inorganic anions in drinking water by ion chromatography. *US Environmental Protection Agency, Cincinnati, OH*.

US EPA. (2010). *Lead and copper rule: Monitoring and reporting guidance for public water systems*. US EPA, Washington, DC. https://www.epa.gov/dwreginfo/lead-and-copper-rule

US EPA. (2021). *National Primary Drinking Water Regulations: Lead and Copper Rule Revisions*. https://www.federalregister.gov/documents/2021/01/15/2020-28691/national-primary-drinking-water-regulations-lead-and-copper-rule-revisions

van den Hoven, T., Buijs, P., Jackson, P., Miller, S., Gardner, M., Leroy, & others. (1999). *Developing a new protocol for the monitoring of lead in drinking water. European commission*. Chemical Analysis, EUR, 19087.

van den Hoven, T., & Slaats, N. (2006). *Lead monitoring*. Wiley.

Van Wazer, J. R., & Callis, C. F. (1958a). Metal complexing by phosphates. *Chemical Reviews*, *58*(6), 1011–1046.

Van Wazer, J. R., & Callis, C. F. (1958b). Metal Complexing By Phosphates. *Chemical Reviews*, *58*(6), 1011–1046. https://doi.org/10.1021/cr50024a001

Vreeburg, I. J. H. G., & Boxall, Dr. J. B. (2007). Discolouration in potable water distribution systems: A review. *Water Research*, *41*(3), 519–529. https://doi.org/10.1016/j.watres.2006.09.028

Wan, B., Elzinga, E. J., Huang, R., & Tang, Y. (2020). Molecular Mechanism of Linear Polyphosphate Adsorption on Iron and Aluminum Oxides. *The Journal of Physical Chemistry C*, *124*(52), 28448–28457. https://doi.org/10.1021/acs.jpcc.0c06127

Wan, B., Huang, R., Diaz, J. M., & Tang, Y. (2019). Manganese Oxide Catalyzed Hydrolysis of Polyphosphates. *ACS Earth and Space Chemistry*, *3*(11), 2623–2634. https://doi.org/10.1021/acsearthspacechem.9b00220

Wan, B., Yang, P., Jung, H., Zhu, M., Diaz, J. M., & Tang, Y. (2021). Iron oxides catalyze the hydrolysis of polyphosphate and precipitation of calcium phosphate minerals. *Geochimica et Cosmochimica Acta*, *305*, 49–65. https://doi.org/10.1016/j.gca.2021.04.031

Wasserstrom, L. W., Miller, S. A., Triantafyllidou, S., Desantis, M. K., & Schock, M. R. (2017a). Scale formation under blended phosphate treatment for a utility with lead pipes. *Journal-American Water Works Association*, *109*(11), E464–E478. https://doi.org/10.5942/jawwa.2017.109.0121

Wasserstrom, L. W., Miller, S. A., Triantafyllidou, S., Desantis, M. K., & Schock, M. R. (2017b). Scale Formation Under Blended Phosphate Treatment for a Utility With Lead Pipes. *Journal AWWA*, *109*(11), E464–E478. https://doi.org/10.5942/jawwa.2017.109.0121

Weesner, F. J., & Bleam, W. F. (1998). Binding characteristics of Pb2+on anion-modified and pristine hydrous oxide surfaces studied by electrophoretic mobility and X-ray absorption spectroscopy. *Journal of Colloid and Interface Science*, *205*(2), 380–389. https://doi.org/10.1006/jcis.1998.5629

Weng, L., Van Riemsdijk, W. H., & Hiemstra, T. (2012). Factors Controlling Phosphate Interaction with Iron Oxides. *Journal of Environmental Quality*, *41*(3), 628–635. https://doi.org/10.2134/jeq2011.0250

Westerhoff, P., Atkinson, A., Fortner, J., Wong, M. S., Zimmerman, J., Gardea-Torresdey, J., Ranville, J., & Herckes, P. (2018). Low risk posed by engineered and incidental nanoparticles in drinking water. *Nature Nanotechnology*, *13*(8), 661–669. https://doi.org/10.1038/s41565-018-0217-9

Wickham, H., Averick, M., Brian, J., Chang, W., McGowan, L., Francois, R., Grolemund, G., Hayes, A., Henry, L., Hester, J., Kuhn, M., Pedersen, T., MIller, E., Banche, S., Muller, K., Ooms, J., Robinson, D., Seidel, D., Spinu, V., … Yutani, H. (2019). Welcome to the tidyverse. *Journal of Open Source Software*, *4*(43), 1686. https://doi.org/10.21105/joss.01686.

Wilkinson, K. J., Balnois, E., Leppard, G. G., & Buffle, J. (1999). Characteristic features of the major components of freshwater colloidal organic matter revealed by transmission electron and atomic force microscopy. *Colloids and Surfaces A: Physicochemical and Engineering Aspects*, *155*(2–3), 287–310. https://doi.org/10.1016/S0927-7757(98)00874-7

Winning, L. (2015). *Investigation of the source and occurrence of lead in the Brandon water supply system* [Master's thesis]. University of Manitoba.

Winning, L. D., Gorczyca, B., & Brezinski, K. (2017). Effect of total organic carbon and aquatic humic substances on the occurrence of lead at the tap. *Water Quality Research Journal*, *52*(1), 2–10. https://doi.org/10.2166/wqrjc.2017.028

Wohlleben, W. (2012). Validity range of centrifuges for the regulation of nanomaterials: From classification to as-tested coronas. *Journal of Nanoparticle Research*, *14*(12), 1300. https://doi.org/10.1007/s11051-012-1300-z

Woodward, R. C., Heeris, J., St. Pierre, T. G., Saunders, M., Gilbert, E. P., Rutnakornpituk, M., Zhang, Q., & Riffle, J. S. (2007). A comparison of methods for the measurement of the particle-size distribution of magnetic nanoparticles. *Journal of Applied Crystallography*, *40*(s1), s495–s500. https://doi.org/10.1107/S002188980700091X

Worms, I. A. M., Al-Gorani Szigeti, Z., Dubascoux, S., Lespes, G., Traber, J., Sigg, L., & Slaveykova, V. I. (2010). Colloidal organic matter from wastewater treatment plant effluents: Characterization and role in metal distribution. *Water Research*, *44*(1), 340–350. https://doi.org/10.1016/j.watres.2009.09.037

Xie, L., & Giammar, D. E. (2007). Chapter 13 Influence of phosphate on adsorption and surface precipitation of lead on iron oxide surfaces. In *Developments in Earth and Environmental Sciences* (Vol. 7, pp. 349–373). Elsevier. https://doi.org/10.1016/S1571-9197(07)07013-9

Xie, Y., & Giammar, D. E. (2011). Effects of flow and water chemistry on lead release rates from pipe scales. *Water Research*, *45*(19), 6525–6534. https://doi.org/10.1016/j.watres.2011.09.050

Xu, Y., Boonfueng, T., Axe, L., Maeng, S., & Tyson, T. (2006). Surface complexation of Pb (II) on amorphous iron oxide and manganese oxide: Spectroscopic and time studies. *Journal of Colloid and Interface Science*, *299*(1), 28–40. https://doi.org/10.1016/j.jcis.2006.01.041

Yang, F., Shi, B., Gu, J., Wang, D., & Yang, M. (2012). Morphological and physicochemical characteristics of iron corrosion scales formed under different water source histories in a drinking water distribution system. *Water Research*, *46*(16), 5423–5433. https://doi.org/10.1016/j.watres.2012.07.031

Yano, J., & Yachandra, V. K. (2009). X-ray absorption spectroscopy. *Photosynthesis Research*, *102*(2), 241. https://doi.org/10.1007/s11120-009-9473-8

Zhang, H., Penn, R. L., Hamers, R. J., & Banfield, J. F. (1999). Enhanced adsorption of molecules on surfaces of nanocrystalline particles. *The Journal of Physical Chemistry B*, *103*(22), 4656–4662. https://doi.org/10.1021/jp984574q

Zhang, Y., & Edwards, M. (2011). Zinc content in brass and its influence on lead leaching. *Journal AWWA*, *103*(7), 76–83. https://doi.org/10.1002/j.1551-8833.2011.tb11496.x

Zhao, J., Giammar, D. E., Pasteris, J. D., Dai, C., Bae, Y., & Hu, Y. (2018a). Formation and aggregation of lead phosphate particles: Implications for lead immobilization in water supply systems. *Environmental Science & Technology*, *52*(21), 12612–12623. https://doi.org/10.1021/acs.est.8b02788

Zhao, J., Giammar, D. E., Pasteris, J. D., Dai, C., Bae, Y., & Hu, Y. (2018b). Formation and Aggregation of Lead Phosphate Particles: Implications for Lead Immobilization in Water Supply Systems. *Environmental Science & Technology*, *52*(21), 12612–12623. https://doi.org/10.1021/acs.est.8b02788

Zidouh, H. (2009). Velocity profiles and wall shear stress in turbulent transient pipe flow. *International Journal of Dynamics of Fluids*, *5*(1), 61–84.

Appendix A Supporting Data for Chapter 2

Table 11 Water quality characteristics of colloidal lead field studies.

Reference	Location	Sampling protocol	Water Quality Characteristics	Characterization method
(Harrison & Laxen, 1980)	Lancaster, England (building)	Flushed	Alkalinity (mg/L as $CaCO_3$): 21	Membrane filtration
			pH: 7.5	
			Total organic carbon (mg/L): 9.4	
			Specific Conductance (uS): 130	
	Glasgow, Scotland (residential)	>6 hour stagnant	Alkalinity (mg/L as $CaCO_3$): 20	
			pH: 6.8	
			Total organic carbon (mg/L): 1.6	
			Specific Conductance (uS): 92	
	Bentham, England (residential)	>6 hour stagnant	Alkalinity (mg/L as $CaCO_3$): 4	
			pH: 6.7	
			Total organic carbon (mg/L): 8	
			Specific Conductance (uS): 42	
(de Mora et al., 1987)	Site 1, Glasgow, Scotland (residential)	30 minute stagnation	Alkalinity (mg/L as $CaCO_3$): 9-12.5	Membrane filtration
			pH: 7.3-7.8	
			Total organic carbon (mg/L): 3.5-6.2	
	Site 2, Glasgow, Scotland (residential)	30 minute stagnation	Alkalinity (mg/L as $CaCO_3$): 6.1-20.5	
			pH: 6.6-9.3	
			Total organic carbon (mg/L): 3.2-6.5	
	Site 3, Glasgow, Scotland (residential)	30 minute stagnation	Alkalinity (mg/L as $CaCO_3$): 8.3-30	
			pH: 7.8-9.4	
			Total organic carbon (mg/L): 2.9-3.3	
	Site 4, Glasgow, Scotland (residential)	30 minute stagnation	Alkalinity (mg/L as $CaCO_3$): 15-22.6	
			pH: 8.7-9.6	
			Total organic carbon (mg/L): 2.9-3.3	
			Alkalinity (mg/L as $CaCO_3$): 13-41	

Reference	Location	Sampling protocol	Water Quality Characteristics	Characterization method
(De Rosa & Williams, 1992)	England (residential)	30 minute stagnation	pH: 7.8-8.1	Membrane filtration
			Total organic carbon (mg/L): 0.9	
			Turbidity (NTU): 0.39–1.8	
(L. McNeill & Edwards, 2002)	Utility A1, USA (residential)	>6 hour stagnant	Alkalinity (mg/L as $CaCO_3$): 46-55	Membrane filtration
			pH: 7.5-8	
	Utility A2, USA (residential)	>6 hour stagnant	Alkalinity (mg/L as $CaCO_3$): 118	
			pH: 7.9	
	Utility B, USA (residential)	>6 hour stagnant	Alkalinity (mg/L as $CaCO_3$): 50	
			pH: 9.6	
	Utility C, USA (residential)	>6 hour stagnant	Alkalinity (mg/L as $CaCO_3$): 135	
			pH: 8.3	
	Utility E1, USA (residential)	>6 hour stagnant	Alkalinity (mg/L as $CaCO_3$): 156	
			pH: 7.4	
	Utility E2, USA (residential)	>6 hour stagnant	Alkalinity (mg/L as $CaCO_3$): 160	
			pH: 8.3-8.5	
	Utility F, USA (residential)	>6 hour stagnant	Alkalinity (mg/L as $CaCO_3$): 50	
			pH: 9.8	
	Utility G, USA (residential)	>6 hour stagnant	Alkalinity (mg/L as $CaCO_3$): 25	
			pH: 8	
	Utility H, USA (residential)	>6 hour stagnant	Alkalinity (mg/L as $CaCO_3$): 71	
			pH: 7.8	
	Utility I, USA (residential)	>6 hour stagnant	Alkalinity (mg/L as $CaCO_3$): 65-85	
			pH: 8-8.4	
(Barkatt et al., 2009)	Washington, D.C., USA (building)	Weekly stagnation	n/a	Membrane filtration with magnetic measurements
(Trueman & Gagnon, 2016a)	Halifax, NS, Canada (residential)	>6 hour stagnant	Alkalinity (mg/L as $CaCO_3$): 20	SEC-ICP-MS, Membrane filtration
			pH: 7.3	
			Total inorganic carbon (mg/L): 1.5	
			Orthophosphate (mg/L $PO4^{3-}$): 0.5	
			Chloride (mg/L): 9	
			Sulfate (mg/L): 8.5	
			Alkalinity (mg/l as $CaCO_3$): 36	FFF-UV-VIS,

Reference	Location	Sampling protocol	Water Quality Characteristics	Characterization method
(Trueman, Anaviapik-Soucie, et al., 2019)	Nunavut, Canada (buildings)	Random daytime	pH: 7	FFF-ICP-MS (0.45 µm filtered samples)
			Dissolved organic carbon (mg/L): 2.8-3.2	
			Specific Conductance (uS): 71.1	
			SUVA (L/mg m): 3.2–3.8	
(Lytle, Schock, et al., 2020)	Newark, NJ, USA	>6 hour stagnant	pH: 7.6	Membrane filtration, SEM EDXS, TEM, XRD
			Total inorganic carbon (mg/L): 7.05–7.15	

Appendix B Supporting Data for Chapter 4

ATR-FTIR of phosphates in solution

A 50-mL volume of phosphate solution was prepared by adding 1 g P L^{-1} of hexametaphosphate (HexametaP, $(NaPO_3)_6$) (Alfa Aesar, Haverhill, MA), sodium trimetaphosphate (TrimetaP, $(NaPO_3)_3$) (Alfa Aesar, Haverhill, MA), sodium tripolyphosphate (TripolyP, $Na_5P_3O_{10}$) (Alfa Aesar, Haverhill, MA), and orthophosphate (ACS grade phosphoric acid, Fisher Chemical, Fairlawn, NJ)) to ultrapure water (18.2 MΩcm, TOC < 2 μg L^{-1}) with a dissolved organic carbon content of 5 mg C L^{-1}. Dissolved organic carbon was achieved by dissolving sodium bicarbonate powder (Fisher Chemical, Fairlawn, NJ). The pH, measured on an Acument XL50, was adjusted to either pH 7 or 9 by the addition of 1N trace metal grade nitric acid (Fisher Chemical, Fairlawn, NJ) or freshly prepared 2N sodium hydroxide (Fisher Chemical, Fairlawn, NJ).

For analyzing the phosphate solutions, a single-beam Fourier transform infrared spectroscopy in attenuated total reflectance mode (ATR-FTIR) (Bruker alpha-P, USA) was used. After pH adjustment, 20 μL of sample was deposited onto the ATR crystal using a pipette and analyzed. Each ATR spectrum was recorded with the blank cell as the background. Fifty scans at a wavenumber range between 400-4000 cm^{-1} were co-added to obtain each spectrum, with a resolution of 4 cm^{-1}. Baseline spectra for ultrapure water with 5 mg C L^{-1} at pH 7 or 9 was measured in a similar way. Spectral subtraction of the IR spectra of baseline water from the sample spectra produced the spectra of dissolved phosphate species (Figure 21).

The peak assignments for the ATR-FTIR spectra of dissolved phosphates were based on the data of condensed phosphates (Guan et al., 2005; Lu et al., 2019; Michelmore et al., 2000; Socrates, 2004).

ATR-FTIR analysis of phosphates adsorbed on to lead carbonate

Sample preparation and collection

A 50-mL suspension of 1 g L^{-1} lead (II) carbonate (Alfa Aesar, Haverhill, MA) was prepared by dissolving sodium bicarbonate powder (Fisher Chemical, Fairlawn, NJ) in ultrapure water (18.2 MΩcm, TOC < 2 μg L^{-1}) to achieve a 5 mg C L^{-1} dissolved inorganic concentration then adding lead (II) carbonate powder. Phosphates were added at 1 g P L^{-1} as either hexametaphosphate (HexametaP, $(NaPO_3)_6$) (Alfa Aesar, Haverhill, MA), sodium trimetaphosphate (TrimetaP, $(NaPO_3)_3$) (Alfa Aesar, Haverhill, MA), sodium tripolyphosphate (TripolyP, $Na_5P_3O_{10}$) (Alfa Aesar, Haverhill, MA), and orthophosphate (ACS grade phosphoric acid, Fisher Chemical, Fairlawn, NJ)). The pH, measured on an Acument XL50, was adjusted to either pH 7 or 9 by the addition of 1N trace metal grade nitric acid (Fisher Chemical, Fairlawn, NJ) or freshly prepared 2N sodium hydroxide (Fisher Chemical, Fairlawn, NJ). The suspensions were placed on a shaker table for 30-mins at 150 rpm. At the end of the reaction period, samples were analyzed with a single-beam Fourier transform infrared spectroscopy in attenuated total reflectance mode (ATR-FTIR) (Bruker alpha-P, USA).

A thin layer of lead (II) carbonate powder from the reactors was deposited onto the ATR crystal using a plastic spoon and analyzed. Each ATR spectrum was recorded with the blank cell as the background. Fifty scans at a wavenumber range between 400-4000 cm^{-1} were co-added to

obtain each spectrum, with a resolution of 4 cm^{-1}. Baseline spectra for lead (II) carbonate at pH 7 or 9 was obtained by adding 1 g L^{-1} of powder to ultrapure water with 5 mg C L^{-1} and mixing for 30-mins at 150 rpm. Spectral subtraction of the IR spectra of baseline suspension from the sample spectra produced the spectra of adsorbed phosphate species.

Sample analysis

The peak assignments for the ATR-FTIR spectra of adsorbed phosphates on lead carbonate are based on the data of condensed phosphates adsorption on titania and metal (hydr)oxides (Guan et al., 2005; Lu et al., 2019; Michelmore et al., 2000; Socrates, 2004). The important features are summarized in table S1. Due to the complexity caused by the solubility of Pb (II) carbonate at these conditions, carbonate bands representative of cerussite were detected at 670 and 835 cm^{-1} in all experiments. This may indicate surface precipitation of Pb carbonate species or be due to the incomplete surface coverage of phosphate on the lead surface.

The vibration band positions of orthophosphate adsorbed onto Pb (II) carbonate were fairly consistent across pH 7 and 9. Orthophosphate at pH 7 contains a mixture of both $H_2PO_4^-$ and HPO_4^{2-}, with bands for both species observed. Vibration bands corresponding to $H_2PO_4^-$ at 878, 948, 1070, and 1150 cm^{-1} were present. Vibration bands corresponding to HPO_4^{2-} at 855 and 940 cm^{-1} were present. The bands at 878 and 948 cm^{-1}, and 1070 and 1150 cm^{-1} are assigned to the symmetric ($\mathbf{v_s}$) and asymmetric ($\mathbf{v_{as}}$) stretching vibration of P-O-P and P-O, respectively. The decreased frequency of the 1077 and 1157 cm^{-1} bands to 1070 and 1150 cm^{-1} indicated a weakening of the P-O bond. While the increased frequency of the 872 and 940 cm^{-1} bands to 878 and 946 cm^{-1} indicated the formation of a P-O-Pb bond. The weak bands at 1070 and 1110

cm^{-1}, and the shift to higher frequencies of the 875 and 944 cm^{-1} bands were attributed to the weakening of the P-O bond during adsorption as well as the stronger P-O-Pb bond compared to P-OH bonds in solution. Increased pH resulted in similar adsorbed phosphate species, but with increased intensities in the vibration bands corresponding to HPO_4^{2-}. The presence of outer sphere, electrostatically adsorbed phosphate (1007 cm^{-1}) was not detected (Figure 22).

Tripolyphosphate adsorption onto Pb exhibited minimal change in the position of phosphate vibration bands across both pH, indicating that the adsorbed species is independent of pH. In the FTIR spectra of adsorbed tripolyphosphate, six peaks dominate the spectra at both pH: 897, 967-975, 1027, 1052, 1108-1115, 1205 cm^{-1}. These were assigned to the $\mathbf{v_{as}}$(P-O-P), $\mathbf{v_{as}}$($P_2O_7^-$), $\mathbf{v_{as}}$(P-OH), $\mathbf{v_{as}}$(terminal PO_3^-), and $\mathbf{v_{as}}$(bridging PO_2). The bands at 1108-1115 cm^{-1} were assigned to $\mathbf{v_{as}}$(terminal PO_3^-) by the comparison of the adsorption bands of orthophosphate to metal oxides (Guan et al., 2005; Tejedor-Tejedor and Anderson, 1990). The 1108-1115 cm^{-1} band fell between the frequency of $\mathbf{v_{as}}$(P-O) bond in $H_2PO_4^-$ and $\mathbf{v_s}$(P-O) bond in HPO_4^{2-}, which were assigned to the $\mathbf{v_{as}}$(P-O) bond in the bidentate complexes formed between the terminal PO_3^- and the lead carbonate surface. After the reaction with lead, the appearance of the 967-975 cm^{-1} bands, attributed to unbound P_2O_7, suggested that not all phosphate groups were bound to the Pb surface (Wan et al., 2020). Additionally, at higher pH, the increased intensity of the bands at 897, 975, and 1115 cm^{-1} at the expense of the band at 1050 cm^{-1} reflected the increased interaction of terminal PO_3^- groups.

The FTIR spectra presented by adsorbed trimetaphosphate or hexametaphosphate were similar across pH (Figure S2). Five distinct peaks dominated trimetaphosphate spectra: bands at 874, 1010, 1088, 1159, and 1268 cm^{-1} were assigned to $\mathbf{v_s}$(P-O-P), bending vibration $\mathbf{v_b}$(P-O), $\mathbf{v_s}$(P-O),

and $\mathbf{v_{as}}$(P-O). The bands at 1159 and 1268 cm^{-1} suggested the formation of a P-O-Pb bond. Furthermore, when compared to trimetaphosphate in solution, the lengthening of the P-O-P and shortening of the P-O bonds in the adsorbed species is observed via the shift of the bands from 902 to 874 cm^{-1} and 1002 to 1010 cm^{-1}, respectively. This suggested the steric conformation of trimetaphosphate on the Pb surface.

Only four distinct peaks were attributed to phosphate species with adsorbed hexametaphosphate: the bands at 874, 996, 1094, and 1270 cm^{-1} were assigned to $\mathbf{v_{as}}$(P-O-P), $\mathbf{v_b}$(P-O), and $\mathbf{v_{as}}$(P-O), respectively (Figure S2). Similarly, the lengthening of the $\mathbf{v_{as}}$(P-O-P) and shortening of the $\mathbf{v_b}$(P-O) bonds indicated steric conformation of hexametaphosphate on the lead surface. Whereas, the shift from 1086 and 1260 to 1094 and 1270 cm^{-1} indicated the depolymerization of hexametaphosphate into shorter chains and the formation of Pb-phosphate structural units (Jha et al., 2015). The shift to lower frequency of the symmetrical P-O-P band at 874 cm^{-1} implied that some of the phosphate groups were not associated with the Pb surface. Moreover, the intensity of the bands at 1008 ,1086, and 1268 cm^{-1} are larger with trimetaphosphate than hexametaphosphate, possibly caused by the binding of more phosphate groups per polyphosphate molecule.

Polyphosphate hydrolysis to orthophosphate within 30 minutes

Experimental design and sample analysis

Polyphosphate hydrolysis experiments were initiated by adding 1 mg Pb L^{-1} $PbNO_3$ (Fisher Chemical, Fairlawn, NJ) in 100 mL of phosphate solution. Sodium bicarbonate powder (Fisher Chemical, Fairlawn, NJ) was dissolved in ultrapure water (18.2 MΩcm, TOC < 2 μg L^{-1}) to achieve

a 5 mg C L^{-1} dissolved inorganic concentration. Polyphosphates were added at 300 or 1000 µg P L^{-1} as either hexametaphosphate (HexametaP, $(NaPO_3)_6$) (Alfa Aesar, Haverhill, MA), sodium trimetaphosphate (TrimetaP, $(NaPO_3)_3$) (Alfa Aesar, Haverhill, MA), and sodium tripolyphosphate (TripolyP, $Na_5P_3O_{10}$) (Alfa Aesar, Haverhill, MA). For blended phosphate experiments, 300 µg P L^{-1} of HexametaP, TrimetaP, or TripolyP were combined with 300 µg P L^{-1} orthophosphate (ACS grade phosphoric acid, Fisher Chemical, Fairlawn, NJ)). The pH, measured on an Acument XL50, was adjusted to either pH 7.5 ± 0.2 by the addition of 1N trace metal grade nitric acid (Fisher Chemical, Fairlawn, NJ) or freshly prepared 1N sodium hydroxide (Fisher Chemical, Fairlawn, NJ). The suspensions were placed on a shaker table for 30-mins at 150 rpm. Prior to the addition of Pb and at the end of the 30 min reaction period, samples were analyzed for orthophosphate (PO_4) via a HACH DR5000 (HACH, CO, USA) using the PhosVer 3 (#8048) method. The detection range for orthophosphate is 0.02 to 2.5 mg/L. Due to the requirement for near-instantaneous PO_4 measurements, the HACH method was chosen over the more sensitive, but longer, ion chromatography method. All experiments were run in triplicate at room temperature (21 ± 2°C).

Results and discussion

Table S5 shows the amount of polyphosphate hydrolysis to orthophosphate at the end of a 30-min reaction time. Results show that hydrolysis followed TripolyP (6.5%) > HexametaP (3.4%) > TrimetaP (1.8%) at equivalent phosphorous to lead ion concentrations. When orthophosphate (300 µg P L^{-1}) and polyphosphate (300 µg P L^{-1}) were blended with 1000 µg Pb L^{-1}, hydrolysis followed a similar pattern as above: Blends with TripolyP, TrimetaP, or HexametaP presented 9.4, 6.5, and 7.6% hydrolysis to orthophosphate. The 1000 µg Pb L^{-1} concentration was higher

than what was seen in the reactors with blended phosphates but was chosen to promote Pb-ion facilitated hydrolysis.

Table 12 Summary of conditions and results of the CSTR dissolution experiments.

ID	pH	Short stagnation (30 mins)					Long stagnation dissolution (24 hr)				
		Lead dissolution (µg Pb m^{-2})		Phosphorous and phosphate removed in the reaction		Dissolved lead in effluent (mol)	Lead (µg Pb m^{-2})		Phosphorus and phosphate removed in the reaction		Dissolved lead in effluent (mol)
		Dissolved (<0.2 µm)	<0.45 µm filtrate	Phosphorus (%)	Phosphate (%)		Dissolved (<0.2 µm)	<0.45 µm filtrate	Phosphorous (%)	Phosphate (%)	
Phosphate free	7.5	104.4 ± 4.3	118.6 ± 12.1	*	*	0.39 ± 0.02	168.4 ± 10.6	344.3 ± 13.1	*	*	0.64 ± 0.04
OrthoP (150 µg P L^{-1})	7.5	75.3 ± 6.7	80.1 ± 6.5	93.6 ± 1.9	*	0.28 ± 0.03	93.5 ± 0.8	109.7 ± 2.6	99.9 ± 3.2	*	0.28 ± 0.003
OrthoP (300 µg P L^{-1}) (Ref)	7.5	65.7 ± 16.1	77.1 ± 10.2	3 ± 1.3	*	0.25 ± 0.06	97.1 ± 3.1	108 ± 6.3	4.1 ± 0.2	*	0.37 ± 0.01
OrthoP (600 µg P L^{-1})	7.5	32.1 ± 13.3	55.4 ± 8.6	3.7 ± 3.4	*	0.12 ± 0.05	84.2 ± 4.9	97.6 ± 1.2	3.4 ± 0.2	*	0.32 ± 0.02
OrthoP (1000 µg P L^{-1})	7.5	6.1 ± 2	19.2 ± 3.9	0.9 ± 0.7	*	0.02 ± 0.01	28.5 ± 2.8	98.7 ± 11.3	16.3 ± 4.9	*	0.11 ± 0.01
OrthoP (Ref) + TrimetaP (300 µg P L^{-1})	7.5	94 ± 3.3	102.6 ± 9.4	66.8 ± 0.7	97.9 ± 1.3		122.6 ± 5.9	139 ± 13.6	67.7 ± 0.2	87 ± 32.	
OrthoP (Ref) + TrimetaP (700 µg P L^{-1})	7.5	95 ± 11.3	102.8 ± 16.1	25.2 ± 1.1	98.2 ± 1.1		148.7 ± 2.5	161.1 ± 9.2	29.8 ± 0.2	87.3 ± 32.7	
OrthoP (Ref) + HexametaP (300 µg P L^{-1})	7.5	64.5 ± 10.9	67 ± 14.9	1.3 ± 1.8	8.34 ±		454.2 ± 19.1	615.5 ± 31.4	63.7 ± 1.7	7.4 ± 2.9	
OrthoP (Ref) + HexametaP (700 µg P L^{-1})	7.5	2122 ± 145	2232.9 ± 118.2	6 ± 4	10.2 ± 1.6		1467 ± 160.7	2887.1 ± 81.6	33.3 ± 1.2	9.1 ± 3.7	

OrthoP (Ref) + Tripoly P (300 µg P L^{-1})	*7.5*	*788.2 ± 35.7*	*843.7 ± 27.4*	*19.2 ± 6.4*	*12.6 ± 2.6*		*399.2 ± 35.9*	*446 ± 42.8*	*13.8 ± 4.6*	*11.2 ± 4.8*	
OrthoP (Ref) + Tripoly P (700 µg P L^{-1})	*7.5*	*2631.5 ± 43.9*	*2626.6 ± 59.7*	*3.4 ± 1.4*	*-3.4 ± 4.*		*1987.3 ± 7.1*	*2217.3 ± 36.6*	*18.7 ± 9.9*	*-3.0 ± 4.2*	
Trimeta P (1000 µg P L^{-1})	*7.5*	*188.6 ± 23.3*	*265.1 ± 12.6*	*3.1 ± 0.9*	*	*0.71 ± 0.02*	*167.7 ± 6.5*	*340.9 ± 31.8*	*8.3 ± 0.7*	*	*0.63 ± 0.02*
Hexam etaP (1000 µg P L^{-1})	*7.5*	*2333.3 ± 156.1*	*2503.8 ± 211.9*	*6.6 ± 5*	*	*6.0 ± 0.09*	*2942.9 ± 111.2*	*2970.5 ± 112.1*	*7.7 ± 3*	*	*7.0 ±0.16*
Tripoly P (1000 µg P L^{-1})	*7.5*	*2906.4 ± 27.6*	*2969.9 ± 72.2*	*0.5 ± 2.8*	*	*11.0 ± 0.10*	*2907.7 ± 20.9*	*3008.3 ± 21.9*	*8.8 ± 3.7*	*	*11.0 ± 0.08*

*Data not available

Table 13 Summary of energy dispersive spectroscopy (EDS) results of CSTR solids. Data is presented in weight percent (wt. %).

ID	*Calcium*	*Orthophosphate*	*Trimetaphosphate*	*Hexametaphosphate*	*Tripolyphosphate*	*P*	*Pb*	*C*	*O*
	mg Ca L^{-1}	*µg P L^{-1}*				*wt.% (mean ± std dev)*			
OrthoP (Ref) + TrimetaP (300 µg P L^{-1})	*0*	*300*	*300*	*0*	*0*	*25.82 ± 7.26*	*24.05 ± 6.1*	*17.16 ±8.82*	*32.94 ± 9.39*
OrthoP (Ref) + TrimetaP (700 µg P L^{-1})	*0*	*300*	*700*	*0*	*0*	*6.44 ± 2.42*	*65.84 ± 6.74*	*8.87 ±4.57*	*20.65 ± 4.64*
OrthoP (Ref) + HexametaP (300 µg P L^{-1})	*0*	*300*	*0*	*300*	*0*	*13.79 ± 3.46*	*57.64 ± 8.45*	*12.24 ± 6.04*	*16.34 ± 1.51*
OrthoP (Ref) + HexametaP (700 µg P L^{-1})	*0*	*300*	*0*	*700*	*0*	*0.24 ± 0.11*	*73.34 ± 6.36*	*7.63 ± 2.49*	*18.92 ± 4.29*
OrthoP (Ref) + TriployP (300 µg P L^{-1})	*0*	*300*	*0*	*0*	*300*	*41.69 ± 3.74*	*46.92 ± 9.96*	*3.75 ± 2.01*	*7.71 ± 4.48*

OrthoP (Ref) + TriployP (700 µg P L^{-1})	*0*	*300*	*0*	*0*	*700*	*1.55 ± 1.41*	*68.55 ± 4.56*	*10.8 ± 3.21*	*19.1 ± 8.84*

*ND: below detection limit

Table 14 Standard XRD patterns and their PDF entry numbers.

Phase	PDF entry No.
Hydroxypyromorphite	00-089-6287
Hydrocerussite	96-901-1389
Cerussite	00-076-2056
Calcite	00-005-0586

Table 15 Standard ATR-FTIR patterns and their RUFF entry numbers.

Phase	RUFF entry No.
Hydroxypyromorphite	NA
Hydrocerussite	R160062
Cerussite	R040069
Calcite	R040070

Table 16 Summary of polyphosphate hydrolysis experiments.

ID	OrthoP	TrimetaP	HexametaP	TripolyP	Lead	Initial PO_4	PO_4 at end of 30-min HRT	Hydrolysis (%)
	µg P L^{-1}				µg Pb L^{-1}	mg PO_4 L^{-1}	mg PO_4 L^{-1}	
TripolyP (1000 µg P L^{-1})	0	0	0	1000	1000	0.01	0.21±0.01	6.5±0.3
TrimetaP (1000 µg P L^{-1})	0	1000	0	0	1000	0.01	0.06±0.02	1.8±0.8
HexametaP (1000 µg P L^{-1})	0	0	1000	0	1000	0.01	0.11±0.01	3.4±0.4
OrthoP (Ref) + TripolyP (300 µg P L^{-1})	300	0	0	300	1000	0.94±0.01	1.03±0.01	9.4±0.5
OrthoP (Ref) + TrimetaP (300 µg P L^{-1})	300	300	0	0	1000	0.94±0.01	0.99±0.02	6.5±1.5

OrthoP (Ref) + HexametaP (300 µg P L^{-1})	*300*	*0*	*300*	*0*	*1000*	*0.94±0.01*	*1.01±0.02*	*7.2±0.5*

Note: values is red are below detection limit and were assigned half the detection limit value (0.01 mg PO_4 L^{-1}).

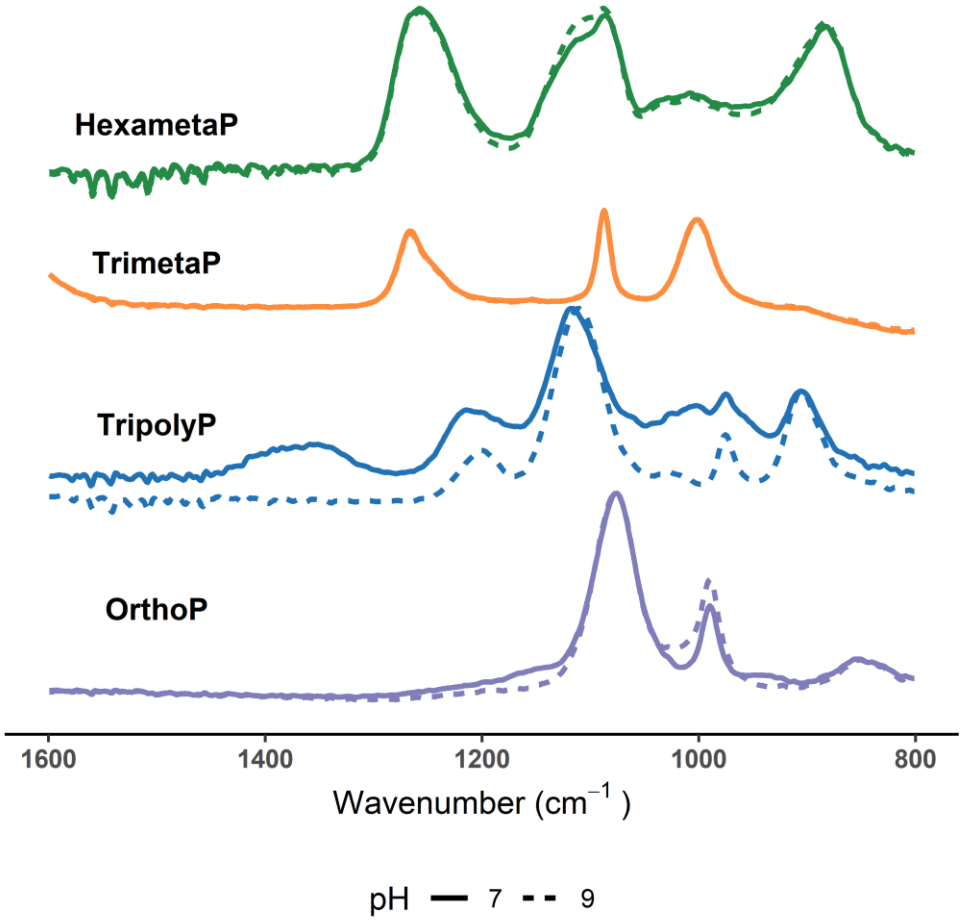

Figure 23 ATR-FTIR spectra of phosphate standards (1 g P L^{-1}) in solution at pH 7 and 9. ATR-FTIR spectra were recorded in the 5 mg L^{-1} DIC background electrolyte solution.

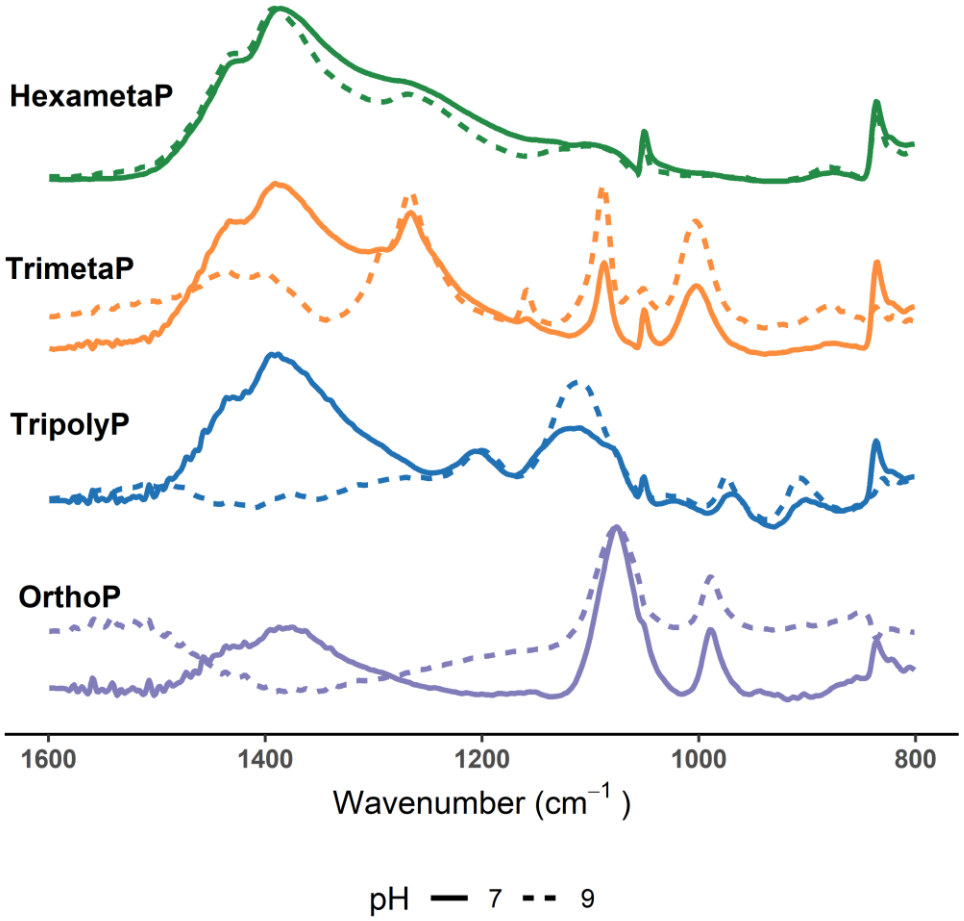

Figure 24 ATR-FTIR spectra of phosphates (1 g P L^{-1}) adsorbed onto lead carbonate at pH 7 and 9. ATR-FTIR spectra were recorded in the 5 mg L^{-1} DIC background electrolyte solution.

Appendix C Supporting Data for Chapter 5

Field-flow fractionation

Suspensions from the corrosion cells were fractionated using an asymmetric flow field-flow fractionation (A4F) system (Postnova AF2000 multiflow) with a 300 Da poly(ethersulfone) membrane, a 500 µm spacer, and a 1 mL polyether ether ketone sample loop. The system was sequentially coupled to a UV absorbance detector (Shimadzu SPD-20A) at 254 nm, and an ICP-MS (ThermoFisher iCAP-RQ). The mobile phase was a 50 mM tris (hydroxymethyl)aminomethane buffer, adjusted to pH 7.5 with trace metal grade HCl. The FFF effluent was mixed with internal standards (Sc, In, and Tb in 2% HNO_3) using a mixing tee prior to entering the ICP-MS.

The details of the A4F method described in Trueman *et al.* (2022)are summarized below. A run was 53 minutes long. The focus period was 10 minutes. During each run, the crossflow was maintained at 2.0 mL/min for the first 31 minutes. It was then set to decay linearly over 2 minutes to 0.1 mL/min. The crossflow was maintained at 0.1 mL/min for 10 minutes. It was then set to zero for 10 minutes to rinse the A4F channel.

Inductively coupled plasma mass spectrometry

The ICP-MS data were acquired using a ThermoFisher iCAP-RQ operated in kinetic energy discrimination mode with He as the collision gas. The ICP-MS was calibrated on each analysis with a multielement standard in 2% HNO_3 at 25, 100, and 250 µg L^{-1}. Standards were introduced to the nebulizer after mixing with A4F channel effluent via a mixing tee. Detection limits were

estimated using a 3σ method. The median detection limits were 0.11 µg Fe L^{-1}, 0.002 µg Mn L^{-1}, 1.65 µg P L^{-1}, and 9 µg Si L^{-1}, respectively.

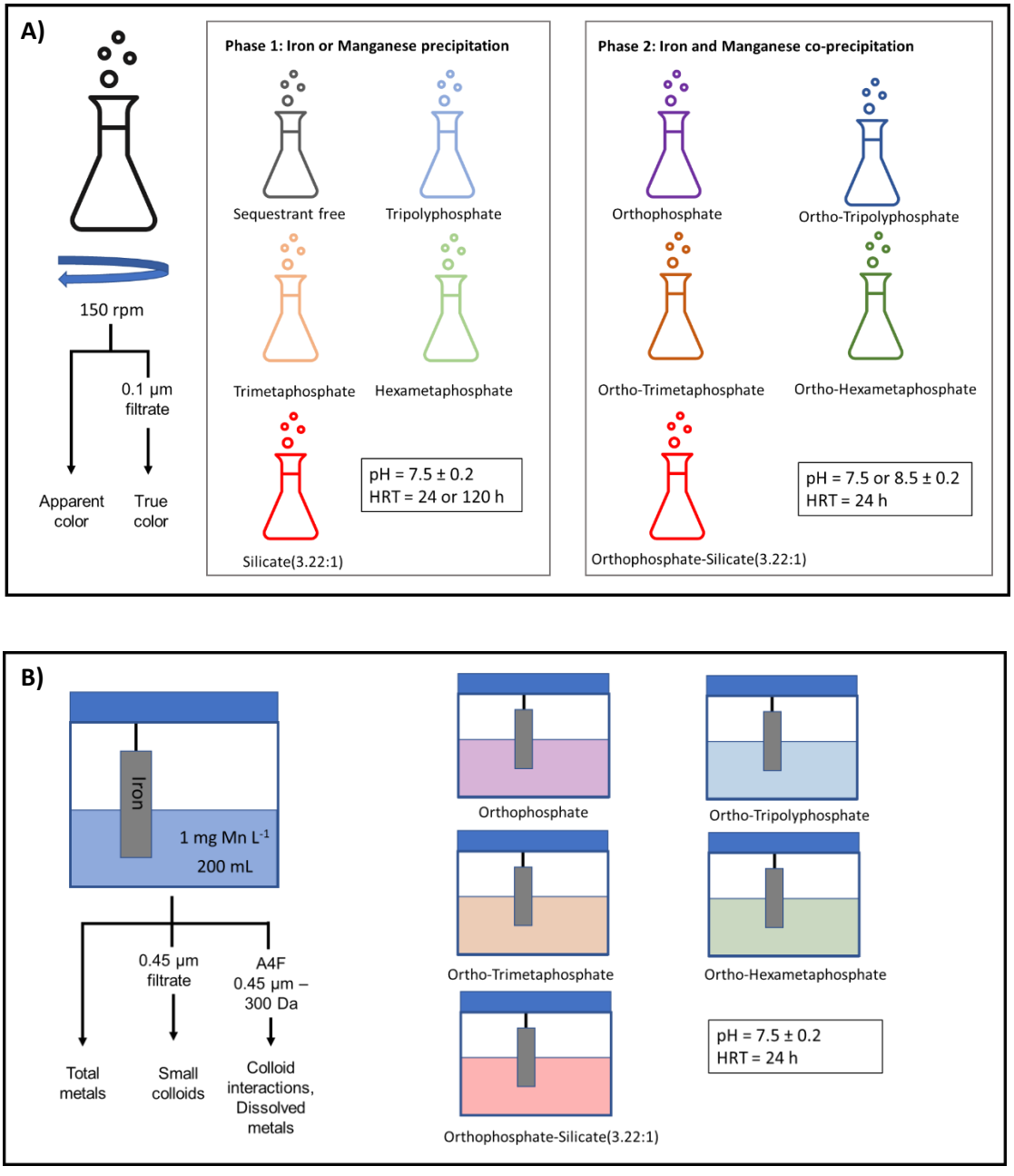

Figure 25 A schematic overview of the (A) precipitation and (B) corrosion cell experiments. The background electrolyte was 5 mg C L^{-1} DIC with a free chlorine residual of 1 mg Cl_2 L^{-1}.

A) **C)**

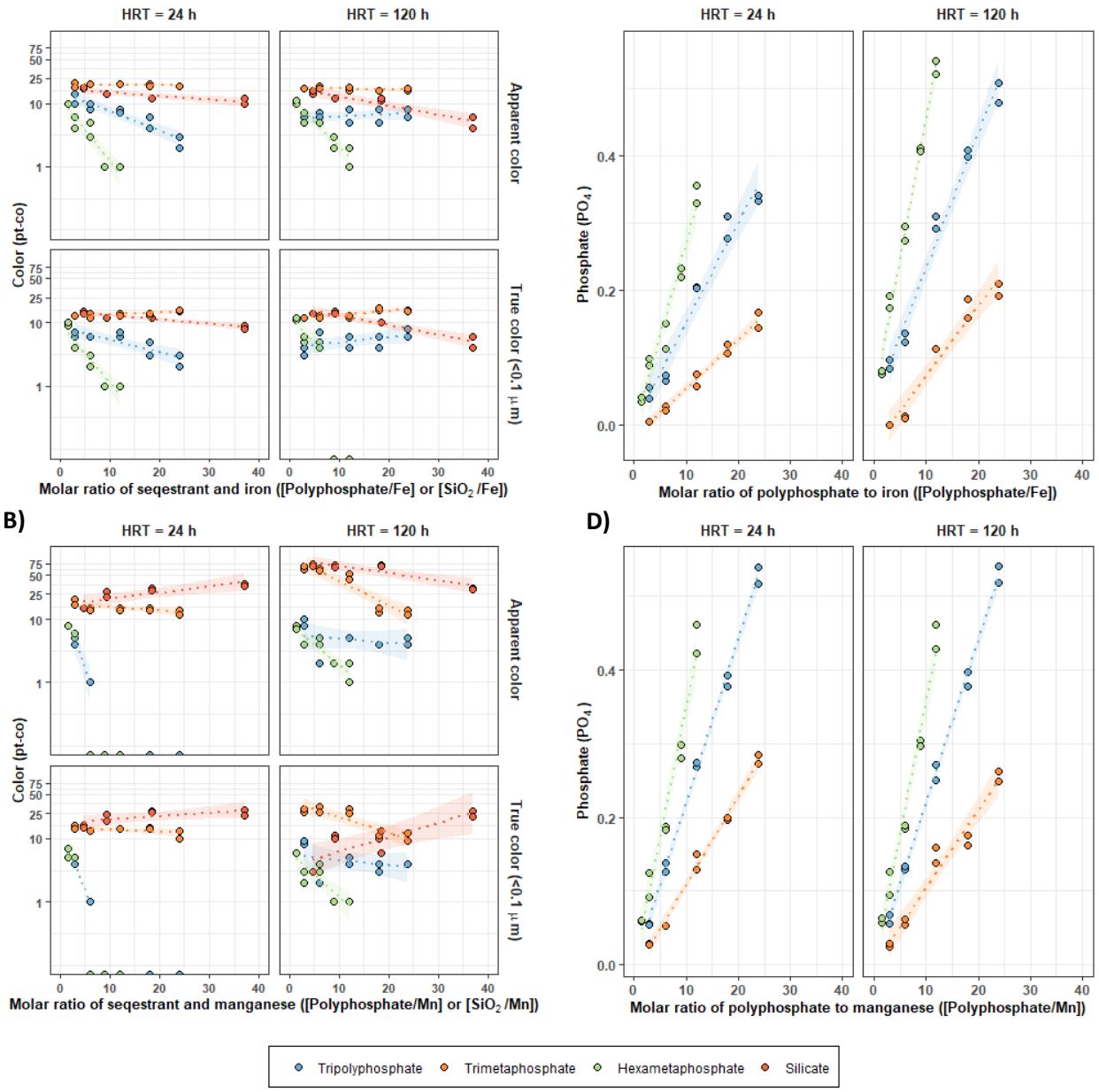

Figure 26 Effect of sequestrants on color reduction and polyphosphate hydrolysis with Fe (A, C) and Mn (B,D) (1 mg L^{-1}, 18 µM) after 24 and 120 h. The background electrolyte solution was buffered with $NaHCO_3$ (5 mg C L^{-1}) at a free chlorine residual of 1 mg L^{-1} and pH 7.5.

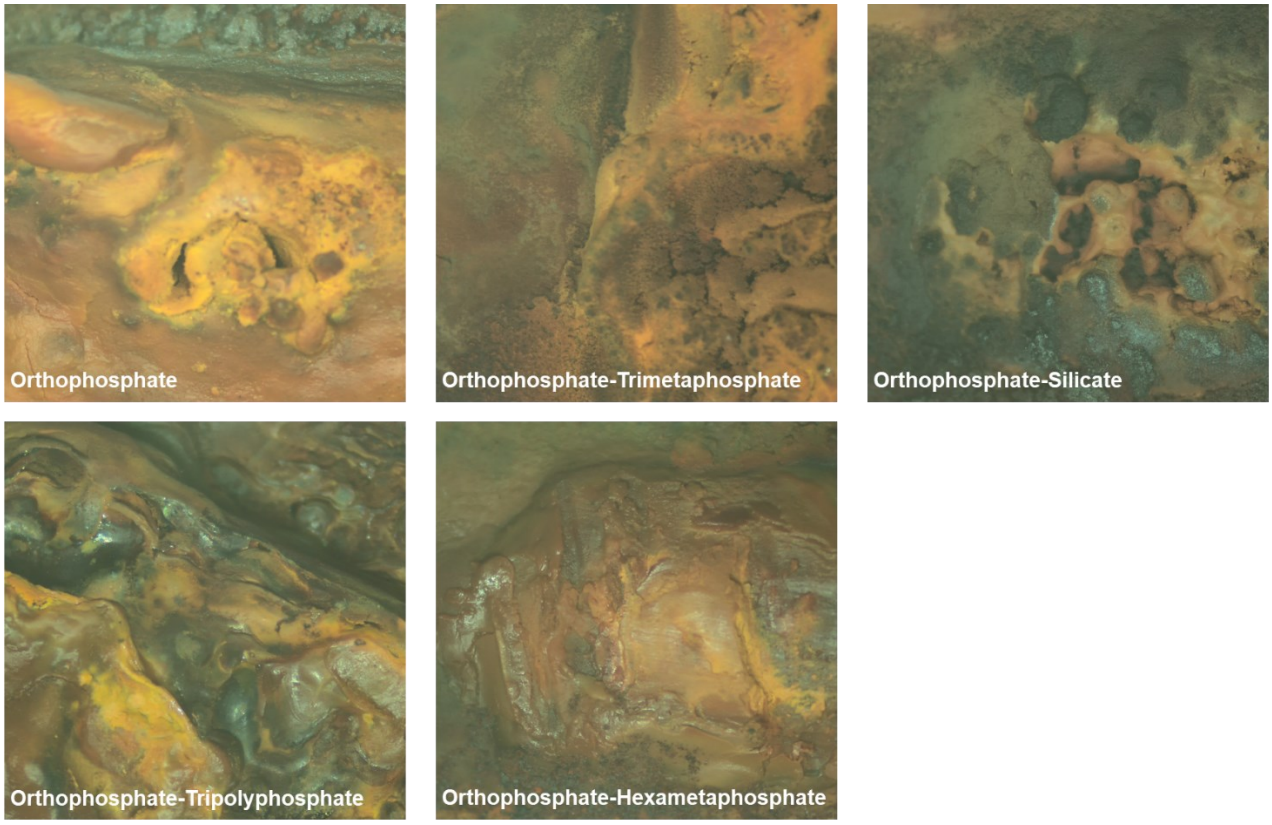

Figure 27 Optical imaging of corroded iron coupon surfaces in $NaHCO_3$ (5 mg C L^{-1}) buffered pure water systems at pH 7.5, free chlorine residual of 1 mg L^{-1}, and temperature of 21 ± 1 °C. (A) the reference system with orthophosphate (300 µg P L^{-1}, ~10 µM), (B) orthophosphate (300 µg P L^{-1}, ~10 µM) - tripolyphosphate (300 µg P L^{-1}, ~10 µM), (C) orthophosphate (300 µg P L^{-1}, ~10 µM) - trimetaphosphate (300 µg P L^{-1}, ~10 µM), (D) orthophosphate (300 µg P L^{-1}, ~10 µM) - hexametaphosphate (300 µg P L^{-1}, ~10 µM), and (E) orthophosphate (300 µg P L^{-1}, ~10 µM) - sodium silicate (12 mg SiO_2 L^{-1}, ~200 µM).

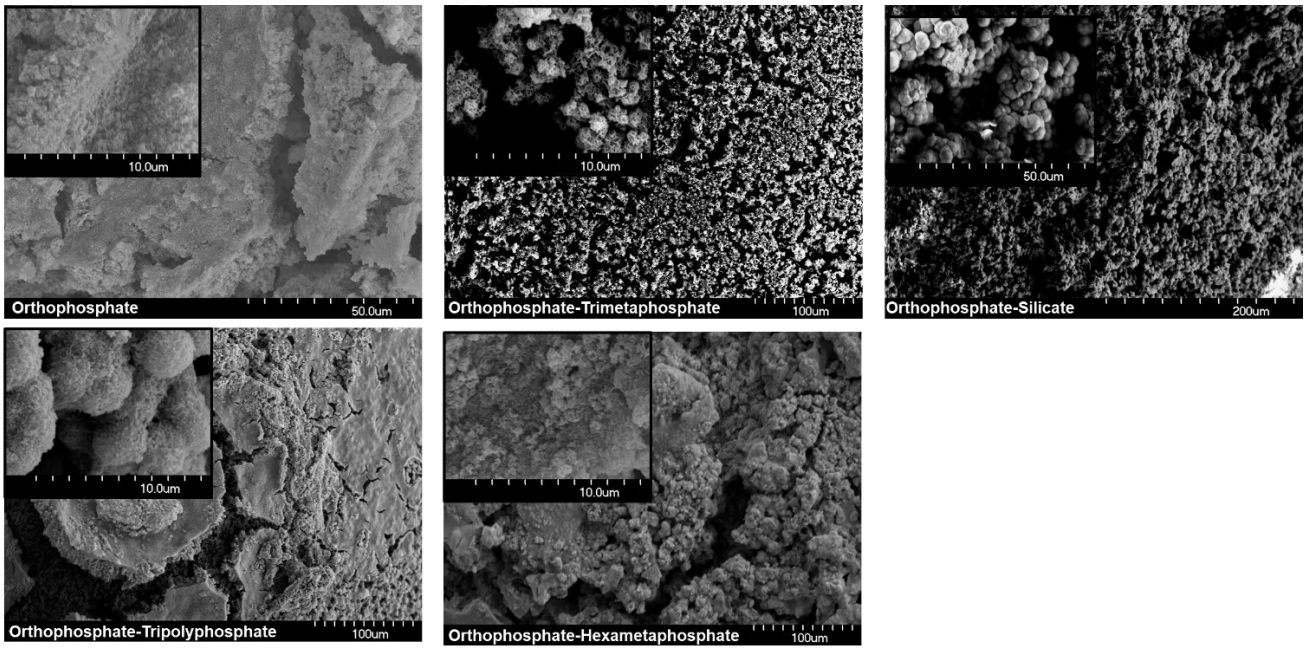

Figure 28 Scanning electron micrographs of corroded iron coupon surfaces in $NaHCO_3$ (5 mg C L^{-1}) buffered pure water systems at pH 7.5, free chlorine residual of 1 mg L^{-1}, and temperature of 21 ± 1 °C. (A) the reference system with orthophosphate (300 µg P L^{-1}, ~10 µM), (B) orthophosphate (300 µg P L^{-1}, ~10 µM) - tripolyphosphate (300 µg P L^{-1}, ~10 µM), (C) orthophosphate (300 µg P L^{-1}, ~10 µM) - trimetaphosphate (300 µg P L^{-1}, ~10 µM), (D) orthophosphate (300 µg P L^{-1}, ~10 µM) - hexametaphosphate (300 µg P L^{-1}, ~10 µM), and (E) orthophosphate (300 µg P L^{-1}, ~10 µM) - sodium silicate (12 mg SiO_2 L^{-1}, ~200 µM).